

Millimetre Wave for Fifth Generation of Wireless Communications

Saurav Dahal

B. Eng., M. Eng.

Institute for Sustainable Industries & Liveable Cities

College of Engineering and Science

Victoria University

Submitted in fulfilment of the requirements for the degree of

Doctor of Philosophy

August 19, 2020



To my family and friends

Abstract

Mobile communication technology is continuously evolving. Early Fifth generation (5G) products, due 2020, should support high capacity, higher data rates, lower latency, lower energy consumption and should be cost effective. High data rates will require wider bandwidths, which are available in the higher frequency millimetre wave (mmWave) bands. Millimetre waves have much shorter wavelengths compared to today's microwave mobile systems. Understanding mmWave propagation characteristics is important in the physical layer design of future wireless systems. Statistical Channel models are required in the standardization process to evaluate implementation proposals without the expense of building costly hardware test-beds. Statistical channel models are described by a few key parameters and a variance. For example, transmission path loss is a function of environment, range, path loss exponent (PLE) and the standard deviation (σ) of a statistical (shadowing) component. These parameters are generated by fitting an equation, in a minimum mean square error (MMSE) fashion, to a collated measurement database from a number of research organizations in different countries. Considering this, a number of channel sounding empirical measurements at mmWave frequencies were conducted to characterize, model and evaluate the propagation channel properties in different 3rd Generation Partnership Projects (3GPP) scenarios (environments) under Australian conditions. Particular outdoor areas of interest were Rural Macro (RMa), Urban Macro (UMa) and Urban Micro (UMi) while indoor areas (InH) of interest included office and shopping malls.

An in-house channel sounder was modified to obtain signal strengths with respect to (wrt) location and angle of arrival (AoA). Angular resolution was nominally 10°, 20° and

55° depending upon the size of the horn antenna. The equipment covered frequencies between 24 GHz to 40 GHz and was capable of measuring path losses up to 160 dB with the appropriate antenna. The experimental work involved performing measurements in different scenarios and then comparing to existing channel models (if such exist) and suggesting improvements where appropriate. The thesis focuses on outdoor and outdoor to indoor mmWave wireless propagation channels and contains contributions in each of the key scenarios as follows:

Rural Macro (RMa) channel measurements were performed at 24 GHz. Average path loss and Angle of Arrival (AOA) spread were close to 3GPP predictions limited to sub 7 GHz frequencies. The results were submitted to the Third Generation Partnership Project (3GPP) enabling the extension of the existing RMa model to 30 GHz.

Urban Macro (UMa) have base station (BS) antennas above roof-top height. Measurements at 27.1 GHz were performed in two environments; dense urban and light urban, both classified as NLOS UMa. The results were compared against two competing 3GPP path loss models; the alpha beta (AB) model and the close-in free space reference distance (CI) model. The AB model had the lower RMS error. The AB model required input parameters such as average building height and street width etc. which made it sensitive to the choice of input parameters, whereas the CI model required no input parameters and was preferred if the cell consists of wide variety of dense and light urban regions.

Urban Micro (UMi) have BS antennas below roof-top height. Measurements were conducted at 39.5 GHz in Open Square (OS) and Street Canyon (SC) scenarios. Results showed that the extracted parameters are in close agreement with 3GPP specifications,

particularly for the CI model. Additionally, we reported 31 dB for 100 m down the SC side streets out of which 18 dB loss occurs just around the corner. We further analysed the base station (BS) height gain effect in OS and found a marginal benefit of 0.5 dB for a 4 m height change. Cross polar discrimination were also reported in SC which reduced by 2.5 dB per 10 dB increase in path loss using directional antennas while correlation disappeared on a omnidirectional basis.

We presented a double-directional measurements for an UMi OS environment. Results showed that multiple Angles of Departure from a given user equipment (UE) position often result in few (often one) Angles of Arrival at the BS. Similarly different UE locations can often share a common angle of arrival at the BS. This could cause rank reduction in some MIMO system.

An outdoor to indoor measurement campaign at 24 GHz emulating the satellite to indoor propagation channel was presented. The results are applicable to the satellite/mobile co-existence problem as well as in-building coverage from high altitude platform. The mean building entry loss increased by 0.43 dB per degree of (satellite) slant elevation angle, almost twice the ITU recommendation. Further we showed that the signal linearly decays with distance with a slope that increases with slant angle. Additionally, we showed that high gain narrow beam antenna outperformed low gain wide beam antenna both in terms of signal maximization to high altitude platform as well as signal minimization to a co-existing satellite uplink channel. Further, there is an antenna gain reduction in this type of environment due to internally generated multipath.

Details of Included Papers

Contributions to standards

1. 3GPP Technical specification group radio access network, “New measurements at 24 ghz in a rural macro environment,” 3rd Generation Partnership Project, Technical Report TDOC R1-164975, June, 2016. [Online]. Available: http://www.3gpp.org/ftp/TSG_RAN/WG1_RL1/TSGR1_85/Docs/R1-164975.zip [1].

Articles in peer-reviewed journals

2. Saurav Dahal, Shabbir Ahmed, Horace King, Ganesh Bharatula, John Campbell and Mike Faulkner, “Slant-Path Building Entry Loss at 24 GHz”, IEEE Access, vol. 7, pp. 158525-158532, 2019 [2].
3. Saurav Dahal, Shabbir Ahmed, Horace King, Ganesh Bharatula, John Campbell and Mike Faulkner, “Urban Microcell 39 GHz Measurements”, IEEE Antennas and Wireless Propagation Letters, vol. 18, no. 10, pp. 2071-2075, 2019 [3].

Peer-reviewed conference papers

4. Saurav Dahal, Euripides A. Stephanou, Nathaniel Talukdar, Shabbir Ahmed, Horace King and Mike Faulkner, “Millimetre Wave Propagation Reverse Measurements for 5G Urban Micro Scenario”, in IEEE 89th International Conference on Vehicular Technology, 2019 [4].
5. Saurav Dahal, Shabbir Ahmed, Horace King, and Mike Faulkner. “Antenna gain in a Millimeter-Wave Multipath Environment”, 3rd Australian Microwave Symposium (AMS), pp. 93-94, 2018 [5].

6. S. Dahal, M. Faulkner, H. King, and S. Ahmed, "27.1 GHz millimeter wave propagation measurements for 5G urban macro areas", in IEEE 85th International Conference on Vehicular Technology, pp. 1-5, 2017 [6].

During my PhD study, I have also contributed to the following papers and standards.

However, these are **not included** in the thesis.

7. ITU, "ITU-R P. 2346-2: compilation of measurement data relating to building entry loss", ITU Tech. Rep., pp. 220-245, 2017 [7].
8. ITU-R, "Measurements on urban building clutter loss," International Telecommunication Union, Report ITU-R WP3K Contribution 102, 2017. [Online]. Available: <https://www.itu.int/md/R15-WP3K-C-0102/en> [8].
9. Saurav Dahal, Shabbir Ahmed, Horace King, Ganesh Bharatula, John Campbell and Mike Faulkner, "Millimetre wave Propagation Measurements in a Multipath NLOS Environment", to be submitted to IEEE Access, 2020.
10. Saurav Dahal, Shabbir Ahmed, Horace King, Ganesh Bharatula, John Campbell and Mike Faulkner, "K-factor and Antenna Gain in Measured Urban Macro Millimetre wave Environments", needs revision and will be submitted to IEEE Open Journal of Vehicular Technology, 2020.

Note: The standards are NOT peer reviewed.

Thesis including published works declaration

I, Saurav Dahal, declare that the PhD thesis entitled ‘Millimetre Wave for Fifth Generation of Wireless Communications’ is no more than 100,000 words in length including quotes and exclusive of tables, figures, appendices, bibliography, references and footnotes. This thesis contains no material that has been submitted previously, in whole or in part, for the award of any other academic degree or diploma. Except where otherwise indicated, this thesis is my own work.

This thesis includes six original publications; one has been published in in a 3GPP standardisation document, two have been published in Q1 ranked journals and three have been published in peer-reviewed IEEE conferences. The core theme of the thesis is millimetre wave channel characterization for fifth generation of mobile systems. The ideas, development and writing up of all the papers in the thesis were the principal responsibility of myself, the student, working within the Institute of Sustainable Industries and Liveable Cities (ISILC) under the supervision of Dr. Horace King, Professor Mike Faulkner and Dr. Shabbir Ahmed.

In the case of Chapters 5 to 10, my contributions to the work involved are presented in the table below:

Signed:

Candidate Name: Saurav Dahal

August 19, 2020

Thesis Chapter	Publication Title	Type	% of student contribution and Nature	Co-author names, Nature and % of contribution	Co-author affiliated to VU
5	New measurements at 24 GHz in a rural macro environment [1]	Standard	80%. Concept, ideas and simulation analysis	Telstra, submitted to 3GPP and review of drafts 20%	No
6	27.1 GHz Millimetre Wave Propagation Measurements for 5G Urban Macro Areas [6]	Conference	80%. Concept, ideas, analysis, and paper writing draft	Mike Faulkner, contribution to theory 10% Horace King, draft review 3% Shabbir Ahmed, hardware design 7%	Yes Yes Yes
7	Urban Microcell 39 GHz Measurements [3]	Journal	80%. Concept, ideas, analysis, and paper writing draft	Shabbir Ahmed, helped in measurement 5% Horace King, review of draft 2% Ganesh Bharatula and John Campbell, review of draft 5% Mike Faulkner, overall supervision and contribution to theory 8%	Yes Yes No Yes
8	Millimetre Wave Propagation Reverse Measurements for 5G Urban Micro Scenario [4]	Conference	80%. Concept, ideas, analysis, and paper writing draft	Euripides A. Stephanou and Nathaniel Talukdar, helped in measurements, 10% Shabbir Ahmed and Horace King, review of drafts, 5% Mike Faulkner, overall supervision and contribution to theory 5%	Yes Yes Yes
9	Slant-Path Building Entry Loss at 24 GHz [2]	Journal	80%. Concept, ideas, analysis, and paper writing draft	Shabbir Ahmed and Horace King, helped in measurement 5% Ganesh Bharatula and John Campbell, review of draft 5% Mike Faulkner, overall supervision and contribution to theory 10%	Yes No Yes
10	Antenna gain in a Millimetre-Wave Multipath Environment [5]	Conference	80%. Concept, ideas, analysis, and paper writing draft	Shabbir Ahmed and Horace King, helped in measurement 10% Mike Faulkner, overall supervision and contribution to theory 10%	Yes Yes

Acknowledgements

Firstly, my special thanks and gratitude goes to my supervisors, Dr. Horace King, Prof. Mike Faulkner and Dr. Shabbir Ahmed, for all their devoted support, advice and encouragement. Their endless kindness, patience and knowledge enabled me to not only complete this dissertation, but also become a better researcher.

I would like to thank Telstra for providing the grant to conduct this research. A token of appreciation to Mr. Ganesh Bharatula and Mr. John Campbell for their advice and suggestions during the project.

I would also like to thank Mr. Euripides S. Stephanou, Mr. Nathaniel Talukdar and Tyson Skiba in helping the measurement program.

I would also like to thank the staff of the Graduate Research Centre and the College of Engineering and Science, especially Ms. Elizabeth Smith for her immense support throughout this journey. I acknowledge the financial support provided through the Victoria University Postgraduate Research Scholarship.

Special thanks to my colleagues, who have shared this journey with me and made it exciting and enjoyable. The memories and friendships will always be remembered.

My deepest thanks and appreciation to my parents, sister, for their endless and unconditional love, support and care, for whom I owe all my inspiration in life to follow my dreams.

Last but not least, my deepest gratitude and love goes to my dear wife, Sabita, for all her support and care through years of hard work.

Contents

Abstract	ii
Details of Included Papers	v
Thesis including published works declaration	vii
Acknowledgements	ix
List of Figures	xv
List of Tables	xviii
Abbreviations	xix
Symbols	xxi
1 Introduction	1
1.1 MIMO	3
1.2 Beamforming	8
1.3 Massive MIMO and Hybrid Beamforming	10
1.4 Millimetre waves	13
1.5 Standardisation bodies	14
1.5.1 3GPP	14
1.5.2 ITU	16

1.5.2.1	Development (ITU-D)	17
1.5.2.2	Standardization (ITU-T)	18
1.5.2.3	Radio communication (ITU-R)	18
1.6	Research Objectives	19
1.7	Research Contributions	20
1.8	Thesis Outline	22
2	Antenna and Propagation Fundamentals	26
2.1	Antenna	26
2.1.1	Wire Antennas	27
2.1.2	Aperture Antennas	27
2.1.2.1	Microstrip Antennas	28
2.1.3	Array Antennas	29
2.2	Fundamental Parameters of Antennas	29
2.2.1	Radiation Pattern	30
2.2.1.1	Isotropic, Directional and Omnidirectional Patterns	30
2.2.1.2	Radiation Pattern Lobes	30
2.2.1.3	Radiation Intensity	31
2.2.2	Directivity	32
2.2.3	Gain	32
2.2.4	Half-Power Beamwidth	32
2.2.5	Synthesising Isotropic Measurements from Directional Radiation Patterns	33
2.3	Radio Wave Propagation	34
2.3.1	Large and Small Scale Parameters	34
2.3.2	Free Space Path Loss	35
2.3.3	Angular Spread	36
2.3.4	Delay Spread	37
2.4	Summary	38
3	Literature Review	39

3.1	Frequency attenuation and rain attenuation in millimetre waves	40
3.2	Wireless Channel Modelling Approaches	42
3.3	Propagation Path loss models	45
3.3.1	AB model	46
3.3.2	CI path loss model	49
3.4	Channel characterization	52
3.4.1	Rural Macro (RMa)	53
3.4.2	Urban Macro (UMa)	54
3.4.3	Urban Micro (UMi)	56
3.4.3.1	Path Loss Measurements and models	57
3.4.3.2	3D Path Loss Models	58
3.4.3.3	Multi Beams	59
3.4.3.4	Repeaters and Backhaul	60
3.4.3.5	Delay Spread	61
3.4.3.6	Angular Spread	62
3.4.3.7	Height Gain	62
3.4.3.8	Polarisation	63
3.4.4	Indoor Hotspot (InH) and Outdoor to Indoor (O2I)	64
3.4.4.1	Material Losses	64
3.4.4.2	InH Propagation	66
3.5	Summary	68
4	Hardware Design, Calibration and Performance	70
4.1	OHS Transmission Limits	71
4.2	Swept Frequency measurements using Network Analyser	72
4.2.1	Antenna Calibration	72
4.3	Semi Automatic Receiver Scanning	74
4.3.1	Limited isotropic coverage	74
4.4	Narrowband measurements	76
4.4.1	Signal Generator and Receiver Calibration	77
4.4.2	Link Margin Calculation	78

4.5	Wideband measurements (OFDM)	79
4.5.1	Link Margin Calculation	82
4.6	Summary	83
5	New measurements at 24 GHz in a rural macro environment	86
5.1	Overview	86
5.2	Publication	87
6	27.1 GHz Millimetre Wave Propagation Measurements for 5G Urban Macro Areas	94
6.1	Overview	94
6.2	Publication	95
7	Urban Microcell 39 GHz Measurements	103
7.1	Overview	103
7.2	Publication	104
8	Millimetre Wave Propagation Reverse Measurements for 5G Urban Micro Scenario	112
8.1	Overview	112
8.2	Publication	113
9	Slant-Path Building Entry Loss at 24 Ghz	121
9.1	Overview	121
9.2	Publication	123
10	Antenna gain in a Millimetre-Wave Multipath Environment	134
10.1	Overview	134
10.2	Publication	135
11	Conclusion	138
11.1	Research Contributions	138
11.1.1	RMa	138

Contents

11.1.2 UMa	139
11.1.3 UMi	139
11.1.4 O2I	141
11.2 Future Work	142

References	143
-------------------	------------

List of Figures

1.1	Growth in connected devices(billions) [9].	2
1.2	Global mobile traffic growth (monthly Exabytes) [9].	2
1.3	A 2x2 MIMO [10].	4
1.4	Far-field geometry of n-element array of antennas.	9
1.5	Phase array antenna beamforming to two users.	10
1.6	Massive MIMO prototype (Lund university at 2.6 GHz) [11].	11
1.7	Major types of hybrid beamforming: (a) Fully-connected hybrid beamforming, (b) Sub-connected hybrid beamforming [12].	12
1.8	Frequency bands for cellular communication	13
1.9	Regional Standard Setting Organizations (SSOs) [13].	14
1.10	3GPP distributed organization structure [13].	15
1.11	ITU structure.	17
2.1	A (folded) dipole antenna [14]	27
2.2	Horn antenna; an example of aperture antenna. The wave-guide to coaxial cable transition is on the left and the aperture in the right. Nominal gain ranges from 25 dBi (top) to 10 dBi (bottom).	28
2.3	Patch antenna [15]	28
2.4	A layout of the 8x8 array of patches [16].	29
2.5	Radiation pattern of an antenna showing pattern lobes [17].	31
2.6	Radiation pattern of a directional antenna showing HPBW and First Null Beamwidth (FNBW) [18].	33
2.7	Radiation pattern of a directional antenna [5].	34
2.8	Free space path loss at 2.4, 24 and 39 GHz as a function of distance	36

3.1	Radio channel and propagation channel [19].	40
3.2	Atmospheric absorption across mmWave frequencies in dB/km [20–22].	40
3.3	Rain attenuation in dB/km across frequency at various rainfall rates [21, 23].	41
3.4	Wireless channels modelling techniques [19]	43
3.5	Cluster-based channel model [24]	44
3.6	Break point distance [25]	48
3.7	Delay spread in UMa, measured from Victoria University, Footscray Campus	62
3.8	Impulse response. LHS Horn-to-horn reference through free space, RHS with a 22 cm thick brick wall. Measurement bandwidth 0-40 GHz, time resolution 0.025 ns [26]	65
3.9	Theoretical shadowing gain due to perfectly conducting cylinders at 2.4 GHz and 60 GHz [19]	66
3.10	BEL measurements with Tx on the ground and Rx on different levels of a building [27]	67
4.1	40 GHz Anritsu 37369 Network analyser measuring loss through builders 'sarking' (Courtesy of Inderjeet Singh, Maninder Jit Singh and Gaurav Jain - VU Course Work students, 2018)	72
4.2	Antenna Measurements over a 2 m test distance. (a) 25 dBi horn (b) 20 dBi horn (c) 10 dBi horn (nominal gains).	73
4.3	Automated equipment developed for receiving signals at 7° steps in az- imuth covering 0° to 360°; and 10° steps in elevation covering -20° to 40°[28].	74
4.4	Antenna position in AoA measurement hardware when covering -20° to 40°.	75

4.5	CW transmissions. (a) LHS Two signal generators, for Horizontal and Vertical polarisation (HP8360 and Agilent N5230A). Example frequencies: 39.499 GHz and 39.501 GHz (b) RHS Receiver with 2 LNAs (Miteq JS426004000-30-10P) feeding spectrum analyser (R& S FSIQ40).	77
4.6	Wideband Tx (top) and Rx (bottom) hardware [28].	79
4.7	Software Signal Processing Flow for Tx (top) and Rx (bottom) [28]. . .	80
4.8	Result from a 2 m test range with large horns (2 x 24 dBi) and 30 dB attenuation added to the Tx signal path. TL (Top Left) – Raw received signal; TR – Channel Estimate (after filtering, frequency domain decimation by 4 and modulation removal); BL – Debug output; BR – Channel Impulse Response with threshold level (red line) and zoomed response.	81
4.9	Rx spectrum with Transmitter disabled. Noise floor, showing DC leak and an unwanted spur from the USRP receiver.	81

List of Tables

1.1	5G frequency bands 2 (FR2)	19
3.1	Summary of LOS Path loss models [29]	48
3.2	Summary of NLOS Path loss models [29]	49
3.3	Material penetration loss at 28 GHz [26].	66
4.1	Power Density Limits [30] and peak Tx power for 20 dBi horn	71
4.2	Antenna gains	73

Abbreviations

2D	Two-dimensional
3D	Three-dimensional
3G	3rd Generation
4G	4th Generation
5G	5th Generation
3GPP	3rd Generation Partnership Project
AB	Alpha-Beta
AoA	Angle of Arrival
AoD	Angle of Departure
BEL	Building Entry Loss
BS	Base Station
BW	Bandwidth
CDF	Cumulative Distribution Function
CI	Close in free space reference
dB	Decibel
DG	Diversity Gain
GRF	Gain Reduction Factor
HPBW	Half-power Beamwidth
IEEE	Institute of Electronics and Electrical Engineers
IF	Intermediate Frequency
InH	Indoor Hotspot
ITU	International Telecommunication Union
K	Ricean K factor
LNA	Low Noise Amplifier

Abbreviations

LO	Local Oscillator
LOS	Line-of-Sight
LTE	Long Term Evolution
MEG	Mean effective gain the user equipment antenna
MIMO	Multiple-Input-Multiple-Output
MMSE	Minimum Mean Squared Error
mmWave	Millimetre Wave
MPC	Multipath Component
MS	Mobile Station
MU-MIMO	Multi-User Multiple-Input-Multiple-Output
NF	Noise Floor
NLOS	non Line-of-Sight
NYU	New York University
O2I	Outdoor to Indoor
OFDM	Orthogonal Frequency-Division Multiplexing
PA	Power Amplifier
PL	Path Loss
PLE	Path Loss Exponent
PG	Path Gain
RF	Radio Frequency
RMa	Rural Macro
RMS	Root Mean Square
Rx	Receiver
SNR	Signal-to-Noise Ratio
Tx	Transmitter
UE	User Equipment
UMa	Urban Macro
UMi	Urban Micro
UMTS	Universal Mobile Telecommunication System
WiFi	Wireless Fidelity
XPD	Cross polar discrimination

Symbols

a_i	power delay profile amplitude in dB
α	Path Loss Exponent
G_{BS}	Specified gain of the base station antenna
G_{UE}	Specified gain of the user equipment antenna
ΔG	Height Gain
h	Height
H	Angular arrival spectrum
PG_{peak}	Peak path gain
PG_{omni}	Omni path gain
P_t	Transmit power
P_r	Receive power
θ	elevation angle
ϕ	azimuth angle
τ	Delay spread
σ	standard deviation
σ_τ	RMS Delay spread

Chapter 1

Introduction

Cellular networks were originally designed for voice only, using analogue transmission channels. In 1990s, digital Second generation (2G) systems were emerged enabling new services such as text messaging and circuit switched data access. The low data rate services provided by 2G systems did not fulfil the need for mobile Internet access. This led to a demand for new Third generation (3G) standards in 2000s, which evolved to provide fast data services and more capacity for voice. As the demand for more data increased, 3G also couldn't handle the demand. LTE (Long Term Evolution), a Fourth-generation phase of mobile cellular system, developed in around 2010, is a wireless communication standard which provides high capacity and highest rate data service for mobile multimedia. Thus, each of the cellular standards has evolved around a set of key use cases:

- 1G- Voice services
- 2G- Improved voice and text messaging

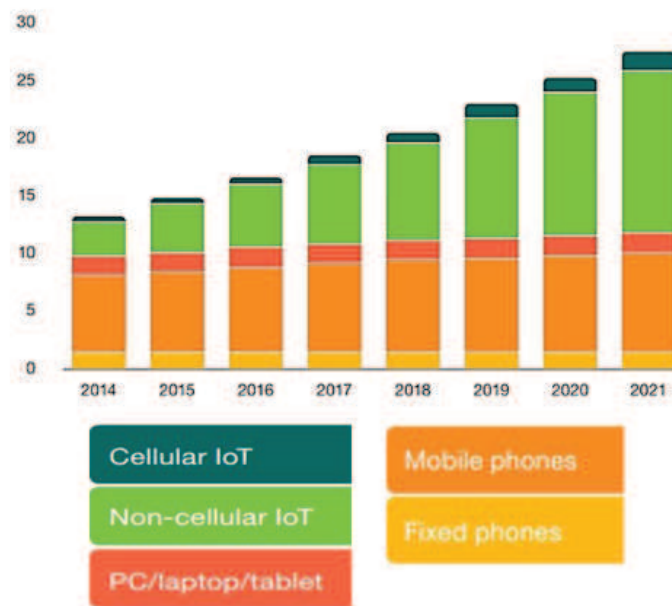


FIGURE 1.1: Growth in connected devices(billions) [9].

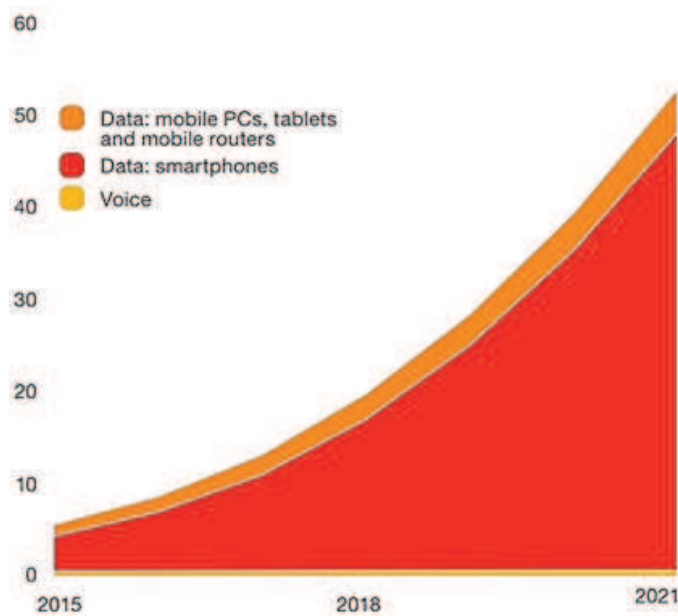


FIGURE 1.2: Global mobile traffic growth (monthly Exabytes) [9].

- 3G- Voice and mobile internet
- 4G- High capacity mobile multimedia

Fig. 1.1 shows the growth trend and prediction for the number of connected devices from 2014 to 2021. Much higher data rates than today's 4G systems are required due

to, e.g., high-quality video streaming and cloud computing [9]. As shown in Fig. 1.2, by 2021 the amount of mobile data traffic is predicted to be a decade more than in 2015 [9], [31]. The current 4G systems such as LTE and Mobile WiMAX utilize advanced innovations such as orthogonal frequency-division multiplexing (OFDM), spatial frequency reuse, cooperative multiple-input multiple-output (Co-MIMO) [32], multi-user diversity, relays and interference mitigation between base stations in order to achieve spectral efficiencies nearer to the theoretical limit in terms of bits per second per Hertz per cell [33, 34]. Thus, there is a constrained space for further improvement in spectral efficiency.

Fifth generation (5G) mobile systems is the upcoming technology which tends to overcome the limits of current systems and is based upon use cases such as huge number of devices with different needs, very high throughput, low latency and ultra reliability for mission critical applications [35]. Some of the features that 5G will incorporate are MIMO, beamforming, massive MIMO, hybrid beamforming and millimetre waves.

1.1 MIMO

Multiple-input multiple-output (MIMO) is a method for multiplying the capacity of a radio link using multiple transmission and receiving antennas to exploit multipath propagation. It generates a number of parallel data streams to the user simultaneously over the same radio channel, thus increasing the data rate. It also helps to get rid of fading by providing spatial diversity. Fig. 1.3 shows an example of 2x2 MIMO.

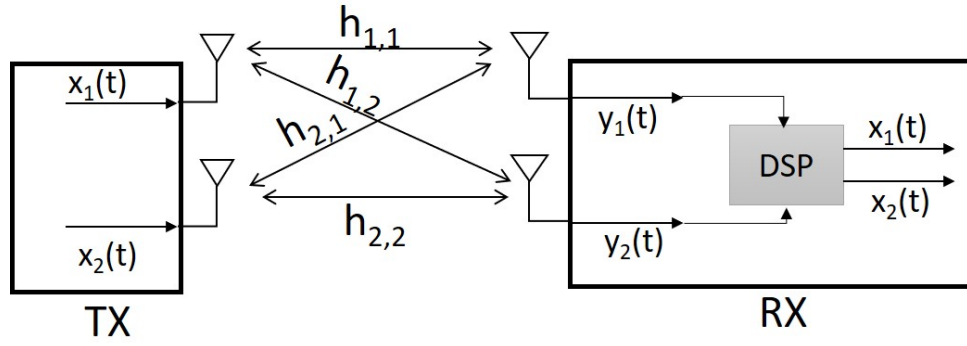


FIGURE 1.3: A 2x2 MIMO [10].

A MIMO radio system with N_t transmit antennas and N_r receive antennas can be described as:

$$\mathbf{H} = \begin{bmatrix} h_{1,1} & h_{1,2} & \dots & h_{1,N_t} \\ h_{2,1} & h_{2,2} & \dots & h_{2,N_t} \\ \cdot & \cdot & \cdot & \cdot \\ h_{N_r,1} & h_{N_r,2} & \dots & h_{N_r,N_t} \end{bmatrix}$$

where, \mathbf{H} is the channel information matrix, $h_{m,n}$ is the impulse response between the n th transmitting and m th receiving antenna. The input-output relation of the MIMO channel can be represented as [36, 37]

$$y = \mathbf{H} \otimes x + n \quad (1.1)$$

where \otimes denotes the convolution operator, y is the received signal vector and x is the transmitted signal vector. For a narrowband (i.e. frequency flat) MIMO link, this

relation can be written as

$$\begin{aligned}y &= \mathbf{H}x + n \\ \Rightarrow x &= \mathbf{H}^{-1}y\end{aligned}\tag{1.2}$$

To recover the transmitted data (original data) from the received data we need to take inverse of the channel information matrix. Unfortunately not all matrices are invertible.

To workaround these problems, we change the channel information matrix into three matrices by the method called Singular Value Decomposition (SVD). According to SVD theory, there exists orthogonal matrices $U = [u_1, \dots, u_m]$, $V = [v_1, \dots, v_n]$ and Σ such that

$$\mathbf{H} = U \Sigma V^*\tag{1.3}$$

$$\Rightarrow U^* \mathbf{H} V = \Sigma\tag{1.4}$$

and $U^*U = I$ and $V^*V = VV^* = I$; I =identity matrix

where

$$\Sigma = \begin{bmatrix} \sigma_1 & 0 & \dots & 0 \\ 0 & \sigma_2 & \dots & 0 \\ \cdot & \cdot & \cdot & \cdot \\ 0 & 0 & \dots & \sigma_k \end{bmatrix}$$

σ is a diagonal matrix of singular values. These values represent the power gain of each parallel data stream.

Substituting the SVD of \mathbf{H} in 1.2 gives

$$y = U \sum V^* x + n \quad (1.5)$$

At the receiver, multiply by U^*

$$U^* y = U^* (U \sum V^* x + n) \quad (1.6)$$

$$\Rightarrow \tilde{y} = \sum V^* x + \tilde{n} \quad (1.7)$$

At the transmitter, perform $x = V\tilde{x}$ where $V\tilde{x}$ is the precoding of the transmitted symbols. Then,

$$\tilde{y} = \sum V^* V\tilde{x} + \tilde{n} \quad (1.8)$$

$$\Rightarrow \tilde{y} = \sum \tilde{x} + \tilde{n} \quad (1.9)$$

Now the channel information matrix is a simple ‘diagonal matrix’ which can be used to decode the transmitted symbol.

The general MIMO channel capacity for AWG Rayleigh fading channel, assuming channel state information (CSI) is known at receiver, but not at transmitter, is given by

$$C = \log_2 \left(\det \left(I_m + \frac{E_{tot}/n}{N_0} HH^* \right) \right) \quad (1.10)$$

$$= \sum_{i=1}^{\min(m,n,p)} \log_2 \left(1 + \frac{E_{tot}/n}{N_0} \sigma_i^2 \right) \quad (1.11)$$

where H = $m \times n$ channel matrix

I_m = m -dimensional identity matrix

E_{tot} =total transmitted power

N_0 =noise power

σ_i^2 =eigen value of HH^*

The number of usable (strong) data streams, k is:

$$k = \min(n, m, p) \quad (1.12)$$

which is the minimum of the number of Tx antennas, the number of Rx antennas and the number of resolvable paths (p). The latter is a function of the channel and the antenna system. For a narrowband system (such as a single OFDM sub-carrier) this is related to the angle of arrival (AoA) profile of the incoming waves and the resolving capability of the antenna system. If the number of resolvable paths are limited this can result in capacity loss [38, 39]. High resolution antenna arrays require a wider aperture to separate out closely spaced incoming rays, which has cost implications. Therefore, knowing the angular distribution of the received signal is an important parameter for a propagation measurement campaign. Chapter 8 discusses this in more detail.

1.2 Beamforming

Beamforming is a signal processing technique by which an array of antennas can be steered to transmit radio signals in a specific direction. Beamforming allows the steering of beam and allows the energy to be concentrated in the users' environment only rather than broadcast across the whole cell. The steering of the beam is enabled by changing the phase shift along the antenna array. Beamforming has several advantages as follows:

- It increases the throughput capacity of a cellular tower by focusing the beam in the desired direction and cell edge users can experience reasonable data rates because of improved SNR.
- It reduces interference among users by minimising signal spillover in unwanted directions..
- It enables spatial multiplexing by the use of multiple independently directed beams.
- It increases the frequency reuse if there is beam co-ordination between adjacent base stations.

For a linear array of N-elements (Fig. 1.4) with $d = \lambda/2$ spacing, the array factor power gain for an N-element linear array is given as [40]

$$AF = \frac{1}{N} \left\{ \sum_{n=0}^{N-1} w_n * e^{j(nkdsin\phi - n\psi)} \right\}^2 \quad (1.13)$$

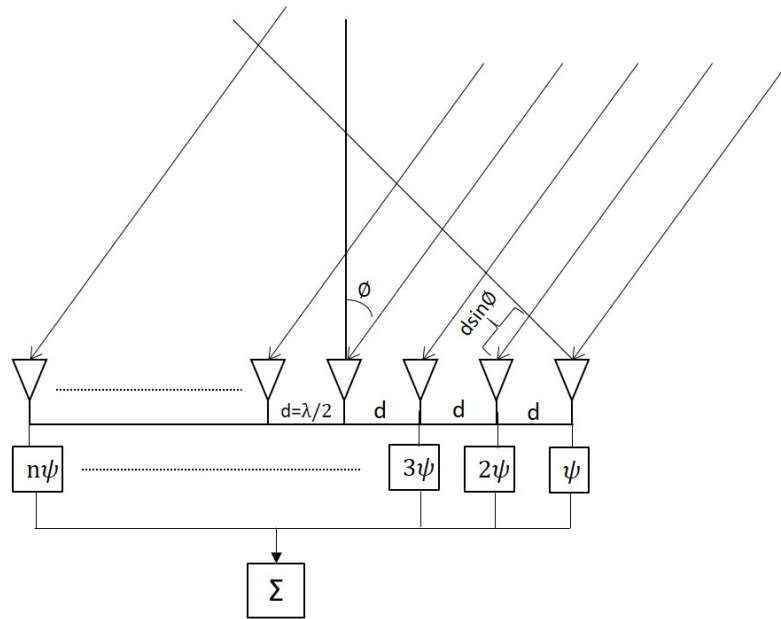


FIGURE 1.4: Far-field geometry of n-element array of antennas.

where, $k = 2\pi/\lambda$ and w_n is a weighting factor given to each element to control side lobes. The phase array look angle is ϕ and $n\psi$ is the electrical phase shift on the n 'th element of the phase array that beam steers the phase array to the desired direction.

Now the total gain of the array antenna is given as: $Gain_{total} = AF \times \text{antenna gain}$

Fig. 1.5 shows a phase array beamforming to two users; spatially separated users operating at the same frequency and at the same time .

Beamforming is very effective in open line-of-sight (LOS) conditions or predominantly open LOS conditions such as from high macro sites. In NLOS situations from UMi sites, the beams must point to the dominant interacting objects, which often scatter the signal in all directions. Propagation data is required to identify just how many users can be multiplexed under such conditions. Chapter 8 describes double directional UMi measurements from which the spatial multiplexing gain can be characterised.

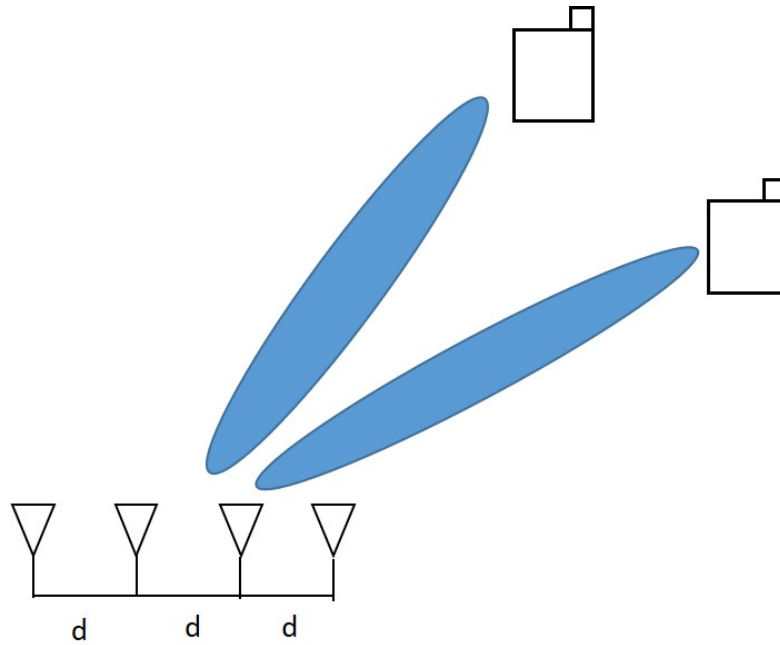


FIGURE 1.5: Phase array antenna beamforming to two users.

1.3 Massive MIMO and Hybrid Beamforming

The ever increasing demand of wireless communication system depends heavily on spectral efficiency (SE). Multiple-input multiple-output (MIMO) technology, the use of multiple antennas at transmitter (Tx) and receiver (Rx), is considered as one of the promising way to improve SE [12, 41]. SE can be improved from MIMO by two ways: 1) multiple user equipments (UEs) can communicate to a base-station (BS) on the same time-frequency-space resources and 2) a BS can send multiple data streams to each UE [12]. The original MIMO concept developed into the multi-user MIMO (MU-MIMO) of 4G from which massive MIMO evolved.

Massive MIMO requires the number of antenna elements to be much greater than the number of data streams. The number of antenna elements at the BS can reach hundreds or thousands multiplying the capacity of a wireless connection many times without requiring more spectrum. Massive MIMO can help in the reduction of small-scale fading

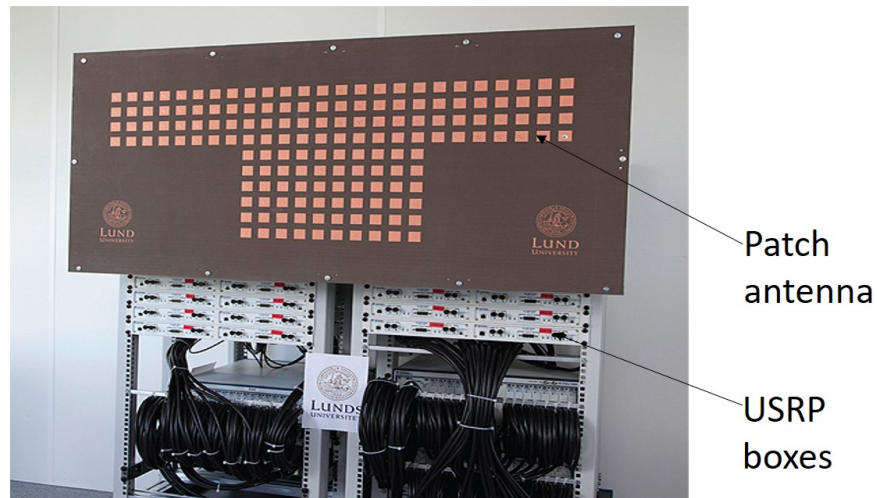


FIGURE 1.6: Massive MIMO prototype (Lund university at 2.6 GHz) [11].

(also known as channel hardening), accommodate multiple users per channel and improve the performance in terms of link reliability, spectral efficiency and transmit energy efficiency [42–44]. Fig. 1.6 shows a prototype of massive MIMO developed by Lund University in Sweden.

In mmWave massive MIMO systems, the beamforming improves Effective Isotropic Radiated Power (EIRP) and receiver gain array to compensate for the additional path loss created by the increased frequency and the increase transmission bandwidth. Three different types of beamforming techniques can be applied:

- **Analog Beamforming:** In this type, precoding is applied to the Intermediate frequency (IF)/ Radio Frequency (RF) analog signal after up conversion. There is a gain and phase adjuster for each antenna. The drawback of this beamforming is the difficulty in generating more than one signal beam.
- **Digital Beamforming:** In this type, precoding is applied to digital signal or base-band signal before Digital to Analog conversion (DAC). After the DAC and RF up conversion, the signal is transmitted over the air. This requires one distinct radio

frequency (RF) chain per antenna [43, 45, 46]. The generation of multiple beams is the key advantage. The drawback is the high power consumption and the high cost of mixed-signal and RF chains (analog-to-digital converters (ADC)/digital-to-analog converters (DAC), data converters, mixers, local oscillators) [47].

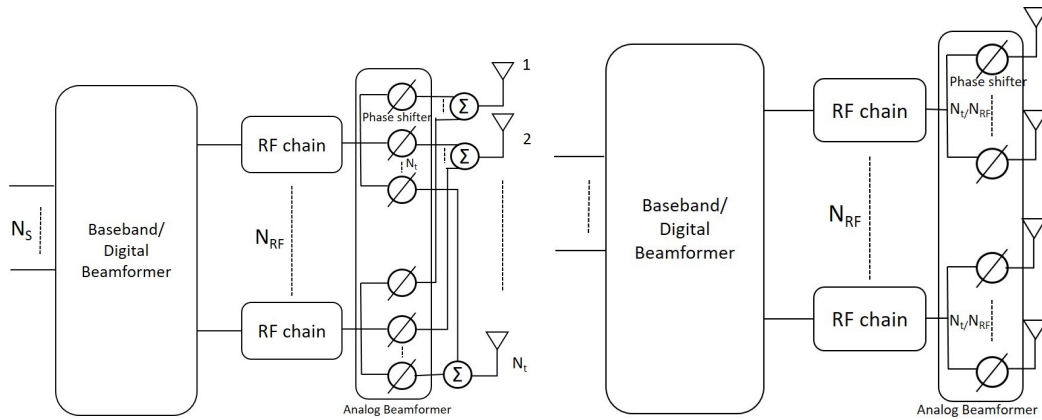


FIGURE 1.7: Major types of hybrid beamforming: (a) Fully-connected hybrid beamforming, (b) Sub-connected hybrid beamforming [12].

- **Hybrid Beamforming:** In this type, there is a balance between digital and analog beamforming, operating in the baseband and analog domains. It combines the benefits of both analog and digital beamforming. Here precoding is applied in both the analog domain and the digital domain at radio frequencies (RF) and baseband frequencies respectively. Thus hybrid beamforming techniques reduce the number of RF chains by combining each chain with an analog beamformer. Hybrid beamforming methods are designed to jointly optimize the analog and digital beamformers to maximize the achievable rate. Unlike the conventional microwave architecture, the hybrid beamforming architecture seems to be more applicable to mmWave, since the beamforming is performed in the analog domain, and multiple sets of beamformers can be connected to a reduced number of ADCs or DACs [12, 48].

The hybrid beamforming architectures are broadly divided into two types: 1) Fully connected, in which each RF chain is connected to all antennas via analog gain and phase adjusters and summers (Fig. 1.7(a)). 2) Sub-connected or partially connected, in which each RF chain is connected to its own subset of antenna elements as shown in Fig. 1.7(b) [12].

1.4 Millimetre waves

As the mobile data demand is continuously increasing, the sub 6 GHz spectrum is continuously becoming more congested. On the other hand, a vast amount of spectrum in the higher frequency range 30—300 GHz range remains underused. The frequency range from 300 MHz to 30 GHz is generally termed as microwaves and the frequency range from 30 GHz to 300 GHz is termed as the millimetre wave (mmWave) bands with wavelengths from 10 mm to 1 mm. Fig. 1.8 shows the presently used frequency bands and the millimetre frequency bands that can be used for future mobile systems.

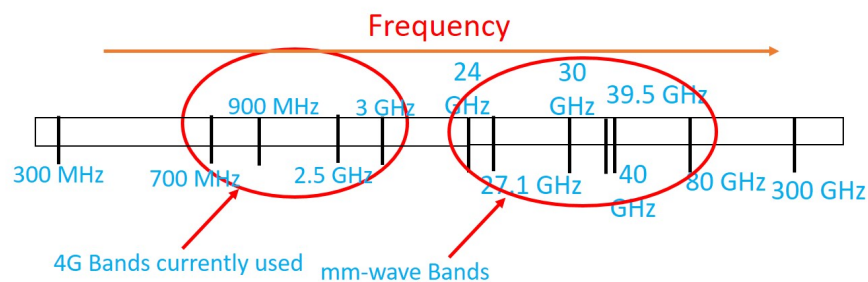


FIGURE 1.8: Frequency bands for cellular communication

The propagation properties of mm-wave frequencies are widely different from those

of sub-GHz frequency bands. These bands possess several challenges in terms of coverage area limitations, signal attenuation, path and penetration losses, as well as scattering. For example, path loss increases 20 dB per decade of frequency. Additionally, mmWave signals are susceptible to blockage from buildings and other structures, particularly in higher-density urban areas. So, in order to facilitate the development of mmWave systems, the propagation characteristics of mmWave wireless channels need to be characterized, modelled and evaluated, which requires a lot of research. A good channel estimation with a single antenna system is difficult to achieve because of higher path loss and too low a signal to noise ratio (SNR). Therefore, antennas must be grouped into arrays forming a beam with high gain. Thus, channel estimation is now between the beams rather than the individual antennas.

To use the new frequency bands, standardization bodies such as Third Generation Partnership Project (3GPP) and International Telecommunication Union (ITU) develop standards which then will be applied across the world.

1.5 Standardisation bodies

1.5.1 3GPP



FIGURE 1.9: Regional Standard Setting Organizations (SSOs) [13].

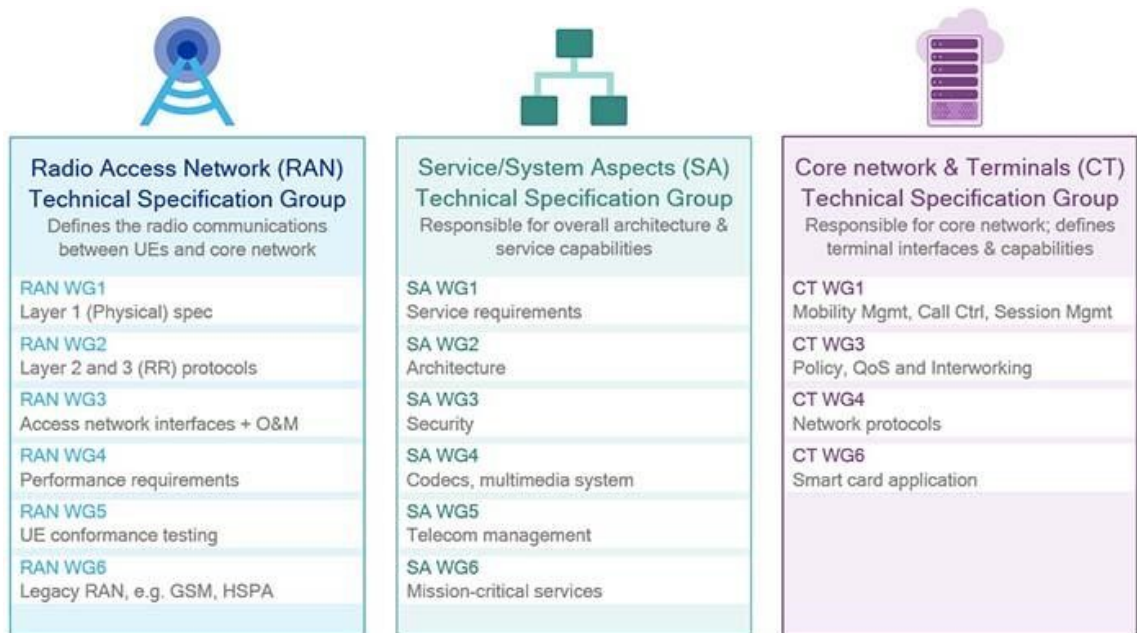


FIGURE 1.10: 3GPP distributed organization structure [13].

The 3GPP (3rd Generation Partnership Project) was established in December 1998 and is a collective of seven global telecommunications standards organizations. This collaboration has worked to create and organize the standards for a number of mobile communication systems including 2G, 3G, HSPA and LTE. It develops technical specifications. These technical specifications are then translated into standards by the seven regional Standards Setting Organizations (SSOs) that form the 3GPP partnership (Fig. 1.9). The regional SSOs are also responsible for establishing and enforcing an Intellectual Property Rights (IPR) policy.

3GPP specifications and studies are contribution-driven, by member companies, in Working Groups (WG) under the Technical Specification Group (TSG) level. The three Technical Specification Groups (TSG) in 3GPP are:

- Radio Access Networks (RAN)
- Services and Systems Aspects (SA)

- Core Network and Terminals (CT)

Under three TSGs, 3GPP is organized into 16 specialized Working Groups (WGs) as seen in Fig. 1.10. Among these 16 WGs, RAN WG1 is responsible for channel model standardization and the focus of this work.

Defining channel models for the key use cases (Rural Macro (RMa), Urban Macro (UMa), Urban Micro (UMi), Indoor Hotspot (InH)) is the first technical task of the standardisation process. Models are required for understanding the behaviour of the mmWave channels and comparing the performance of different candidate systems suggested by competing organisations. In this way the best performing system is selected. For 5G, the models had to be defined by June 2016. Providing input to 3GPP by this date was the first goal of this research. Another goal was to obtain mmWave propagation knowledge under Australian conditions and provide inputs to other standardization bodies such as ITU, which had suggested a number of potential frequency bands between 24 GHz and 40 GHz. Thus, this thesis focuses on the characterization of the millimetre wave (mmWave) propagation channel, especially at 24, 27.1 and 39.5 GHz in different use case scenarios.

1.5.2 ITU

The International Telecommunication Union (ITU), formed in 1865, in Paris, is responsible for coordinating the use of the shared global radio spectrum, promoting in assigning satellite orbits through international cooperation, improving telecommunication infrastructure in the developing world and assisting in the development and coordination

of worldwide technical standards [49].

The ITU is active in areas of broadband Internet, latest-generation wireless technologies, aeronautical and maritime navigation, radio astronomy, satellite-based meteorology, convergence in fixed-mobile phone, Internet access, data, voice, TV broadcasting and next-generation networks [49].

ITU is divided into three structures as shown in Fig. 1.11.

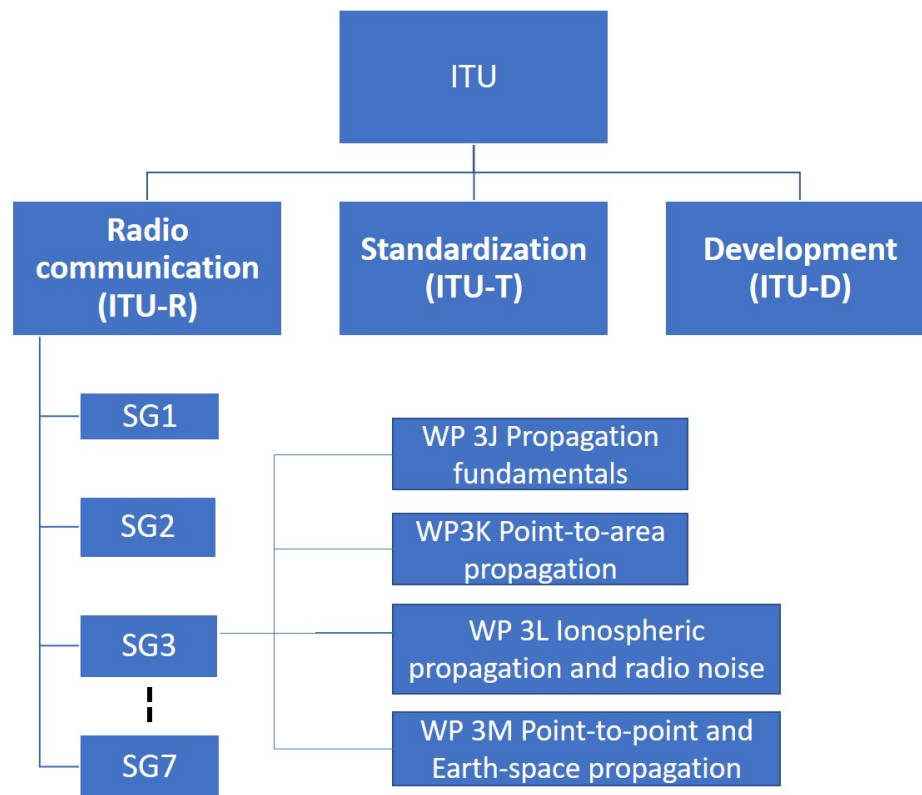


FIGURE 1.11: ITU structure.

1.5.2.1 Development (ITU-D)

ITU-D, established in 1992, helps spread equitable, sustainable and affordable access to information and communication technologies (ICT) [49].

1.5.2.2 Standardization (ITU-T)

ITU-T was firstly established in 1956 as the International Telephone and Telegraph Consultative Committee (CCITT) before becoming ITU-T in 1993. This sector standardizes global telecommunications, except for radio [49].

1.5.2.3 Radio communication (ITU-R)

ITU-R was established as the International Radio Consultative Committee (CCIR) in 1927 and in 1992 it became ITU-R. This sector manages the international radio-frequency spectrum and satellite orbit resources. The ITU-R consists of 7 Study Groups (SGs) which develop the technical bases for decisions taken at World Radiocommunication Conferences (WRC) and develop global standards (Recommendations), reports and handbooks on radiocommunication matters. Among these SGs, SG 3 is responsible for propagation of radio waves in ionized and non-ionized media and the characteristics of radio noise for the purpose of improving radiocommunication systems. SG 3 consists of four Working Parties (WP) which draft the Recommendations in the ITU-R P Series such as [7, 50–52]. Our interest is on WP 3K Point-to-area propagation.

The World Radio Conference in 2015 (WRC-15) approved a number of candidate frequency bands for 5G for further study (24.25-27.5 GHz, 31.8-33.4 GHz, 37-43.5 GHz, 45.5-50.2 GHz, 50.4-52.6 GHz, 66- 76 GHz, and 81- 86 GHz) and final decision in final meeting in 2019 (WRC-19). The study was required because some of these frequencies are shared with other services (notably satellite and radar services). A key requirement was therefore to perform co-existence studies involving the measurement

of interference signals leaking from one system into another. For example, mobile to satellite and vice-versa. The National Broadband Network (NBN) Satellite is one such example of great interest to Australia. Measurements are required for outdoor to satellite co-existence and indoor to satellite co-existence. Some results pertaining to the latter are presented in Chapter 9.

After WRC-19, the following bands were approved for 5G operation as listed in Table 1.1.

TABLE 1.1: 5G frequency bands 2 (FR2)

Band	Frequency	Bandwidth (MHz)
n257	26.50 – 29.50	50, 100, 200, 400
n258	24.25 – 27.50	50, 100, 200, 400
n260	37.00 – 40.00	50, 100, 200, 400
n261	27.50 – 28.35	50, 100, 200, 400

1.6 Research Objectives

The research objectives are:

- Broader aims
 - To contribute to 3GPP and ITU channel models for standardisation purposes.
 - To understand the behaviour of the mmWave channel between 24 GHz and 40 GHz in the Australian context to better predict the capacity cost trade-off of deploying a 5G network at these frequencies.

- Specific aim
 - To measure and characterize the mmWave wireless channel by calculating path loss, angle of arrival, angle of departure, height gain, diversity gain, side scatter, cross polar discrimination and effective antenna gain in key 3GPP scenarios; Rural Macro (RMa), Urban Macro (UMa), Urban Micro (UMi), Outdoor to Indoor (O2I), Indoor (InH) Atrium and Indoor Office.

1.7 Research Contributions

The research has led to the following contributions to standard bodies and papers:

1. We presented the world's first Rural measurements at mmWave frequency for mobile rural applications and submitted as a 3GPP contribution via Telstra and Ericsson who sponsored the work. This included path loss, tree loss results. This contribution was accepted and led to the extension of the previous 3GPP rural macro (RMa) non line-of-sight (NLOS) model [53] from 7 GHz (previously) to 30 GHz (now) (Chapter 5) [1].
2. We contributed two documents to ITU; in-building entry loss and clutter loss, presented via Telstra since Universities are generally not members of 3GPP and ITU standardization bodies. Outdoor to indoor (O2I) measurements for different slant angles in a traditional building (low thermal insulation) were presented. We also

presented clutter loss from buildings, foliage and other scatter objects (cars, humans) in sub-urban environment. These new input documents [7, 8] contributed to the standard [54].

3. The standard on building entry loss (BEL) [54] only applied to omnidirectional antennas and left directional antennas to future work. To address this issue, we used our slant-path O2I measurements to study the effect of antenna beamwidth on a desired signal (e.g., from a HAP) and on an unwanted signal (e.g., co-existence with satellite uplink channels). We showed that narrow beamwidth, high gain antennas have better performance in both cases. We introduced a new term combined building entry loss (CBEL) which included the effect of antenna gain in building entry loss [2]. We showed narrow beamwidth high gain antennas have better performance than omnidirectional antennas in both cases. Results were also presented in IEEE Access journal (Chapter 7) [2]. We show that a directional antenna cannot utilize its full specified gain in NLOS multipath environments (Chapter 10) [55].
4. We presented results from two different urban microcell (UMi) environments, Open Square (OS) and Street Canyon (SC). Our NLOS path loss extracted parameters closely aligned with those of the 3GPP NLOS standard [29] (Chapter 7), particularly for the close-in free-space reference distance model with path-loss exponents within 3%. We also showed that changes in BS antenna height of a few (~ 4) meters had little effect on the measured path loss in the OS scenario. We reported the scattering loss into SC side streets at 18 dB for “just around the corner” rising to 31 dB ~ 100 m down the side street. Narrower streets have

higher losses. Cross polar discrimination (XPD) appeared to be uncorrelated with path loss in SC [3].

5. We presented a double-directional measurement campaign to find out the path loss, angle of arrival (AoA) and angle of departure (AoD) in an UMi NLOS Open Square (OS) environment. We showed that many angles of departure from the user equipment resulted in few angles of arrival at the base station (Chapter 8) [4]. This hampers MIMO performance by limiting the number of usable spatial streams.
6. We presented empirical results from NLOS suburban macro (UMa) scenario. Different path loss models such as Alpha-Beta (AB), the close-in free space reference distance (CI), AB-3GPP and CI-NYU (New York University) were compared. Results were analysed for both the strongest signal (“peak”) and summation of all signals from all directions (“omni”). With “omni” measurement, AB-3GPP outperforms CI-NYU in the more sub-urban setting while the CI-NYU prefers the more dense environments and also performs well when the coverage area includes zones with vastly different parameter sets, such as street widths and building heights (Chapter 6) [56].

1.8 Thesis Outline

This thesis is organised in eleven chapters. A brief description of each chapter is outlined below:

Chapter 1 provides history of mobile communication starting from the first generation (1G) to the fifth generation (5G). Some of the features that 5G will incorporate such as multiple-input multiple-output (MIMO), massive MIMO, beamforming and millimetre waves are presented. A brief description of standardization bodies, 3GPP and ITU are presented along with the key use cases they consider. The chapter concludes with the research objectives and key contributions of the work.

Chapter 2 reviews relevant background information on antennas, and propagation. Different types of antenna are presented such as patch, aperture, microstrip and array, along with some fundamental parameters such as radiation pattern, directivity, gain and half-power beamwidth in terms of propagation, large and small scale parameters identified. Equations for a free space path loss (FSPL), shadow fading (χ), angular spread and delay spread are presented.

Chapter 3 reviews the state of the art in the field of mmWave channel measurements. Wireless channel modeling approaches, propagation path loss models such as AB, CI and 3GPP models are discussed in brief. Channel characterization works from different authors are presented.

Chapter 4 describes the hardware used in our work for this thesis. Narrow band and wide band transmitter and receiver designs are presented. This includes the calibration of test equipment and the use of spectrum and network analysers. Calibration of three different horn antennas along with their radiation patterns are shown. We also showed the error analysis of our angle of arrival measurement receiver.

Chapter 5 describes the contribution submitted to the 3GPP standard for Rural Macro

(RMA) environment. Path loss values and the extracted parameters are compared against the old RMA model for frequencies below 7 GHz [53]. The results enabled the extension of [53] up to 30 GHz [29].

Chapter 6 describes the paper for Urban Macro (UMa) scenario. Different path loss models such as AB, CI, AB-3GPP and CI-NYU are compared for two different UMa measurement scenarios. The 3GPP model is more suited to measurement zones with a consistent parameter set (building height, street width etc) whereas the CI model is competitive when the measurement zone consists of regions with vastly different parameter sets.

Chapter 7 describes the paper for Urban Micro (UMi) scenario. Here, as well, we firstly compare different path loss models. Then we analysed cross-street path gain and cross polar discrimination (XPD) in UMi SC and height gain and diversity in UMi OS environments. We show that XPD does not change with path loss and there is no appreciable height gain effects in NLOS environments.

Chapter 8 describes the paper for reverse measurements in an Urban Micro (UMi) scenario. We briefly discuss the forward and reverse measurement set up. We show a few examples of polar plots at the receiver end in the forward campaign to find out the angle of arrivals (AoA) which later on became angle of departures (AoD) for the reverse campaign. For each angle of departure at the user terminal end, we showed the angle of arrival (AoA) at the base station. The AoAs at the base station were nearly same for most of the AoDs, implying a potential reduction in MIMO performance.

Chapter 9 describes the paper for slant path propagation in an outdoor to indoor

(O2I) scenario. These measurements evaluate signal penetration into buildings from elevated transceivers. Isotropic building entry loss (BEL) with depth inside the building for two different receiver antennas and for different slant angles (elevation angles) are presented. We model this as a linear dB variation with building depth. A comparison against the ITU standard is presented. The ITU standard is based on isotropic antennas and does not include the effect of directive (beamformed) antennas as used by mmWave transceivers. This paper is one of the first to address such a situation. The introduction of new term ‘combined building entry loss’ (CBEL) enabled the analysis of two cases; the desired signal case, where a good signal is desired at the indoor receiver from a high altitude platform (e.g. satellites, drones, balloons); and the co-existence case, where interference from the indoor mobile terminal into a satellite uplink channel should be limited. We show that both cases are improved with adaptive beamforming.

Chapter 10 describes a short paper on effective antenna gain based on our outdoor to indoor (O2I) measurements. A reduction in the specified gain of the antenna is presented.

Finally, conclusions are discussed in Chapter 11 along with some potential future works.

Chapter 2

Antenna and Propagation

Fundamentals

This chapter overviews some of the basics of antennas and propagation as applied to this thesis.

2.1 Antenna

An antenna is defined as “a usually metallic device for radiating or receiving radio waves”. The IEEE Standard defines antenna as “a means for radiating or receiving radio waves” [57]. In other words, the antenna is the transitional structure between free-space and a guiding device. The guiding device or transmission line may take the form of a coaxial line or a waveguide (hollow pipe) and it is used to transport electromagnetic energy from the transmitting source to the antenna or from the antenna to the receiver. Good references for antennas are [57, 58]. Some antenna types are discussed next.

2.1.1 Wire Antennas

They can be seen virtually everywhere-on automobiles, buildings, ships, aircraft, spacecraft and so on in various shapes such as straight wire, dipole, loop and helix. They are often based on the half wave dipole (Fig. 2.1) or quarter wave monopole [59]. These structures become difficult to fabricate at millimetre wavelengths and so other structures are preferred as described next.



FIGURE 2.1: A (folded) dipole antenna [14]

2.1.2 Aperture Antennas

They are usually in the shape of pyramidal horn, conical horn and rectangular waveguide. The horn has a hollow pipe of different cross sections, tapered to a larger opening and is mainly used as a feed element for large radio astronomy, satellite tracking and communication dishes [60]. The type, direction and amount of taper can have an effect on the overall performance of the element as a radiator. Generally speaking the larger the aperture area the higher the antenna gain and the narrower the antenna beamwidth (Fig. 2.2).



FIGURE 2.2: Horn antenna; an example of aperture antenna. The wave-guide to co-axial cable transition is on the left and the aperture in the right. Nominal gain ranges from 25 dBi (top) to 10 dBi (bottom).

2.1.2.1 Microstrip Antennas

A very thin metallic strip (patch) placed on a grounded substrate constitute microstrip antennas. The microstrip patch is designed so its pattern maximum is normal to the patch. Often they are also referred to as patch antennas. The radiating elements and the feed lines are usually photoetched on the dielectric substrate. Fig. 2.3 shows a microstrip patch antenna.

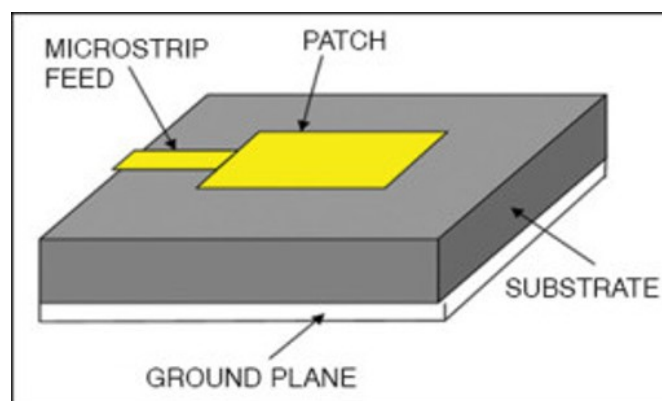


FIGURE 2.3: Patch antenna [15]

2.1.3 Array Antennas

A single element may not provide required radiation characteristics for many applications. In such situation, an aggregate of radiating elements in an electrical and geometrical arrangement (an array) should be used which will result in the desired radiation characteristics. The arrangement of the array may be such that the radiation from the elements combines up to provide a maximum radiation in a particular desired direction while minimum in others.

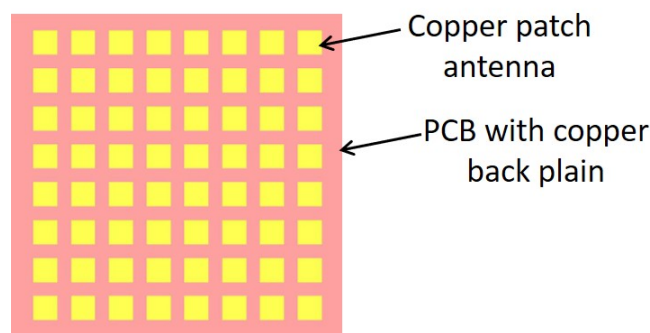


FIGURE 2.4: A layout of the 8x8 array of patches [16].

Patch antennas, horn antennas and array antennas are some of the options for mmWaves. Array antennas based on 8x8 patch element modules (Fig. 2.4) form the basis of early basestation designs [61]. Horn antennas are used in this thesis.

2.2 Fundamental Parameters of Antennas

Performance of an antenna can be defined by various parameters.

2.2.1 Radiation Pattern

An antenna radiation pattern or antenna pattern is defined as “a mathematical function or a graphical representation of the radiation properties of the antenna as a function of space coordinates” [62]. Generally, the radiation pattern is determined in the far-field region ($> 2D^2/\lambda$ where D is the maximum linear dimension of the antenna) and is represented as a function of the directional coordinates. Radiation properties include power flux density, radiation intensity, field strength, directivity phase or polarization.

2.2.1.1 Isotropic, Directional and Omnidirectional Patterns

An isotropic radiator is defined as “a hypothetical lossless antenna having equal radiation in all directions” [59, 63]. It is an ideal radiation pattern which is not physically realizable, but is taken as a reference for expressing the directive properties of actual antennas.

A directional antenna is the one “having the property of radiating or receiving electromagnetic waves more effectively in a particular direction than in others” [59, 63].

An omnidirectional antenna is the one “having non-directional pattern in a given plane and directional pattern in any orthogonal plane” [59, 63].

2.2.1.2 Radiation Pattern Lobes

A radiation pattern’s various parts are referred to as lobes, which can be classified into major, minor, side and back lobes (Fig. 2.5). A major lobe is defined as the radiation

lobe containing the direction of maximum radiation. A minor lobe is any lobe except a major lobe. A side lobe is a radiation lobe in any direction other than the intended lobe. A back lobe is a radiation lobe whose axis makes an angle of approximately 180° with respect to the major lobe. The level of minor lobes is usually expressed as a ratio of the power density in the lobe in question to that of the major lobe. This ratio is often termed the side lobe ratio [40].

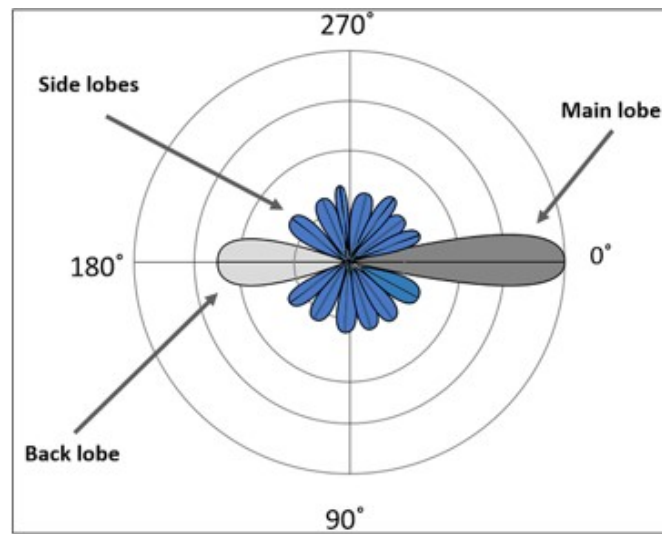


FIGURE 2.5: Radiation pattern of an antenna showing pattern lobes [17].

2.2.1.3 Radiation Intensity

Radiation intensity in a given direction is defined as the power radiated from an antenna per unit solid angle [40]. The radiation intensity is a far-field parameter and can be obtained by simply multiplying the radiation density by the square of the distance as

$$U = r^2 W_{rad} \quad (2.1)$$

where U = radiation intensity (W/unit solid angle) and W_{rad} = radiation density (W/m²)

2.2.2 Directivity

Directivity of an antenna is defined as the ratio of the radiation intensity (U) in a given direction from the antenna to the radiation intensity averaged over all directions (U_0).

U_0 is equal to the total power radiated (P_{rad}) by the antenna divided by 4π [40].

$$D = \frac{U}{U_0} = \frac{4\pi U}{P_{rad}} \quad (2.2)$$

where $U_0 = \frac{P_{rad}}{4\pi}$ and P_{rad} is the total radiated power (W).

2.2.3 Gain

Gain of an antenna is defined as the ratio of the intensity in a given direction to the isotropic radiation intensity. The radiation intensity corresponding to the isotropically radiated power is equal to the power accepted by the antenna divided by 4π , represented as [40]

$$Gain, G = 4\pi \frac{\text{radiation intensity}}{\text{total accepted power}} = 4\pi \frac{U(\theta, \phi)}{P_{in}} \quad (2.3)$$

2.2.4 Half-Power Beamwidth

The half-power beamwidth (HPBW) of an antenna is defined as the angle between the two directions in which the radiation intensity is half the maximum value of the main lobe i.e. 3 dB down from the peak of the main lobe (Fig. 2.6).

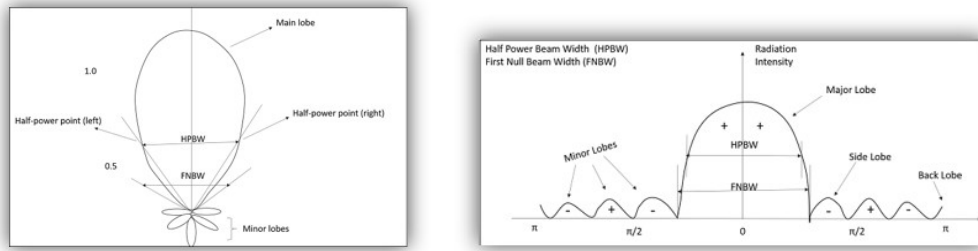


FIGURE 2.6: Radiation pattern of a directional antenna showing HPBW and First Null Beamwidth (FNBW) [18].

2.2.5 Synthesising Isotropic Measurements from Directional Radiation Patterns

Most standardised channel models (i.e from ITU and 3GPP) specify path loss as the loss between two 0 dBi antennas. To perform measurements at mmWave frequencies with isotropic antennas requires high transmit powers. Alternatively high gain narrow beam antennas can be used to scan all direction from which the maximum signal (called “peak” (P_{Peak})) and isotropic performance P_{Omni} can be synthesised [64]. The approach is to sample the received signal in both azimuth and elevation at angular steps of HPBW (yellow dots in Fig. 2.7) and sum the results. Removing the antenna gain from the summation gives the synthesised isotropic received signal, P_{Omni} .

$$P_{Peak} = \max(P(\theta, \phi)) \quad (2.4)$$

$$P_{Omni} = \sum \sum P(\theta_i, \phi_j) \cos(\theta_i)$$

Where azimuth $\phi_j = 0 : HPBW : 360$ and elevation $\theta_i = -20 : HPBW : 40$ and $P(\theta, \phi)$ is the received signal power seen by the measuring antenna pointing in the ϕ and θ direction. The cosine term compensates for reduced arc as the elevation angle

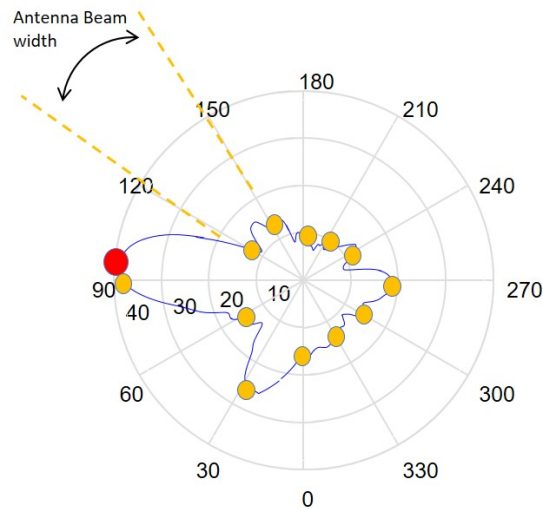


FIGURE 2.7: Radiation pattern of a directional antenna [5].

approaches $\pm 90^\circ$ (vertical) (see Chapter 10 for further details).

2.3 Radio Wave Propagation

2.3.1 Large and Small Scale Parameters

Rays travelling from transmitter (Tx) to receiver (Rx) constitute multipath components, whose temporal and angular characteristics can be derived from large-scale and small-scale parameters [65]. Small-scale parameters define the signal's properties in fine detail over a short distance, for example a single multipath component's path delay, angle of arrival (AOA) and angle of departures (AOD), while large-scale parameters define variations over longer distances usually of a statistical nature, such as the expected path loss (PL) root-mean-square (RMS) delay spread, angular spread, shadow fading (SF) and the Rician K-factor [66].

2.3.2 Free Space Path Loss

The path loss can be defined as the ratio of the transmit power to the received signal power as a function of the Tx-Rx separation distance. The free space path loss (FSPL) is the path loss for two isotropic antennas in free space separated by a distance d , and is given by [36]

$$\text{FSPL}(d) = \left(\frac{4\pi d}{\lambda}\right)^2 = \left(\frac{4\pi d f}{c_0}\right)^2 \quad (2.5)$$

Eq. 2.5 shows that FSPL is proportional to the square of the carrier frequency, i.e. $\text{FSPL} \propto f^2$, indicating an increased FSPL for mmWave systems. Fig. 2.8 shows the FSPL at 2.4, 24 and 39 GHz as a function of distance. Compared to the FSPL for a given distance at 2.4 GHz, the FSPL is about 20 dB larger for 24 GHz and 25 dB larger for 39 GHz. Antennas with higher gain or phased array antennas can be used to compensate the increased FSPL at mmWave frequencies. However, in a realistic multipath environment, the antennas might not be in free space and the signal will reach the Rx through several different paths. For these cases, the path loss is often modelled by a log-distance power law which in units of dB can be written as [19, 36]

$$PL(d) = PL(d_0) + 10n \log_{10}\left(\frac{d}{d_0}\right) + \chi_{\sigma} \quad (2.6)$$

where d is the distance, n is the path loss exponent, $PL(d_0)$ is the path loss at a reference distance of d_0 and χ_{σ} is a random variable that describes the large scale fading about the distance dependent mean path loss and can be modelled as a log-normal distribution

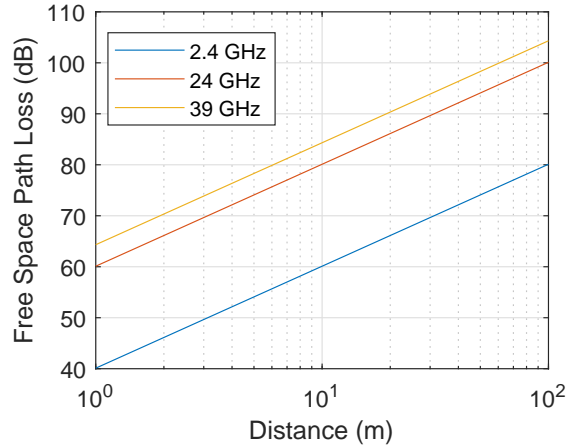


FIGURE 2.8: Free space path loss at 2.4, 24 and 39 GHz as a function of distance

which in the dB-domain corresponds to a zero-mean Gaussian distribution with standard deviation σ , i.e. $\chi_\sigma \sim N(0, \sigma^2)$. The reference value $PL(d_0)$ can be estimated based on measurement data, or based on reference measurements at this distance. For LOS scenario, it can be deterministically calculated based on the free space path loss as

$$PL(d_0) = 20 \log_{10} \left(\frac{4\pi d_0}{\lambda} \right) \quad (2.7)$$

2.3.3 Angular Spread

Angular spread is measured by the method of Fleury [67] as specified by the ITU channel model. The mean arrival angle $\bar{\theta}$ is obtained from:

$$\mu_\theta = \sqrt{\frac{\sum_i P(\theta_i) e^{j\theta_i}}{\sum_i P(\theta_i)}} \quad (2.8)$$

and

$$\bar{\theta} = \arg(\mu_\theta) \quad (2.9)$$

The RMS angular spread is:

$$\mu_{\theta} = \sqrt{\frac{\sum_i P(\theta_i) |e^{j\theta_i} - \mu_{\theta}|^2}{\sum_i P(\theta_i)}} \quad (2.10)$$

Where $P(\theta_i)$ is the received power at angle θ_i . The highest angular spread is $180/\pi$ and corresponds to a uniform power wrt angle (i.e. equal powers from all directions).

2.3.4 Delay Spread

The power delay profile (PDP) (a_i) gives the intensity of a signal received through a multipath channel as a function of time delay. The time delay is the difference in travel time between multipath arrivals. It is easily measured empirically and can be used to extract certain channel's parameters such as the delay spread.

The delay spread is a measure of the multipath richness of a communications channel. In general, it can be interpreted as the difference between the time of arrival of the earliest significant multipath component (typically the line-of-sight component) and the time of arrival of the latest multipath components. The delay spread is mostly used in the characterization of wireless channels. The mean delay spread is given as:

$$\bar{\tau} = \frac{\sum_i \tau_i a_i^2}{\sum_i a_i^2} \quad (2.11)$$

Thus RMS delay spread is calculated as:

$$\sigma_{\tau}^2 = \overline{\tau^2} - (\bar{\tau})^2 \quad (2.12)$$

Where

$$\overline{\tau^2} = \frac{\sum_i \tau_i^2 a_i^2}{\sum_i a_i^2} \quad (2.13)$$

2.4 Summary

In this chapter, a brief overview of different types of antennas along with antenna characteristics such as radiation patterns, directivity, gain, half-power beamwidth are presented. Also, some basics on radio wave propagation are detailed. These include some large scale parameters such as free space path loss (FSPL), shadow fading, angular spread and delay spread. In chapter 3, a detailed literature review related to the millimetre wave propagation channel is presented.

Chapter 3

Literature Review

In Chapter 2, we provided some basic information on antennas and propagation applicable to this thesis. In this chapter, various aspects related to the millimetre wave propagation channel are discussed. We start with the attenuation of mmWaves with frequency and rain and then show that mmWaves can be applied to cellular systems. Different channel modelling techniques related to mmWave systems are presented. Some well known propagation path loss channel models are discussed. Finally the state of the art from other researchers in the field is described.

An RF signal power attenuates in the environment when travelling from Tx to Rx due to numerous factors such as scattering, reflection, diffraction and fading. Path loss propagation models help in calculating the loss in the relevant frequency band. The difference between a radio channel and a propagation channel is shown in Fig 3.1 [19]. The radio channel includes the effects of the Tx and Rx antenna in the channel, whereas

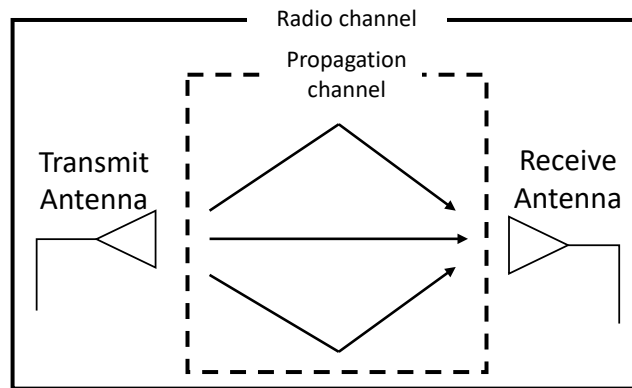


FIGURE 3.1: Radio channel and propagation channel [19].

the propagation channel only describes the effect of the channel without including antennas. Ideally, the propagation channel is the channel that the radio system would experience when using isotropic Tx and Rx antenna.

3.1 Frequency attenuation and rain attenuation in millimetre waves

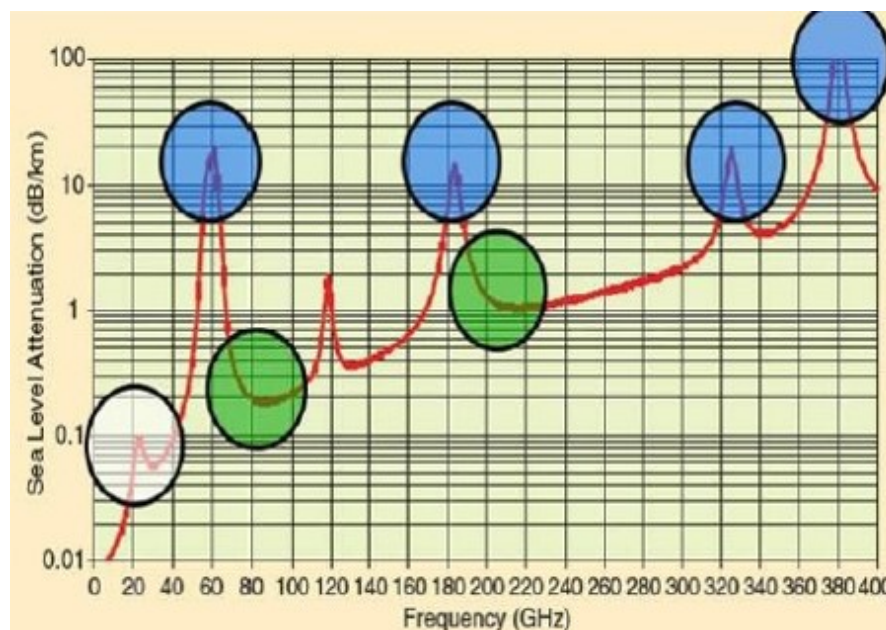


FIGURE 3.2: Atmospheric absorption across mmWave frequencies in dB/km [20–22].

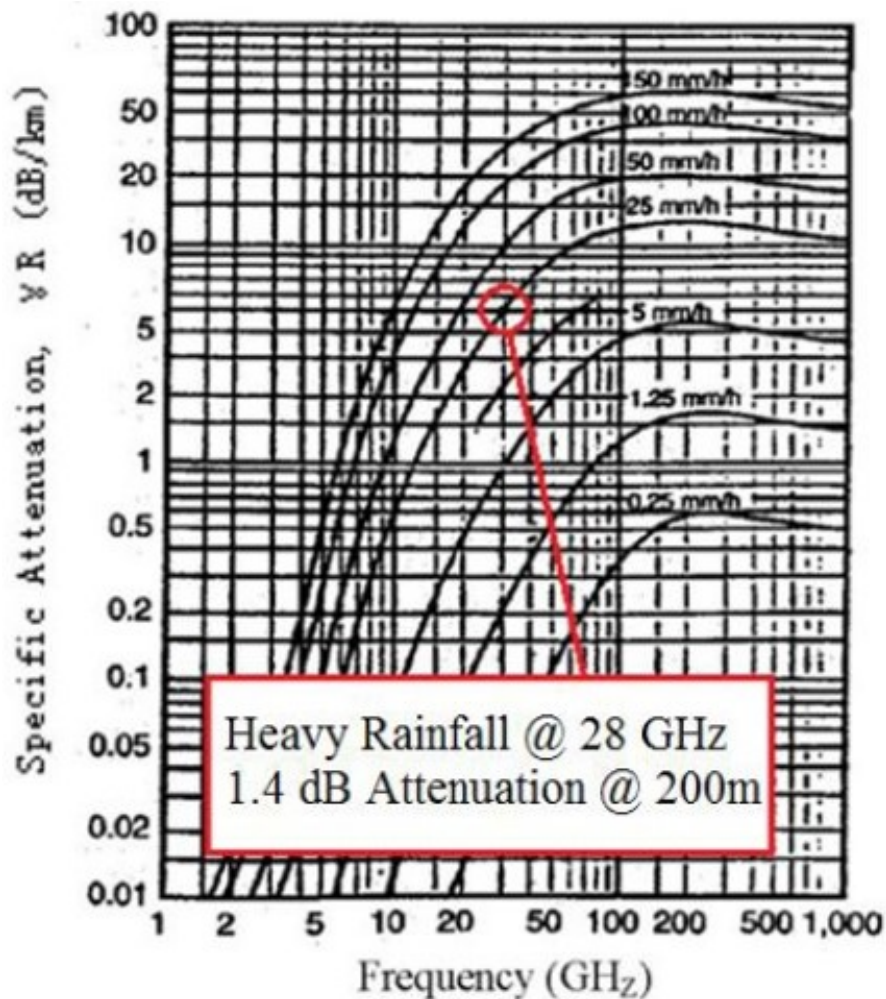


FIGURE 3.3: Rain attenuation in dB/km across frequency at various rainfall rates [21, 23].

A common misconception in the wireless engineering community is that rain and atmosphere make mmWave spectrum useless for mobile communications. However, being the cell sizes on the order of 200 m (particularly in the urban environments), mmWave in cellular systems can overcome these issues. Fig. 3.2 and Fig. 3.3 show the atmospheric absorption and rain attenuation characteristics of mmWave propagation. Atmospheric absorption does not create significant additional path loss for mmWaves for cell sizes on the order of 200 m, particularly at 28 GHz and 38 GHz where the loss is less than 0.02 dB. Even at a heavy rain rate of 7.6 mm/hour, the rain attenuation for a 200 m cell radius is only 0.6 dB at 28 GHz and 0.8 dB at 38 GHz. Only 7 dB/km of

attenuation is expected due to heavy rainfall rates of 1 inch (25 mm)/hour for cellular propagation at 28 GHz, which is only 1.4 dB at 28 GHz and 1.6 dB attenuation at 38 GHz per 200 m distance. Work by many researchers has confirmed that for small distances (less than 1 km), rain attenuation will present a minimal effect on the propagation of mmWaves at 28 GHz to 38 GHz [20, 23]. Frequencies from 70 to 100 GHz and 125 to 160 GHz have higher loss, but still manageable in a cellular environment.

3.2 Wireless Channel Modelling Approaches

A realistic wireless channel model is vital for the development of a reliable wireless system. Before any detailed design can be performed, accurate characterization and modelling of the propagation channel is required. A good wireless channel model can efficiently reproduce the typical behaviour of the wireless channel and give insights into the most relevant radio propagation mechanisms. These channel models are often implemented in channel simulators so that the performance of many different parts of the wireless system of interest can be evaluated and optimized.

Fig. 3.4 shows a classification of the most common types of channel modelling approaches [19]. The two main categories are deterministic and stochastic modelling approaches. The deterministic approach can be further sub-divided into field theory or electromagnetic wave theory using Maxwell's equations and ray tracing. Exact knowledge of the topology and material make up of the environment is required. Also measured data can be used directly in deterministic modelling approach.

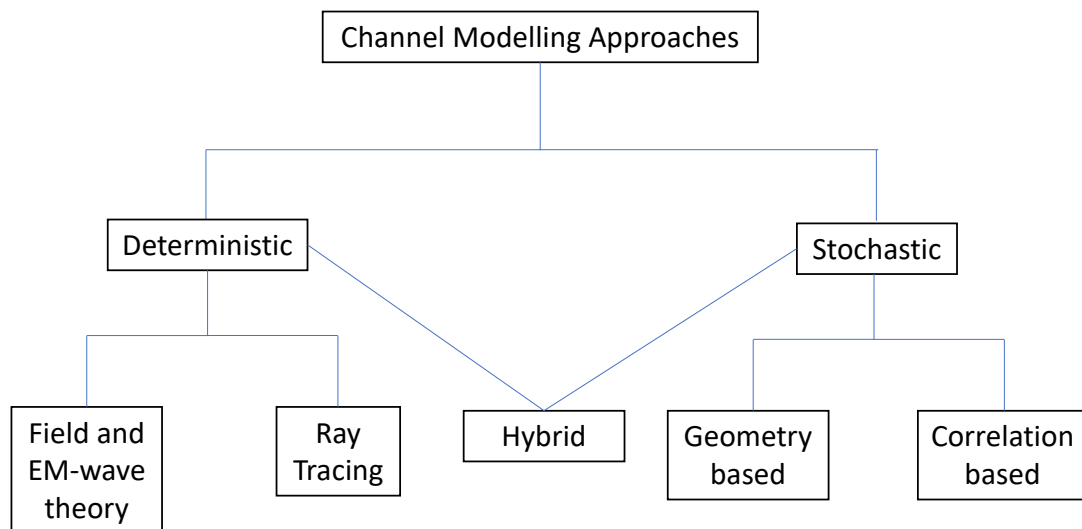


FIGURE 3.4: Wireless channels modelling techniques [19]

Stochastic approaches reproduce the statistical behaviour of the channel. Correlation methods model the correlation properties of the channel. This can be done using the full correlation matrix between all Tx and Rx elements for a given MIMO channel. However, using the full correlation matrix requires a large number of model parameters, which often makes it too complex. Instead, simplified models, such as Kronecker model [68, 69] are often used. The more sophisticated Weichselberger model [70] is another popular correlation based model.

The radio channel typically consists of several distinct multipath components (MPCs) departing from the Tx and arriving at the Rx with specific directions and delays due to reflections and diffractions from scattering objects in the surrounding environment [71]. The MPCs often tend to appear as clusters (Fig. 3.5), i.e. groups of closely located MPCs that have propagated along a similar path. Authors in [72] presented twin-clusters to represent multipath components in order to correctly reflect directions of arrival (DoA), directions of departure (DoD) and delays. To evaluate the performance

of wireless communication systems in this situation, geometry-based stochastic models (GBSMs) [73–77] are widely used. GBSMs can accurately reflect realistic channel properties and are suitable for the massive MIMO channel. GBSMs of massive MIMO can be classified into 2D and 3D channel models. When a linear array is employed at the base station and the tilt angle is fixed, the 2D channel model is enough for performance prediction. For spherical, cylindrical or rectangular antenna array configurations, the 3D model, covering both azimuth and elevation, is needed.

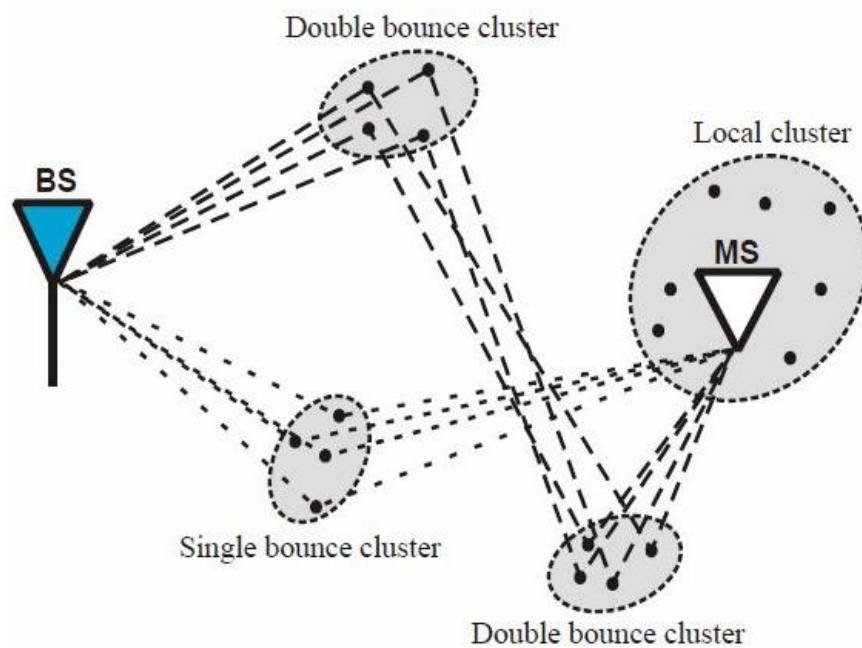


FIGURE 3.5: Cluster-based channel model [24]

Hybrid models combine deterministic with stochastic parts. For example, ray-tracing can determine the cluster positions while GSCM can stochastically model the MPCs within the cluster.

3.3 Propagation Path loss models

Millimetre wave (mmWave) channel modelling plays an important role in the design of future mobile systems. Many different groups around the world are contributing to the development of mmWave channel models. Three major organizations are involved in standardizing propagation models for mobile applications. They are the 3rd Generation Partnership Project (3GPP) [29, 78], the International Telecommunication Union (ITU) [79, 80] and the Institute of Electrical and Electronic Engineers (IEEE). Other organizations involved in the development of channel models often target specific frequency bands based on their target application. These include the European Cooperation in Science and Technology (COST 2100), the Mobile and Wireless Communications Enablers for the Twenty-Two Information Society (METIS) (valid up to 100 GHz) [81], the 5G mmWave Channel Model Alliance (0.5-100 GHz) [82], IEEE 802.11 ad/ay and IEEE 802.15.3e (for the 60 GHz band) [83, 84], IEEE 802.15.3d (for the 300 GHz band) [85], Millimetre Wave Evolution for Backhaul and Access (MiWEBA) (60 GHz band) [86], mmWave based Mobile Radio Access Network for 5G Integrated Communications (mmMAGIC) (6-100 GHz) [87]. Also there are universities and industry participants such as Fraunhofer HHI, which developed the Quasi Deterministic Radio channel Generator (QuaDRiGa) [88] and NYU WIRELESS (for 0.5-100 GHz) [89] and many more [90–93]. Due to the overlap between participants in the organisations, there is often a great deal of similarity in the models.

Often the statistical channel models proposed by these different groups can be narrowed down to two structures; the Alpha Beta (AB) and the close-in free space reference distance (CI) forms [94]. These are discussed next.

3.3.1 AB model

The Alpha Beta (AB) model was developed by WINNER II and predicts signal strength as a function of propagation distance. It gives the path loss using a model given by [95, 96]:

$$PL^{AB}(d) \text{ [dB]} = \beta + \alpha 10 \log_{10}(d) + \chi_{\sigma}^{AB} \quad (3.1)$$

where $PL^{AB}(d)$ denotes the path loss in decibels over frequency and distance, d . The path loss at unit distance, β , and the path loss exponent (PLE), α , are obtained by a least square fit over the measured distances. The shadow fading (SF) term, χ_{σ} , is a zero-mean Gaussian random variable with standard deviation σ in dB. The AB model parameters α , β , and σ are obtained from measured data using closed-form solutions that minimize the SF standard deviation, as shown below [97].

Let $B = PL^{AB}(d) \text{ [dB]}$, $D = 10 \log_{10}(d)$ in eq. 3.3.1. Then the SF is given by

$$\chi_{\sigma}^{AB} = B - \alpha D - \beta \quad (3.2)$$

Then, the SF standard deviation is

$$\sigma^{AB} = \sqrt{\frac{\sum \chi_{\sigma}^{AB^2}}{N}} = \sqrt{\frac{\sum (B - \alpha D - \beta)^2}{N}} \quad (3.3)$$

where N denotes the number of path loss data points.

Minimizing the fitting error is equivalent to minimizing $\sum(B-\alpha D-\beta)^2$, which means its partial derivatives with respect to α and β should be zero as:

$$\frac{\partial \sum(B-\alpha D-\beta)^2}{\partial \alpha} = 2\left(\alpha \sum D^2 + \beta \sum D - \sum DB\right) = 0 \quad (3.4)$$

$$\frac{\partial \sum(B-\alpha D-\beta)^2}{\partial \beta} = 2\left(\alpha \sum D + N\beta - \sum B\right) = 0 \quad (3.5)$$

Solving eq. 3.4 and 3.5, we obtain the closed form solutions for α and β as shown below:

$$\alpha = \frac{\sum B \sum D - N \sum DB}{(\sum D)^2 - N \sum D^2} \quad (3.6)$$

$$\beta = \frac{\sum D \sum DB - \sum B \sum D^2}{(\sum D)^2 - N \sum D^2} \quad (3.7)$$

Therefore, the minimum SF standard deviation for AB model can be obtained by substituting values of α and β in eq. 3.3.

The model was adopted by ITU [98] and 3GPP for a number of scenarios, each with a unique expressions for α and β parameters (Table 3.1 and Table 3.2). The path loss expressions depend upon a number of input parameters such as base station height (h_{BS}), user terminal height (h_{UT}), average street width (W), average building height (h), transmitter-receiver separation distance (d) and carrier frequency (f_c). For each scenario the model takes two forms, line of sight (LOS) and non line-of-sight (NLOS). For LOS

TABLE 3.1: Summary of LOS Path loss models [29]

Scenario	Models	Path Loss(dB) Note: f_c in GHz and d in meters	Shadow fading std (dB)	Applicability range, antenna height default values
RMa	3GPP	$20\log_{10}(40\pi d f_c/3)$ $+ \min(0.03h^{1.72}, 10)\log_{10}(d)$ $- \min(0.044h^{1.72}, 14.77)$ $+ 0.0002\log_{10}(h)d$	4	$10 \text{ m} < d < 5000 \text{ m}$ $5 \text{ m} < h < 50 \text{ m}$ $5 \text{ m} < W < 50 \text{ m}$ $10 \text{ m} < h_{BS} < 150 \text{ m}$ $1 \text{ m} < h_{UT} < 10 \text{ m}$
UMa	3GPP	$32.4 + 20 \log_{10}(d) + 20 \log_{10}(f_c)$	4	$h_{BS} = 25 \text{ m}$ $1.5 \text{ m} < h_{UT} < 22.5 \text{ m}$
UMi	3GPP	$32.4 + 21.9 \log_{10}(d) + 20 \log_{10}(f_c)$	4	$h_{BS} = 10 \text{ m}$ $1.5 \text{ m} < h_{UT} < 22.5 \text{ m}$
InH	3GPP	office: $32.4 + 17.3 \log_{10}(d) + 20 \log_{10}(f_c)$ mall: $32.4 + 17.3 \log_{10}(d) + 20 \log_{10}(f_c)$	3 2	$1 \text{ m} < d < 100 \text{ m}$ $1 \text{ m} < d < 150 \text{ m}$

the model is close to the path loss FRIIS formula of equation 3.9, because at mmWave frequencies the break-point distance is unlikely to be reached in today's cellular layouts (order of 10 kms) (Fig. 3.6) [25]. The expressions are shown in Table 3.1 for LOS and Table 3.2 for NLOS. It is much harder to predict NLOS performance and this shows up in the higher sigma values. This thesis concentrates on NLOS performance.

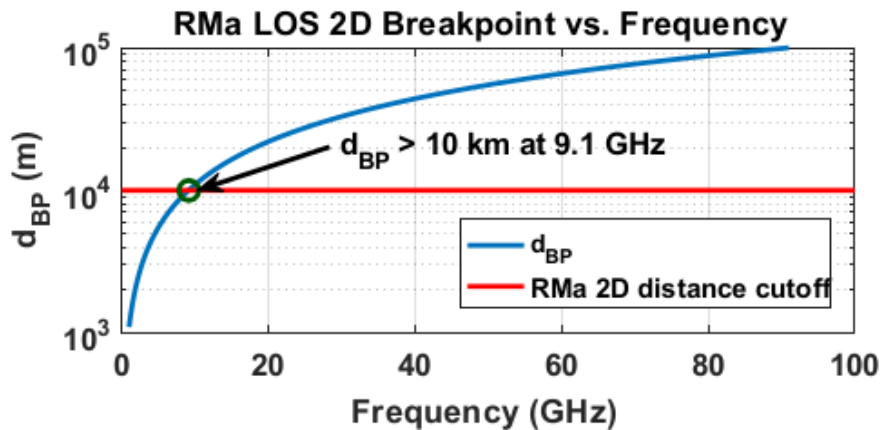


FIGURE 3.6: Break point distance [25]

TABLE 3.2: Summary of NLOS Path loss models [29]

Scenario	Models	Path Loss(dB) Note: f_c in GHz and d in meters	Shadow fading std (dB)	Applicability range, antenna height default values
RMa	3GPP	$161.04 - 7.1 \log_{10}(W) + 7.5 \log_{10}(h)$ $-(24.37 - 3.7 (h/h_{BS})^2) \log_{10}(h_{BS})$ $+ (43.42 - 3.1 \log_{10}(h_{BS})) (\log_{10}(d) - 3)$ $+ 20 \log_{10}(f_c) - (3.2 (\log_{10}(11.75h_{UT}))^2 - 4.97)$	8	$10 \text{ m} < d < 5000 \text{ m}$ $5 \text{ m} < h < 50 \text{ m}$ $5 \text{ m} < W < 50 \text{ m}$ $10 \text{ m} < h_{BS} < 150 \text{ m}$ $1 \text{ m} < h_{UT} < 10 \text{ m}$
UMa	3GPP	$161.04 - 7.1 \log_{10}(W) + 7.5 \log_{10}(h)$ $-(24.37 - 3.7 (h/h_{BS})^2) \log_{10}(h_{BS})$ $+ (43.42 - 3.1 \log_{10}(h_{BS})) (\log_{10}(d) - 3)$ $+ 20 \log_{10}(f_c) - (3.2 (\log_{10}(17.625))^2 - 4.97)$ $- 0.6 (h_{UT} - 1.5)$	6	$h_{BS} = 25 \text{ m}$ $1.5 \text{ m} < h_{UT} < 22.5 \text{ m}$
	CI	$32.4 + 30 \log_{10}(d) + 20 \log_{10}(f_c)$	7.8	-
UMi	3GPP	$35.3 \log_{10}(d) + 22.4 + 21.3 \log_{10}(f_c)$ $- 0.3(h_{UT} - 1.5)$	7.82	$h_{BS} = 10 \text{ m}$ $1.5 \text{ m} < h_{UT} < 22.5 \text{ m}$
	CI	$32.4 + 20 \log_{10}(f_c) + 31.9 \log_{10}(d)$	8.2	-
InH	3GPP	$38.3 \log_{10}(d) + 17.3 + 24.9 \log_{10}(f_c)$	8.03	$1 \text{ m} < d < 86 \text{ m}$
	CI	$32.4 + 20 \log_{10}(f_c) + 31.9 \log_{10}(d)$	8.29	-

3.3.2 CI path loss model

The close-in free space reference distance (CI) path loss model has only one input parameter to describe the propagation path loss over distance at a certain frequency. The general form of the CI path loss model is expressed as [97]

$$\text{PL}^{\text{CI}}(f_c, d)[\text{dB}] = \text{FSPL}(f_c, d_0)[\text{dB}] + 10\alpha \log_{10}\left(\frac{d}{d_0}\right) + \chi_{\sigma}^{\text{CI}}; \quad d \leq d_0 \quad (3.8)$$

where, f_c is the carrier frequency in GHz, d_0 is the close-in free space reference distance in meters, α represents the path loss exponent (PLE) and χ_σ^{CI} denotes the shadow fading with standard deviation σ in dB. The CI model inherently has an intrinsic frequency dependency of path loss already embedded within the FSPL term. 10α in equation (3.8) describes the path loss in decibels per decade of distance beginning at d_0 . The free space path loss (FSPL) in dB at a distance d_0 is given by equation (3.9).

$$\text{FSPL}(f_c, d_0)[\text{dB}] = 20\log_{10}\left(\frac{4\pi f_c d_0 \times 10^9}{c}\right) \quad (3.9)$$

where c is the speed of light. In normal use for mmWaves, the CI model fixes $d_0 = 1\text{m}$ leaving the PLE, α , as the only adjustable parameter [94, 97, 99]. Then equation (3.9) changes to:

$$\text{FSPL}(f_c, 1\text{m})[\text{dB}] = 20\log_{10}\left(\frac{4\pi f_c \times 10^9}{c}\right) \quad (3.10)$$

The PLE model parameter (α) in eq. 3.8 is obtained by first removing the FSPL given by (3.10) from the path loss on the left side of (3.8) for all measured data points as follows:

The expression for the CI model with a reference distance of 1 m is given by [97]:

$$\text{PL}^{CI}(f_c, d)[\text{dB}] = \text{FSPL}(f_c, 1\text{m})[\text{dB}] + 10\alpha\log_{10}(d) + \chi_\sigma^{CI} \quad (3.11)$$

Thus, the SF is

$$\begin{aligned}\chi_{\sigma}^{CI} &= \text{PL}^{CI}(f_c, d)[\text{dB}] - \text{FSPL}(f_c, 1\text{m}) - 10\alpha\log_{10}(d) \\ &= A - \alpha D\end{aligned}\tag{3.12}$$

where $A = \text{PL}^{CI}(f_c, d)[\text{dB}] - \text{FSPL}(f_c, 1\text{m})$ and $D = 10\log_{10}(d)$. Then the SF standard deviation is given as:

$$\sigma^{CI} = \sqrt{\frac{\sum \chi_{\sigma}^{CI^2}}{N}} = \sqrt{\frac{\sum (A - \alpha D)^2}{N}}\tag{3.13}$$

where N denotes the number of path loss data points. Thus, minimizing the SF standard deviation σ^{CI} is equivalent to minimizing the term $\sum (A - \alpha D)^2$. When $\sum (A - \alpha D)^2$ is minimized, its derivative with respect to α should be zero, i.e.,

$$\begin{aligned}\frac{d \sum (A - \alpha D)^2}{d\alpha} &= 0 \\ \Rightarrow \sum 2D(\alpha D - A) &= 0 \\ \Rightarrow n &= \frac{\sum DA}{\sum D^2}\end{aligned}\tag{3.14}$$

The CI model in (3.8) at a reference distance of $d_0 = 1\text{m}$ can be written in the 3GPP/ITU form as:

$$\begin{aligned}
\text{PL}^{\text{CI}}(f_c, d)[\text{dB}] &= \text{FSPL}(f_c, 1\text{m})[\text{dB}] + 10\alpha \log_{10}(d/1\text{m}) + \chi_{\sigma}^{\text{CI}} \\
&= 20 \log_{10} \left(\frac{4\pi f_c \times 10^9}{c} \right) + 10\alpha \log_{10}(d) \\
&= 20 \log_{10} \left(\frac{4\pi \times 10^9}{c} \right) + 20 \log_{10}(f_c) + 10\alpha \log_{10}(d) \\
&= 32.4 + 20 \log_{10}(f_c) + 10\alpha \log_{10}(d) \tag{3.15}
\end{aligned}$$

Therefore, equation (3.8) can be rewritten as:

$$\text{PL}^{\text{CI}}(f_c, d)[\text{dB}] = 32.4 + 10\alpha \log_{10}(d) + 20 \log_{10}(f_c) + \chi_{\sigma} \tag{3.16}$$

For the CI model, the value of PLE (n) is set by the scenario. For instance New York University (NYU) proposed $n = 3.0$ for the NLOS UMa scenario [100] and other scenarios are summarised in Table 3.2 for NLOS.

3.4 Channel characterization

The above two path loss models (eq 3.1 and eq 3.16) describe large-scale propagation path loss with respect to distance, carrier frequency and scenario. The key parameters of these models are the PLE (α), and intercept (β) which are selected to minimise the rms error (shadow fading component) term χ_{σ} . Researchers have therefore performed channel measurements in different geographical locations, to evaluate these parameters

for the key 3GPP scenarios . Prior to recent mmWave studies, the models were only specified for sub 6 GHz frequencies and it was unknown whether mmWaves would be suitable for future cellular communication. At higher frequencies, wavelengths are much smaller and losses are much higher. Hence, there has been a lot of recent studies in the characterization of wireless channels above 6 GHz. In the following subsections we summarise existing work concentrating on scenarios applicable to this thesis, namely RMa, UMa and UMi scenarios.

3.4.1 Rural Macro (RMa)

Millimetre waves, with their high capacity, have traditionally been considered for hotspots. As such, there are very few measurement campaigns to effectively model a mmWave channel in a RMa scenario. To my knowledge only two measurement campaigns exist; our own (June 2016) and New York University's (October 2016). George *et al.* from NYU [25] presented measurement campaign results at 73 GHz from rural macro (RMa) environment. They came up with their own model (which is CI) and claimed it to have improved accuracy, fewer parameters, and better stability as compared with the existing 3GPP RMa path loss model. The Path loss exponent (PLE) was reported as 2.75 and the shadow fading RMS error was reported as 6.7 dB. The authors further analysed the data obtained from the above campaign in [101] and combined this with simulated data from the old 3GPP model (valid <6 GHz), from which a new term was developed a close-in free space reference distance with a novel height dependent model (CIH model). The RMa NLOS CIH model has reducing PLE with increasing BS height. The PLE of 3.2 at 10 m reduced to 2.6 at 150 m height, a reduction of 6 dB path loss per decade of

distance. The model is however based on only one set of measurements at mmWave frequencies and so further measurement confirmation is required.

Before the above campaign, there was not a single work covering the mmWave mobile RMa scenario, infact, it was unknown whether mmWave were applicable to RMa scenarios. So we conducted a measurement campaign and provided this as input to the 3GPP via a joint Ericsson - Telstra submission [1]. Our results extended the validity of the old RMa model from 6 GHz to the current model's 30 GHz, which covers the proposed FR2 mmWave bands n257, n258 and n261.

3.4.2 Urban Macro (UMa)

UMa scenarios involve base station antennas above rooftop height and applies to both dense urban and light urban (suburban) situations. Authors in [99] presented extensive UMa measurement results from 2 to 73 GHz, using directional antennas. They provided a comparison of three large-scale propagation path loss models, i.e., the ABG (four parameters, $\alpha, \beta, \gamma, \chi$), CI (two parameters, α, χ), and CIF (three parameters, α, γ, χ) models, where χ is a gaussian shadow fading term covering the modelling errors. Sensitivity analysis from NYU showed the CI and CIF models to be superior to the ABG model in both stability and prediction accuracy (i.e., SF standard deviation) over a vast frequency range, which is suprising considering the higher degrees of freedom of the ABG model. Authors in [102] provided base-station to mobile propagation situations at 38 GHz carrier frequencies in an outdoor urban environment using directional, steerable antennas. Two directional horn antennas (25 dBi and 13.3 dBi) were used at the receiver. The 13.3

dBi horn antenna outperformed the 25 dBi horn antenna, when pointing in NLOS directions, in terms of path loss, PLE and path loss standard deviation. The larger beamwidth of the 13.3 dBi antenna captures more multipath energy than the 25 dBi antenna (after antenna gains have been removed). We experienced similar phenomena.

Huan *et al.* in [103] studied UMa propagation at 10, 18 and 28 GHz. Four different transmitter heights were chosen. In the NLOS conditions, the Tx height shows significant impact on the path loss. For example, by just raising the Tx heights 10 m from 15 m results in 7.5 dB gain at 10 GHz, and a further 29 m rise brings another 14.8 dB of gain. PLE of 2.5 is reported for 15 m high Tx while PLE reduces to 1.9 for 25 m at 28 GHz. Authors in [104] conducted a 38 GHz cellular outage study for an urban outdoor campus environment using directional antennas at two different transmit locations having heights 36 m and 18 m. They compared the outage with 160 dB and 150 dB path loss threshold. The upper antenna reported 19% outage which increased to 40% with the lower antenna. However no outages occurred within 200 m for either antenna location. Increasing BS height is clearly an advantage in UMa scenarios.

Propagation measurements at 28 GHz were conducted in outdoor urban environments in New York City using four different transmitter locations in [105]. They investigated AOA and AOD of wireless multipath propagation and small-scale fading effects in New York City using highly directional steerable antennas. It was found that small-scale fading is relatively negligible (± 2 dB about the mean power level) over a 10λ distance at fixed AOA using high gain antennas. Wideband propagation measurements and channel modelling for BS to UE were performed at 38 GHz in [106]. They showed that NLOS links have 10 to 50 dB more path loss and higher RMS delay spread. Similarly,

a wideband propagation measurement campaign using rotating directional antennas at 73 GHz was conducted at the New York University (NYU) campus in [107]. They used the measured data to investigate the prediction capability of an empirical Ray Tracing (RT) model. The comparison between the measured and predicted results indicated that a simplified RT model will be able to correctly predict the propagation characteristics at mmWave bands. The study done by authors in [108] achieved the angularly resolved path loss measurement in an urban macrocell scenario at the 28 GHz. The authors stated that the majority of the energy was contained either in a LOS path or in specular reflections or reflections off smaller objects such as scaffolding, drain pipes, light poles, bikes, and balconies. Our measurements (Chapter 6) would add to this list scatters, such as cars and trees which dominate many Australian suburbs.

The authors in [109] focused on frequency dependence of path loss between 2 GHz and 26 GHz. Their LOS results closely followed the Friis formula while the NLOS had an additional loss with frequency, particularly at longer distances, due to a greater reliance on diffraction (which is frequency dependent).

3.4.3 Urban Micro (UMi)

The UMi scenario is characterised by base station antennas below rooftop height; typically in the order of 10 m or so. A lot of interest has been shown by academic and industrial bodies in order to develop channel models above 6 GHz in UMi scenarios because of the high bandwidth requirement of small cell hotspots. We present some of the works carried out by different researchers, categorised according to the nature of the work in the following subsections.

3.4.3.1 Path Loss Measurements and models

Authors in [110] conducted practical measurements at 28 GHz and 73 GHz to derive detailed spatial statistical channel models in the New York (USA) area. The parameters considered were path loss, the number of spatial clusters, angular dispersion, and outage. These parameters were used to provide a realistic assessment of mmWave micro and pico-cellular networks in a dense urban deployment. Authors in [111] presented a empirical path loss data at 28 GHz and 38 GHz for 5G cellular network planning. Using the new mmWave propagation models, they simulated the RF coverage for future 5G cellular networks. Based on the simulation results, they concluded that with completely random beamforming, three times number of BSs are required for 5G networks compared to current networks within a same coverage zone. However, with single best beam only two times more BSs are enough, but with multi-beam combining even fewer BS sites are required. Both authors concluded that an order of magnitude capacity gain was possible (compared to 4G) without additional cell sites.

Authors in [112] studied the UMi wideband measurement at 28 GHz and 38 GHz using an omnidirectional as well as directional steerable antenna. They studied mmWave channel model parameters such as PLE, delay and angular spread and clustering parameters. Results showed that the PLEs value almost equal to that of Friis equation (PLE=2) for the LOS environment, while for the NLOS it was 3.0 at both frequencies. Additionally they showed that other parameters were also equal at both frequencies.

Large-scale path loss parameters at 60 GHz were published for NLOS urban outdoor environments using directional antennas [113]. NLOS links up to 36.6 ns RMS delay

spread and PLE of 4.19 were reported whereas LOS channels provided sub-nanosecond RMS delay spreads with a PLE of 2.23. Similarly, authors in [94] obtained the omnidirectional PLE range from 1.8 to 2.1 and from 2.4 to 3.5 in LOS and NLOS environments respectively at 28, 38 and 73 GHz. Directional path loss models in dense urban environments at 28 and 73 GHz were presented in [64]. They reported same NLOS PLE for both frequencies as 3.4. They concluded that mmWave channels are more directional than conventional UHF/Microwave channels. The article in [114] reported a probabilistic omnidirectional propagation path loss model based on empirical data in [115] using a probability distribution at 28 and 73 GHz. A weighting function enabled a probabilistic model that determined whether the Rx was in LOS of the Tx.

3.4.3.2 3D Path Loss Models

A 3D channel model that includes both azimuth and elevation parameters has been developed at 28 GHz and 73 GHz. Authors in [116] developed a statistical channel impulse response (IR) model for urban LOS and NLOS. The measured power delay profiles, angle of departure, and angle of arrival are used to extract statistics to implement a channel model and simulator which is capable of generating 3D mmWave temporal and spatial channel parameters for arbitrary mmWave carrier frequency, signal bandwidth and antenna beamwidth. Similarly, a path loss model for large-scale high-density urban scenarios has been reported in [117]. They used a “3D ray-tracing” simulation software to design the propagation path loss models for the large-scale future network [118].

3.4.3.3 Multi Beams

In [115], the authors investigated the channel at 73 GHz with directional antennas. A measurement emulating user's location for mobile and backhaul with more than 30 access points was conducted in a high-density urban scenario. The authors concluded more path loss at higher frequency bands using omnidirectional models, thus beam-combining and beam-steering could be beneficial for future wireless technologies by utilizing multipath in a high-density urban environment. Similarly, authors in [119] conducted measurements at 28 GHz in an outdoor environment in Manhattan, New York. The receivers were placed within a distance of 500 m. The parameters that were calculated were path loss with respect to distance, angular distribution of received power and power delay profiles. NLOS communication was shown to be possible out to 200 m by exploiting different multipath AoAs. [120] used the Stanford University Interim (SUI) and standard theoretical free space path loss models to support the benefit of using beam combining at the Rx to receive a strong signal power.

Our measurements in Chapter 8 also show the feasibility of beam combining since a single angle of departure at the Tx can result in many angle of arrivals at the Rx, which can then be coherently summed. We agree that multi-beam combining is necessary, but, for slightly different reasons to the previous authors. We see the primary need is for angular diversity against human blockage as discussed in subsection 3.4.4.1 and in Chapter 7.

3.4.3.4 Repeaters and Backhaul

Samsung modelled the mmWave channels for 5G [121]. They generated a new beam-forming technique and performed outdoor measurements. They established communication links in NLOS sites more than 200 m away by utilising different multipaths coming from reflections off buildings and then recommended the use of repeaters for non-coverage zones. Wireless backhaul is an alternative to repeaters for improving coverage in a low cost fashion and with this in mind, Kyro *et al.* in [122] performed channel measurements at 71-76 and 81–86 GHz for point-to-point communications in a street canyon (SC) scenario in Helsinki, Finland. Extremely high gain antennas (45 dBi) were used and Near-LOS conditions allowed communications up to 1.1 km. A geometry-based single-bounce channel model with scattering was developed and was verified by propagation measurements. Large scale parameters such as RMS delay spread were compared verifying the model. We have also conducted SC measurements in Melbourne CBD, where the emphasis was on the access network with UE's at street level. (Chapter 7 and [3]).

Authors in [123] examined access links and backhaul links for D2D communication, along with the impact of solar radio emissions on outdoor path loss models at 60 GHz. The research highlighted that solar radio emissions reduced carrier to noise ratios (CNR) and could be modelled as an increase in PLE values of path loss channel models. On hot sunny days (as experienced in the Gulf states) the PLE increases by 10% compared to night time operation. As a comment, perhaps a better way of modelling this effect would be to show how solar radiation increases the noise floor, in which case the PLE remains unchanged.

3.4.3.5 Delay Spread

Authors in [124] presented 28 GHz measurements. They used a horn antenna to gather power delay profiles from the environment and synthesized the omni directional power for channel modelling. They verified their model by calculating different large and small scale parameters such as delay spread and AoA/AoD spreads and compared with the experimental data.

Authors in [113] performed an urban cellular and peer-to-peer RF wideband channel measurements at frequencies of 38 GHz and 60 GHz using a directional steerable antenna. They presented the propagation path loss and time delay spread as a function of Tx-Rx distance and antenna pointing angles. At 38 GHz, LOS channels followed FSPL while NLOS have large multipath delay spreads and can utilize many AoAs to provide links. Also, the excess path loss, i.e. beyond free space, is inversely related to the distance between source and destination. A key observation is the RMS delay spread increases for increase in excess path loss for both the peer-to-peer and cellular channels. Smulders *et al* reported a delay spread of less than 50 ns in most locations while the average value was around 20 ns [125, 126]. ,

Delay spread is very much a function of scenario. Small cells generally have less delay spread than large cells. This argument is supported when comparing the above UMi based values with our own measurements taken in a much larger UMa cell (see Fig. 3.7). Each dot in the figure represents a single measurement at a given azimuth, elevation and position. Note the general shape supports the observation in [113], but the maximum value is now 400 ns not 50 ns. The maximum delay spread influences the

the choice of cyclic prefix in an OFDM system and 5G has a number of "numerologies" (or sub-carrier spacings) which enables different cyclic prefixes for different scenarios [127].

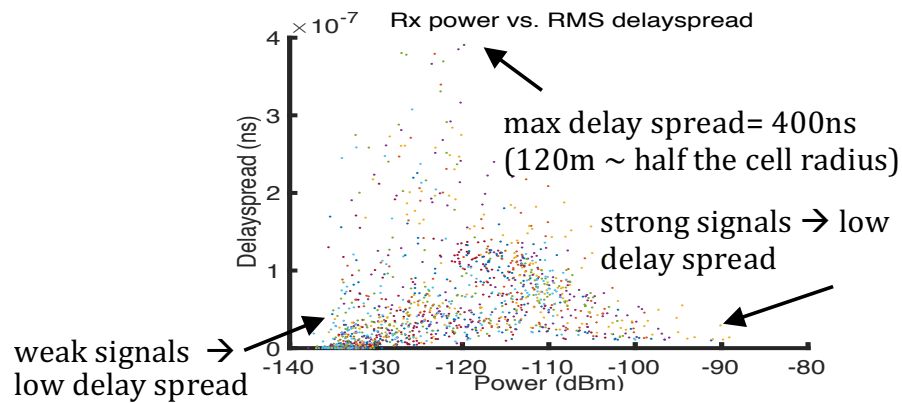


FIGURE 3.7: Delay spread in UMa, measured from Victoria University, Footscray Campus

3.4.3.6 Angular Spread

Average temporal and angular properties of multipaths in UMi measurements at 28 and 73 GHz were derived in combination with ray-tracing [65]. Azimuth and zenith spreads of arrival were found to be 22° and 6.2° at 28 GHz and 37.1° and 3.8° at 73 GHz, respectively in NLOS UMi. In this thesis angular spread analysis is limited to the RMa channel only (chapter 5).

3.4.3.7 Height Gain

The approach in [128] proposed a height-dependent path loss model at 28 and 38.6 GHz for NLOS UMi outdoor scenarios utilizing omnidirectional antennas. They compared their model with the 3GPP 38.900 model [100] and showed that the 3GPP model overestimates the system performance as it predicts lower path loss. They showed path loss

was not effected by BS height in LOS conditions. For NLOS conditions path loss increased with reducing BS height, but the increase was independent of distance (i.e. a fixed offset, or change in β for the AB model) and hence the PLE (α) was unaffected. They concluded that PLE for different heights at 38.6 GHz was constant equal that for 28 GHz.

In this Thesis height gain is discussed in Chapter 7.

3.4.3.8 Polarisation

The large-scale path loss model at 32 GHz band was analysed in [129] and [130] using directional horn antennas. Authors in [129] investigated the effect of co- and cross-polarisation on the CI model PLE. In LOS condition, PLE was 3.4 and 4.3 for co- and cross- respectively. Similarly, authors in [130] obtained 3.1 and 4.3. Additionally they performed NLOS measurements and reported 4.3 and 4.2, which is a strange result indicating a stronger cross-polar signal than co-polar signal! Similarly, authors in [65] at 28 GHz and 73 GHz reported a Gaussian distributed XPD with a mean cross-polar ratio of 29.7 dB and 16.7 dB in LOS and NLOS respectively.

In this Thesis polarisation was studied in the street canyon environment (Chapter 7). Good cross-polar discrimination can aid in MIMO performance based on polarisation (Chapter 7)

3.4.4 Indoor Hotspot (InH) and Outdoor to Indoor (O2I)

Wireless traffic from indoor locations is a significant part of the mobile communications market. Wireless operators are therefore interested in:

1. how much signal enters or leaves a building from outside basestations, in order to estimate coverage, or evaluate potential interference into adjacent cells or co-existing services.
2. how much signal attenuation there is between rooms within a building, in order to plan in-building coverage zones

Material losses play a vital role in determining the above issues. We therefore present path loss measurements of some common materials.

3.4.4.1 Material Losses

Early researchers used 60 GHz equipment, probably because of its unlicensed status and the potential adoption by IEEE for short range data transfer (e.g. IEEE802.11ad and .11ay etc [131]). Authors in [132] identified the problem of building penetration, particularly the high attenuation of concrete, brick walls and thermally efficient glass. Similar findings, in an Australian context, were shown in [26] (Victoria University). Measurements were taken at 24 GHz and a 20 dB loss reported for a double-bricked wall. Some of the attenuation was frequency dependant due to multipath within the structure as demonstrated by the double impulse in Fig 3.8. A summary of material penetration loss at 28 GHz is shown in Table 3.3 [26]. Take home conclusions are

1) Concrete kills mmWave signals, 2) Bricks and reflective glass have high attenuation, potentially providing good isolation between adjacent free standing buildings. 3) Plaster walls and clear glass offer little resistance enabling multiple room indoor coverage.

Trees are another form of loss and [128] measured 17 dB and [133] average value of 19 dB for deciduous trees. We measured a loss of 20 dB through the crown of a euclipt tree (Chapter 5). The human body is another major cause of loss. Losses of 20dB have been measured for partial hand shading, while human body blocking of the direct path near the UE can cause losses of greater than 30 dB [128]. Calculating signal diffraction around a body, modelled as a perfectly conducting cylinder gave similar losses (~ 23 dB) at 60 GHz, but only a 7 dB loss at 2.4 GHz (Fig. 3.9) [19]. This increase in shadowing loss with frequency emphasises the challenge of providing reliable communications to human operated terminals at mmWave frequencies.

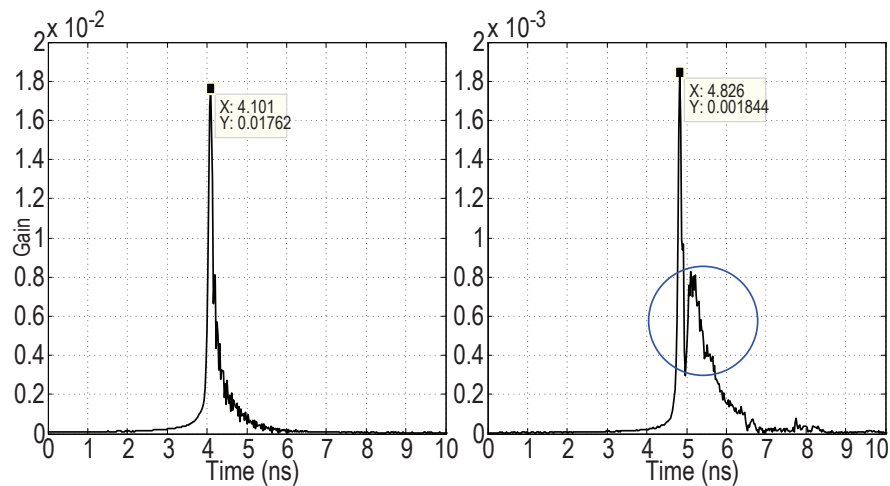


FIGURE 3.8: Impulse response. LHS Horn-to-horn reference through free space, RHS with a 22 cm thick brick wall. Measurement bandwidth 0-40 GHz, time resolution 0.025 ns [26]

TABLE 3.3: Material penetration loss at 28 GHz [26].

	[132]	[134]	[135]	[136]	[26]
Brick Wall	No through signal	28.3 dB	-	-	22 dB
Concrete	No through signal	-	-	117 dB	No through signal
Infra-red Reflective Glass	25-50 dB	24-40 dB	30 dB	31.4 dB	-
Clear Glass	-	3.6 dB	3-5 dB	3.8 dB	-
Plaster wall	-	6.8 dB	-	3.8-7.3 dB	2 dB
Door wood	-	-	-	-	13 dB

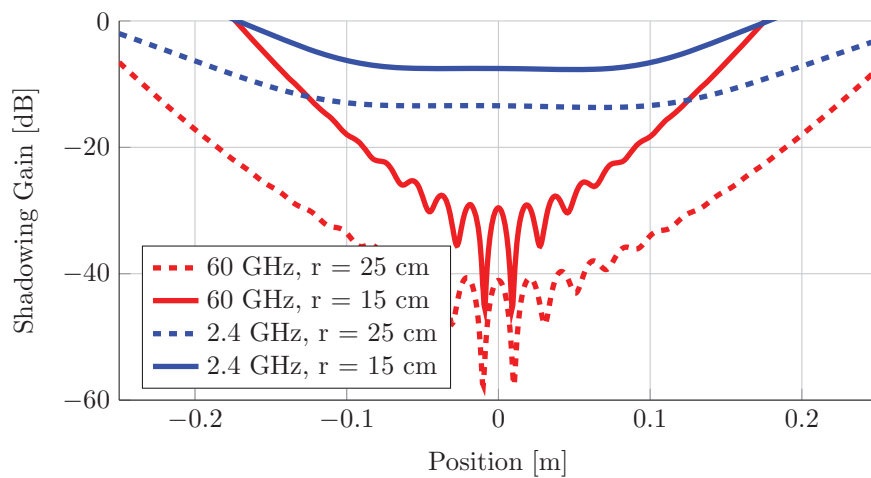


FIGURE 3.9: Theoretical shadowing gain due to perfectly conducting cylinders at 2.4 GHz and 60 GHz [19]

3.4.4.2 InH Propagation

Indoor hotspots are out of the scope of this thesis, however some work has been done in specialised O2I conditions focusing on co-existence with satellite services. Co-existence in this instance means spectrum sharing with Satellite services, and involves measurements at different elevation slant angles (or slant paths). A potential example would be sharing with Australia's National Broadband Network Satellite for remote area access. This sub-section, briefly surveys InH measurements and gives some insight of slant path O2I measurements.

Various researchers have conducted indoor propagation measurements at 28 GHz due to potential 5G frequency band. The authors in [137] conducted the experiments in an ultra-dense indoor office environment and presented a simple path loss model, as compared to the current 3GPP/ITU indoor propagation model. Similarly, the authors in [138] assessed the indoor channel using a multibeam MIMO prototype. They formed multibeam using continuous aperture-phased MIMO (CAP-MIMO), utilizing a lens antenna array. They claimed to use a first-time simultaneous multibeam channel measurement of about 4° beamwidth. They stated that by replacing existing conventional sounder with a CAP-MIMO transceiver, not only enabled spatial resolution, but also allowed the use of simultaneous multibeam, which enhanced network performance. Another author in [139] showed the potential use of mmWaves in indoor environments in shopping malls. More references can be found in the survey paper [140].

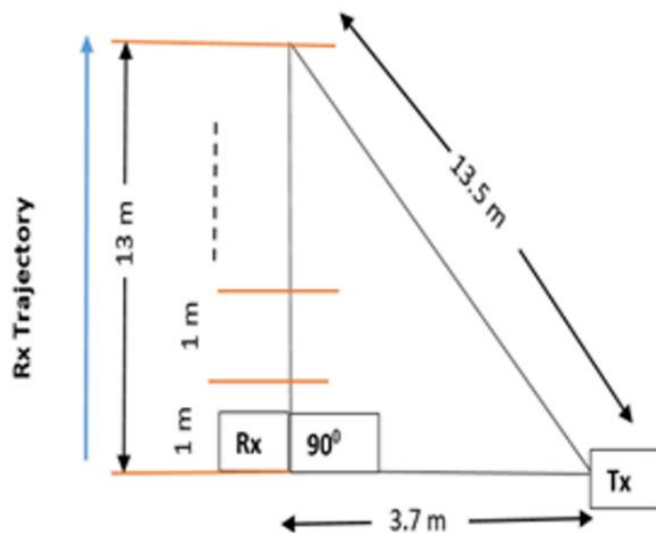


FIGURE 3.10: BEL measurements with Tx on the ground and Rx on different levels of a building [27]

The ITU O2I model has been compiled from a compendium of 28 measurements taken from locations all over the world and documented in [7]. The model covers all frequencies up to 100 GHz, although most measurements are below 6 GHz and do not

include slant paths, i.e. they model horizontal access. Those that do include slant paths use some form of high altitude platform (HAP) such as helicopter drones and balloons. Unfortunately, measurements are usually below 6 GHz [141]. Those at mmWave frequencies tend to use an outdoor ground level transmitter and indoor receivers on different floors of a building (Fig. 3.10 [27]). The O2I model is based on 0 dBi antennas to maintain compatibility with existing ITU path loss models.

Further use cases of mmWave such as in RADAR, vehicular environment are presented in [142–149].

3.5 Summary

In this chapter, most of the previous works related to mmWave channel measurements and characterization in different use case scenarios are presented. In spite of these activities, a number of scenarios and environment still need to be evaluated. Many of the above-mentioned works have used two-dimensional (2D) measurements (azimuth angle of arrival) and ignored the elevation angle. A three-dimensional (3D) analysis is necessary to know the propagation characteristic from different elevations, but such measurements are not always performed in a rigorous way, relying on the operator to identify potential scattering surfaces to which the antenna is pointed. As will be described in the next chapter our equipment uses a scanning pattern covering all azimuth angles having elevations between -20° to $+40^\circ$. Although many scatterers are obvious, we are continually surprised by signals occurring from unexpected directions, which

would have been missed in a manual search. In terms of the various scenarios for mobile access, the measurements described in the following chapters are the only ones covering Australian conditions. Measurements for the mobile RMa channel were the first ever reported. At that time, not a single measurement was conducted to know the channel behaviour in the rural field.

The next chapter (Chapter 4) describes the measurement hardware, its calibration and any modifications required for this Thesis.

Chapter 4

Hardware Design, Calibration and Performance

This chapter describes the design, calibration and performance of the equipment used for the different types of measurements required in this thesis. These are:

- Swept frequency measurements using a network analyzer for measuring frequency response of the antennas and also the path loss of materials at different frequencies. The network analyzer provides excellent time resolution and it is possible to see multi paths within the measured materials.
- Narrow band continuous wave (CW) measurements using signal generator and spectrum analyzer to obtain basic path loss measurements.
- Wide band measurements using a multi tone ‘OFDM like’ signal for measuring path loss and delay spread.

We start with the regulatory requirements for safety.

4.1 OHS Transmission Limits

The International Commission on Non-Ionizing Radiation Protection (ICNIRP) and Australian Radiation Protection and Nuclear Safety (ARPANSA) recommend power density (PD) limits for above 10 GHz as per Table 4.1 for both general public and RF workers [30, 150, 151]. The peak and average power density specifications are shown in the shaded columns. The worst case scenario is when the human body completely covers (touching) the antenna aperture which for a 20 dBi gain horn has an area of $3.5cm \times 2.5cm = 8.7e^{-4}m^2$. Based on this area, the maximum Tx power can be calculated. A maximum RF power of 13 dBm should satisfy all conditions.

TABLE 4.1: Power Density Limits [30] and peak Tx power for 20 dBi horn

	PD_{av} Spec over 20 cm^2	$P_T(av)$ for 20 dBi horn	PD_{peak} Spec over 1 cm^2	$P_T(peak)$ for 20 dBi horn
Public	$10W/m^2$	13 dBm	$200\text{ W}/m^2$	22.4 dBm
RF Workers	$50W/m^2$	20 dBm	$1000\text{ W}/m^2$	29.4 dBm

Since approximately 40% of the incident radiated energy is reflected, a further 2 dB can be added to the above table. We therefore conclude that any Tx powers over 15 dBm require the human body to be separated from the transmitter (Tx) antenna. Since 15 dBm is the limit of our equipment, then transmissions are safe for the general public and staff.

4.2 Swept Frequency measurements using Network Analyser

Swept frequency measurement method can be used in a short coverage range due to the limitation in cable length (~ 10 m). It can obtain high time resolution by sweeping over a wide frequency range and taking an FFT (Fast Fourier Transform) of the frequency response data. It is used for calibrating the antenna and measuring the parameters such as radiation pattern, gain and transmission and reflection losses for typical materials. Fig. 4.1 shows the 40 GHz Anritsu 37369 network analyser measuring transmission loss between two 20 dBi horn antennas.

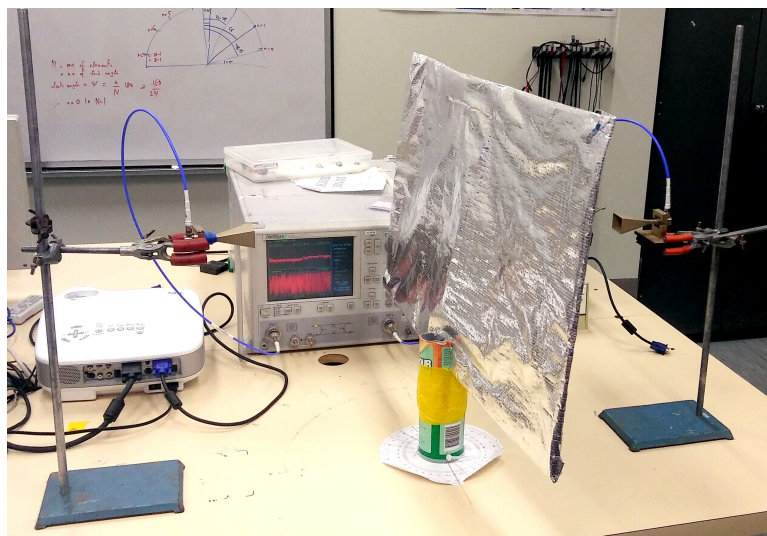


FIGURE 4.1: 40 GHz Anritsu 37369 Network analyser measuring loss through builders ‘sarking’ (Courtesy of Inderjeet Singh, Maninder Jit Singh and Gaurav Jain - VU Course Work students, 2018)

4.2.1 Antenna Calibration

The horn antennas were calibrated using a network analyser, sweeping the frequencies between 20 GHz and 40 GHz. Antennas with gains of 10 dBi, 20 dBi and 25 dBi

TABLE 4.2: Antenna gains

Antenna Gain	24 GHz	27 GHz	39 GHz
25 dBi	23.5	24	25
20 dBi	17	18.5	20.5
10 dBi	9.6	9.9	14.4

were used having a nominal HPBW of $\pm 27.5^\circ$, $\pm 10^\circ$ and $\pm 5^\circ$ @ -3 dB respectively. The antennas were measured on a small test range with 2 m separation between the feed-points which is approximately twice the Rayleigh distance for these antennas. The normalized antenna radiation patterns are plotted in Fig. 4.2 for three frequencies of interest covering two potential 5G bands and the 24 GHz ISM (Industrial, Scientific and Medical) band.

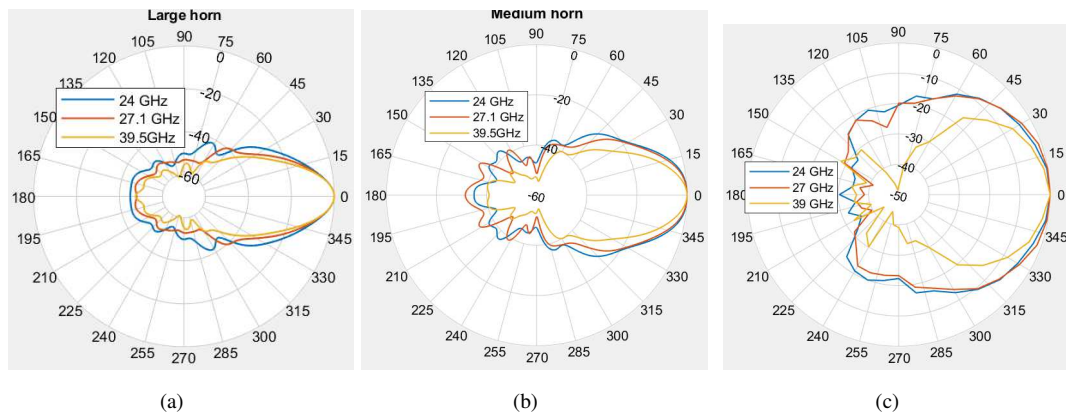


FIGURE 4.2: Antenna Measurements over a 2 m test distance. (a) 25 dBi horn (b) 20 dBi horn (c) 10 dBi horn (nominal gains).

The back-to-front ratios for all antennas are better than 25 dB, and usually greater 35 dB for the medium gain antenna and 45 dB for the high gain antenna. Table 4.2 shows the measured gains of these three antennas at different frequencies.

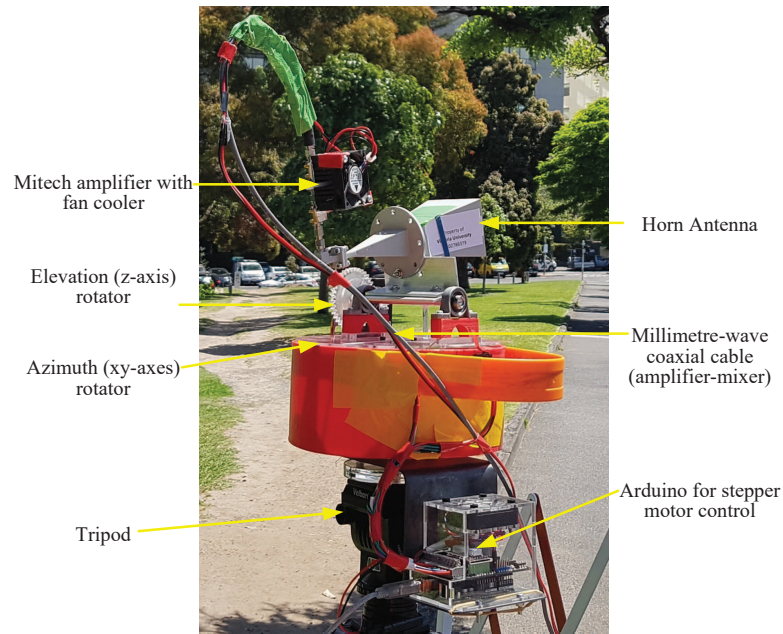


FIGURE 4.3: Automated equipment developed for receiving signals at 7° steps in azimuth covering 0° to 360° ; and 10° steps in elevation covering -20° to 40° [28].

4.3 Semi Automatic Receiver Scanning

Before we dive into further measurement techniques, we discuss the receiver set up for automatic Angle of Arrival (AoA) measurements. An azimuth and elevation (ϕ, θ) adjustment table was developed for one end of the link enabling 360° degree azimuth coverage in steps of 7° in and -20° to $+40^\circ$ in elevation coverage in steps of 10° . The unit was fabricated using 3D printer techniques and driven by stepper motors controlled by Labview software (Fig. 4.3).

4.3.1 Limited isotropic coverage

Ideally it is required to capture all the incoming signals by scanning 0° to 360° in azimuth and -90° to $+90^\circ$ in elevation to accurately synthesise the omnidirectional pattern. Our measurement hardware takes 2.5 minutes for a complete azimuth scan at a single

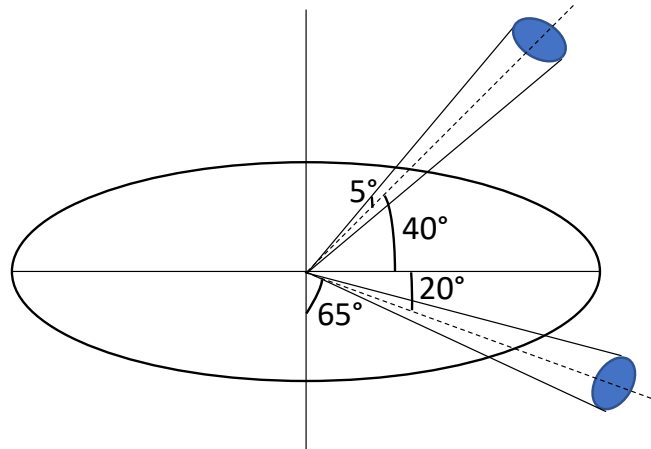


FIGURE 4.4: Antenna position in AoA measurement hardware when covering -20° to 40° .

elevation. For a vertical step size of 10° , the total time to complete a single isotropic measurement would be around 45 minutes, quite a long time. During the measurements, it was found that most signals tend to appear between -10° and $+20^\circ$, with a few at higher elevations. This enabled us to restrict the elevation range to -20° to $+40^\circ$ and reduce the scanning time to around 15 minutes. Fig. 4.4 shows the receiver horn ($\pm 5^\circ$) antenna position when the antenna is at the extreme angles of elevation. The solid angle (Ω st) covered by the 25 dBi horn antenna ($\pm 5^\circ$) is calculated as follows.

$$\begin{aligned}
 \Omega_1 &= 2\pi(\sin\theta) \text{ st} \\
 &= 2\pi(\sin 45) \text{ st} \\
 &= 2\pi \times 0.7 \text{ st}
 \end{aligned} \tag{4.1}$$

Similarly, the solid angle made by the area of aperture of the horn when it is at -20° elevation is given as:

$$\begin{aligned}\Omega_2 &= 2\pi(\sin 25) \text{ st} \\ &= 2\pi \times 0.42 \text{ st}\end{aligned}\tag{4.2}$$

Therefore, the total solid angle covered by the horn is:

$$\begin{aligned}\Omega &= \Omega_1 + \Omega_2 \\ &= 2\pi(0.7 + 0.42) \\ &= 2.24\pi \text{ st}\end{aligned}\tag{4.3}$$

which is 56% of the total 4π steradians in a sphere. Only in one scenario (O2I from high altitude BSs) did we experience signals from outside the coverage range. Here, we increased the scan angle by using a combination of a lower gain antenna (10 dBi) with an increased elevation coverage to give a total $\pm 80^\circ$ or 98% spherical coverage.

4.4 Narrowband measurements

Narrowband measurements use signal generators and a spectrum analyser to measure signal strength. Two transmit antennas are powered at frequencies f and $(f+2)$ MHz respectively (Fig. 4.5(a)). At the receiver site, the spectrum analyser identifies each transmission and automatically logs the data (Fig. 4.5(b)). This enables cross-polarisation

measurements or space diversity measurements. Small scale fading is reduced by a combination of oversampling in the angle domain, averaging in the time domain and repeating the measurements at different antenna heights (effectively applying angle, time and space diversity). The signal generators and spectrum analyser must be calibrated for this measurement in order to remove measurement errors.



FIGURE 4.5: CW transmissions. (a) LHS Two signal generators, for Horizontal and Vertical polarisation (HP8360 and Agilent N5230A). Example frequencies: 39.499 GHz and 39.501 GHz (b) RHS Receiver with 2 LNAs (Miteq JS426004000-30-10P) feeding spectrum analyser (R& S FSIQ40).

4.4.1 Signal Generator and Receiver Calibration

The HP8360 signal generator was calibrated against a power meter (Anritsu) at three spot frequencies (24 GHz, 27 GHz and 39 GHz). The calibration was within less than 0.5 dB. The signal generator was then used to calibrate other equipment, (spectrum analysers, network analysers and USRP receivers, etc.)

4.4.2 Link Margin Calculation

The link margin was measured on a 2 m test range. The received signal was immediately amplified (50 dB using two LNAs) and passed through a 2 m cable (loss=4.5 dB at 24 GHz) to the spectrum analyser. The high RF gain was chosen such that the LNA noise would dominated the spectrum analyser noise floor by at least 10 dB. The transmit power was 8 dBm and the receiver spectrum analyser was set to have 5 MHz span, 50 kHz RBW (Resolution Bandwidth, B) and 10 (video) averages. Based on amplifiers with a noise figure (NF) of 4 dB and a connector loss of 1 dB (giving effective NF = 5 dB), the measurement dynamic range or maximum sustainable path loss (MSPL) is given as:

$$\begin{aligned} MSPL &= P_T + G_T + G_R - \text{Noise Level} (KTBNF) & (4.4) \\ &= 8 + 23.5 + 17 - (-174 + 47 + 5) \\ &= 8 + 23.5 + 17 - (-122) \\ &= 170.5 \text{ dB (with 40.5 dB antenna gain)} \\ &= 130 \text{ dB (Omni to Omni @ } P_T = 8 \text{ dBm)} \end{aligned}$$

where the large horn (25 dBi) is used for receive and the medium horn (20 dBi) is used for transmit, which is the arrangement for most of the measurement schemes. Note, the antenna gains here are for 24 GHz operation (see table 4.2).

4.5 Wideband measurements (OFDM)

We measure the channel impulse response for signals captured by the antenna. The approach uses USRP (Universal Software Radio Peripheral) devices with 100 MHz bandwidth to obtain path resolutions down to 10 ns (3 m). Fig. 4.6 shows the block diagram of Tx and Rx chain. Signal generators provide the up-converter and down-converter local oscillator (LO) signals. Conversion is through a double balanced mixer. The LO signal is chosen to lie in an ISM band (24 GHz) because of the strong leakage. The RF Tx frequency was set at 27.1 GHz (based on ACMA experimental license allocation), and so the USRP generated IF signal was 3.1 GHz.

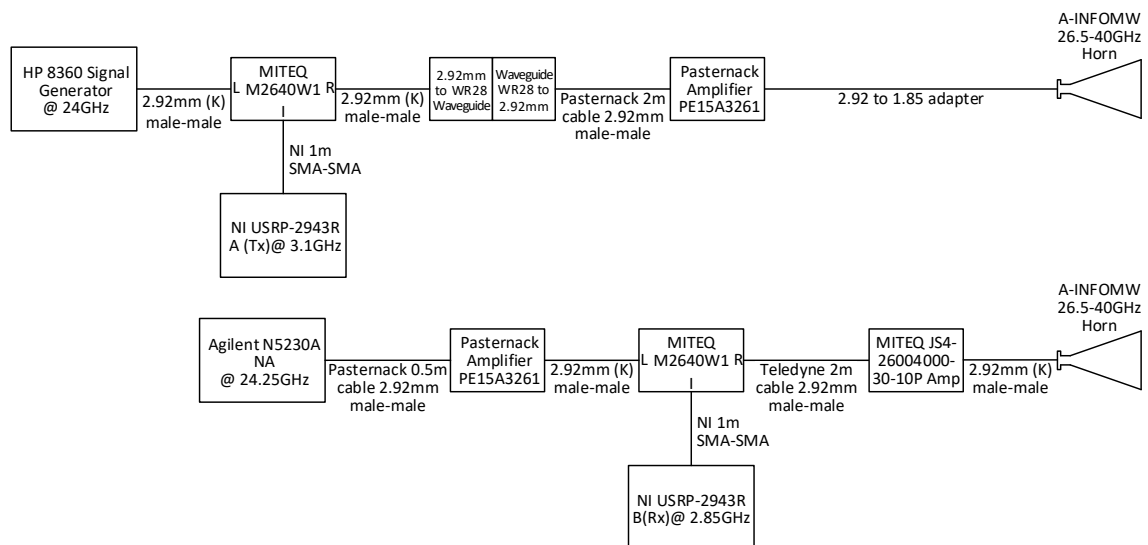


FIGURE 4.6: Wideband Tx (top) and Rx (bottom) hardware [28].

The USRP (Universal Software Radio Peripheral) devices are responsible for the first stage of up/down conversion from/to baseband. The transmitter does continuous transmission and the receiver data logs segments of the received waveform. The remaining software is performed off-line in MATLAB. The software process involves a multi-tone “OFDM like” training sequence with low peak-to-average power ratio (Shapiro-Rubin

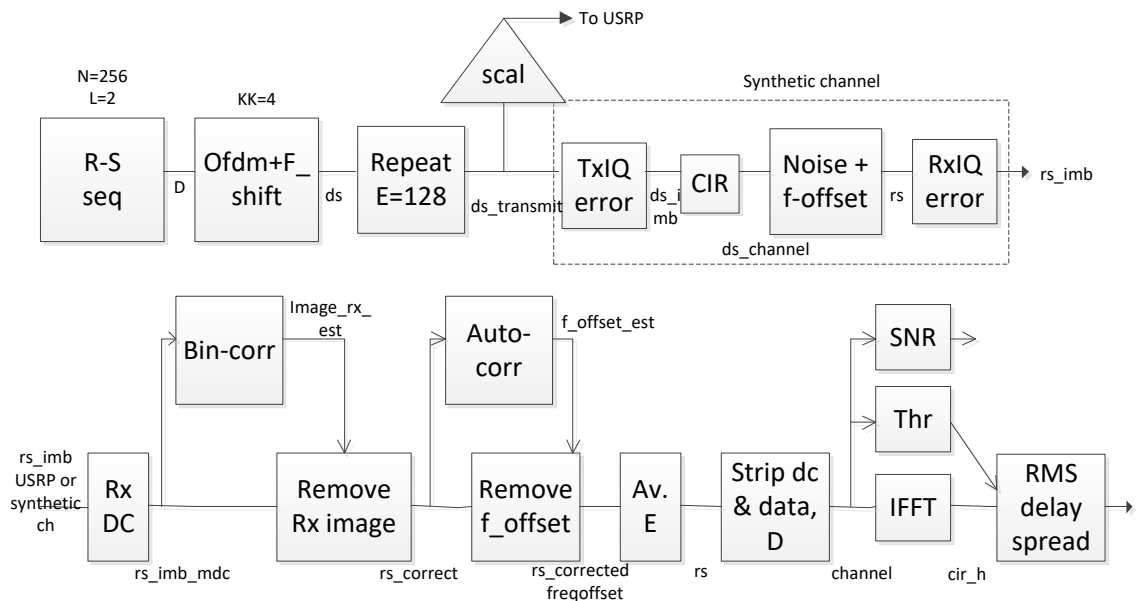


FIGURE 4.7: Software Signal Processing Flow for Tx (top) and Rx (bottom) [28].

sequence). There are 256 active tones oversampled by $L=2$ and spread evenly over 1024 frequency bins. The active tones are arranged in such a way that their images fall in vacant (unused) bins, eliminating the IQ mismatch problem at the transmitter (Tx) side. The signal is repeated 128 times and scaled to an amplitude < 1.0 prior to sending to the USRP (Universal Software Radio Peripheral). Receive side signal processing involves filtering, receiver (Rx) IQ correction, DC offset removal and frequency offset correction. The channel impulse response (CIR) is derived from the inverse fast fourier transform (IFFT) of the channel frequency response. A variable threshold based on signal strength and noise is used to isolate the CIR components from the noise prior to calculating the rms delay spread and coherence bandwidth. The threshold is set approximately 26 dB below the signal power for high SNR's (Signal to Noise ratio) or approximately 12 dB above the noise power for low SNR's. In this way Gibbs ringing and far off noise spurs do not materially effect the rms delay calculation. The working diagram of software for the transmit and receive signal processing is shown in Fig. 4.7. Results from a 2 m test

range are shown in Fig. 4.8 and 4.9.

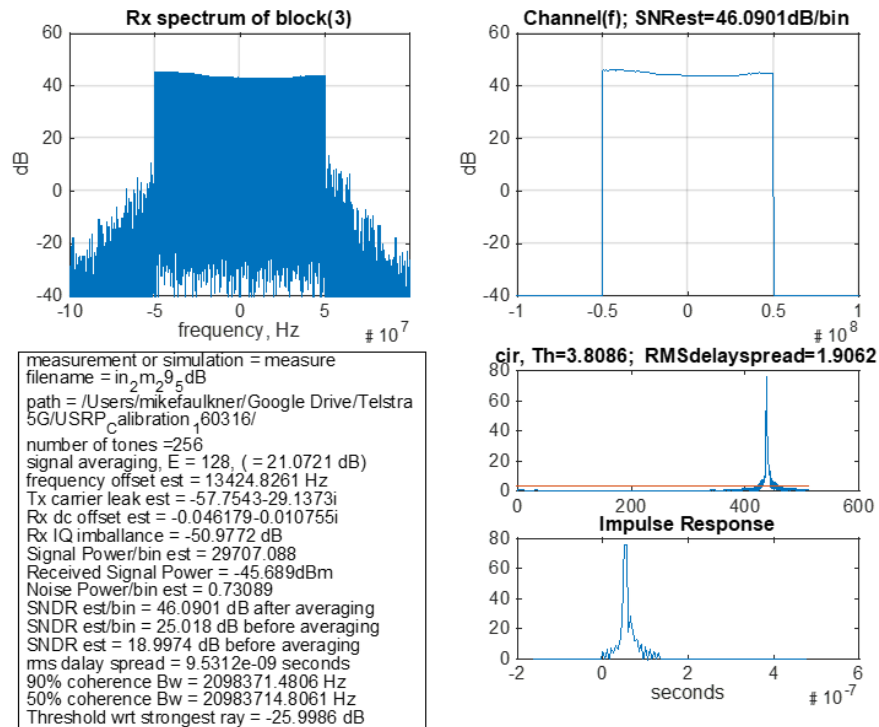


FIGURE 4.8: Result from a 2 m test range with large horns (2 x 24 dBi) and 30 dB attenuation added to the Tx signal path. TL (Top Left) – Raw received signal; TR – Channel Estimate (after filtering, frequency domain decimation by 4 and modulation removal); BL – Debug output; BR – Channel Impulse Response with threshold level (red line) and zoomed response.

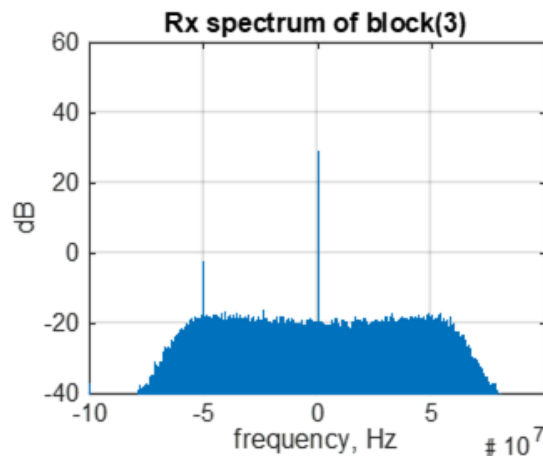


FIGURE 4.9: Rx spectrum with Transmitter disabled. Noise floor, showing DC leak and an unwanted spur from the USRP receiver.

4.5.1 Link Margin Calculation

Comparing Fig 4.8 and Fig. 4.9, the floor of -18 dB, and the signal of +43 dB from a 2 m path with 30 dB attenuation gives a measurement range of 62 dB. After removing 30 dB attenuation, the signal is $62 + 30 \text{ dB} = 91 \text{ dB}$ beyond the 2 m path loss with antenna gains of 47 dB and $P_T = 3.4 \text{ dBm}$. The Maximum Sustainable Path Loss (MSPL) is calculated as below:

$$\begin{aligned} MSPL &= P_T + G_T + G_R - PL(2m) && (4.5) \\ &= 91 + PL(2m) \\ &= 91 + 66 \\ &= 157 \text{ dB (with a total of 48 dB antennagain)} \\ &= 162.5 \text{ dB (with a total of 42.5 dB antennagain)} \\ &= 109 \text{ dB (Omni to Omni @Pt = 3.4 dBm)} \end{aligned}$$

The reduced performance compared to the narrowband solution is due to the lower transmit power and the wider bandwidth over which the energy is spread. The low transmit power is required to limit distortion in the OFDM like signal. It is possible to further boost the MSPL by about 10 dB using software averaging (10 averages) provided the Doppler is low ($< \sim 600 \text{ Hz}$ or $< 20 \text{ kph}$), in the measurement vicinity.

4.6 Summary

In this chapter, the measurement equipment is overviewed. This included, transmit power limits, angle of arrival measurement hardware and calibration of equipment such as antennas, signal generators and the spectrum analyser. Also three different measurement schemes; swept frequency using network analyser, narrowband CW, and wideband OFDM, are discussed. The MSPL based on Omni to Omni transmission is 130 dB for narrowband CW and 109 dB to 119 dB for wideband OFDM measurements. These figures can be boosted by adding antenna gain.

Next chapter, Chapter 5 presents the paper on 24 GHz narrowband measurements.

OFFICE FOR RESEARCH TRAINING, QUALITY AND INTEGRITY

DECLARATION OF CO-AUTHORSHIP AND CO-CONTRIBUTION: PAPERS INCORPORATED IN THESIS

This declaration is to be completed for each conjointly authored publication and placed at the beginning of the thesis chapter in which the publication appears.

1. PUBLICATION DETAILS (to be completed by the candidate)

Title of Paper/Journal/Book:	New measurements at 24 GHz in a rural macro environment		
Surname:	Dahal	First name:	Saurav
Institute:	Institute for Sustainable Industries and Liveable	Candidate's Contribution (%):	80
Status:		Date:	
Accepted and in press:	<input type="checkbox"/>	Date:	
Published:	<input checked="" type="checkbox"/>	Date:	May 2016

2. CANDIDATE DECLARATION

I declare that the publication above meets the requirements to be included in the thesis as outlined in the HDR Policy and related Procedures – policy.vu.edu.au.

<input type="text"/>	<input type="text"/>	<input type="text"/>	18-12-2019
	Signature		Date

3. CO-AUTHOR(S) DECLARATION

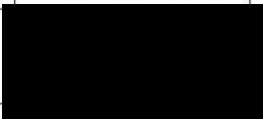
In the case of the above publication, the following authors contributed to the work as follows:

The undersigned certify that:

1. They meet criteria for authorship in that they have participated in the conception, execution or interpretation of at least that part of the publication in their field of expertise;
2. They take public responsibility for their part of the publication, except for the responsible author who accepts overall responsibility for the publication;



- 3. There are no other authors of the publication according to these criteria;
- 4. Potential conflicts of interest have been disclosed to a) granting bodies, b) the editor or publisher of journals or other publications, and c) the head of the responsible academic unit; and
- 5. The original data will be held for at least five years from the date indicated below and is stored at the following **location(s)**:

Name(s) of Co-Author(s)	Contribution (%)	Nature of Contribution	Signature	Date
Telstra	20	submitted to 3GPP and review of drafts		20/02/20

Updated: September 2019

Chapter 5

New measurements at 24 GHz in a rural macro environment

5.1 Overview

A number of measurement campaigns were conducted over the span of one and half years from March 2016 to August 2017 in different scenarios imitating different propagation conditions. The first measurement was in a Rural Macro (RMa) scenario because, at that time, no mmWave measurements existed for the 3GPP rural model. The channel model discussion document, R1-163909 [53] supported frequencies up to 100 GHz for all scenarios (UMa, UMi, InH etc.) except RMa. The RMa model was only valid to 7 GHz [53], and the deadline for defining the channel model for 5G was in June 2016. That is the model would be frozen at that date so that evaluation could be performed

on the different proposals for 5G. Telstra and Ericsson requested VU to obtain results before that date. The attached document was the result of this request.

The input into the standards can be done only by member organisations (industries). We conducted measurements, collected data, analysed the data and prepared a draft report before submitting to 3GPP (by Telstra and Ericsson). Ericsson restructured the discussion and conclusion into 3GPP template. This involved defining a number of 'observations' and 'proposals'.

The key observation was that 'path loss measurements at 24 GHz in a rural macro environment agree on average with the WF (World Forum) RMa path loss model'. The key proposal was 'Extend the applicability of the new RMa path loss model in R1-163909 [53] to 24 GHz'.

At the meeting conclusion the path loss model was extended to 30 GHz.

5.2 Publication

The following paper has been enlisted as a contribution to RMa channel model in 3GPP for higher frequencies.

3GPP. New measurements at 24 GHz in a rural macro environment. Technical Report TDOC R1-164975, Telstra, Ericsson, May 2016
<https://portal.3gpp.org/ngppapp/CreateTdoc.aspx?mode=view&contributionId=704277>

The full-text of this article is subject to copyright restrictions, and cannot be included in the online version of the thesis.



OFFICE FOR RESEARCH TRAINING, QUALITY AND INTEGRITY

DECLARATION OF CO-AUTHORSHIP AND CO-CONTRIBUTION: PAPERS INCORPORATED IN THESIS

This declaration is to be completed for each conjointly authored publication and placed at the beginning of the thesis chapter in which the publication appears.

1. PUBLICATION DETAILS (to be completed by the candidate)

Title of Paper/Journal/Book:	27.1 GHz Millimetre Wave Propagation Measurements for 5G Urban Macro Areas		
Surname:	Dahal	First name:	Saurav
Institute:	Institute for Sustainable Industries and Liveable	Candidate's Contribution (%):	80
Status:		Date:	
Accepted and in press:	<input type="checkbox"/>	Date:	
Published:	<input checked="" type="checkbox"/>	Date:	04-06-2017

2. CANDIDATE DECLARATION

I declare that the publication above meets the requirements to be included in the thesis as outlined in the HDR Policy and related Procedures – policy.vu.edu.au.

<input type="text"/>	<input type="text"/>	<input type="text"/>	18-12-2019
	Signature		Date

3. CO-AUTHOR(S) DECLARATION

In the case of the above publication, the following authors contributed to the work as follows:

The undersigned certify that:

1. They meet criteria for authorship in that they have participated in the conception, execution or interpretation of at least that part of the publication in their field of expertise;
2. They take public responsibility for their part of the publication, except for the responsible author who accepts overall responsibility for the publication;



- 3. There are no other authors of the publication according to these criteria;
- 4. Potential conflicts of interest have been disclosed to a) granting bodies, b) the editor or publisher of journals or other publications, and c) the head of the responsible academic unit; and
- 5. The original data will be held for at least five years from the date indicated below and is stored at the following **location(s)**:

Name(s) of Co-Author(s)	Contribution (%)	Nature of Contribution	Signature	Date
Mike Faulkner	10	contribution to theory		28/02/2020
Horace King	3	Draft review		26/02/20
Shabbir Ahmed	7	Hardware design		26/02/20

Updated: September 2019

Chapter 6

27.1 GHz Millimetre Wave

Propagation Measurements for 5G

Urban Macro Areas

6.1 Overview

In Chapter 5, we showed the measurement campaign in RMa scenario and extended the old RMa model up to 30 GHz. In the following paper, we present the empirical results from Urban Macro (UMa) scenario. The background to this paper is the recent removal of the 'suburban' scenario from the 3GPP channel model. Australian cities have large suburban areas characterised by low height dwellings, wide streets, gardens and trees, and are quite different to Urban areas where high rise buildings are closely attached. To analyse this situation the UMa scenario is divided into UMa-Light and UMa-Dense.

Additionally, there is some discussion within 3GPP and ITU as to the selection of the most appropriate model. The two competing models are fixed intercept, known as the CI model, and the floating intercept, known as the AB model. We compare these models in the above two scenarios.

6.2 Publication

The following article has been published in the IEEE Vehicular Technology (VTC) Conference 2017.

S. Dahal, M. Faulkner, H. King and S. Ahmed, "27.1 GHz Millimetre Wave Propagation Measurements for 5G Urban Macro Areas," 2017 IEEE 85th Vehicular Technology Conference (VTC Spring), Sydney, NSW, 2017, pp. 1-5, doi: 10.1109/VTCSpring.2017.8108208.

The full-text of this article is subject to copyright restrictions, and cannot be included in the online version of the thesis.

The published version is available from: <https://ieeexplore.ieee.org/document/8108208>

OFFICE FOR RESEARCH TRAINING, QUALITY AND INTEGRITY

DECLARATION OF CO-AUTHORSHIP AND CO-CONTRIBUTION: PAPERS INCORPORATED IN THESIS

This declaration is to be completed for each conjointly authored publication and placed at the beginning of the thesis chapter in which the publication appears.

1. PUBLICATION DETAILS (to be completed by the candidate)

Title of Paper/Journal/Book:	Urban Microcell 39 GHz Measurements		
Surname:	Dahal	First name:	Saurav
Institute:	Institute for Sustainable Industries and Liveable	Candidate's Contribution (%):	80
Status:		Date:	
Accepted and in press:	<input type="checkbox"/>	Date:	
Published:	<input checked="" type="checkbox"/>	Date:	27-08-2019

2. CANDIDATE DECLARATION

I declare that the publication above meets the requirements to be included in the thesis as outlined in the HDR Policy and related Procedures – policy.vu.edu.au.

	18-12-2019
Signature	Date

3. CO-AUTHOR(S) DECLARATION

In the case of the above publication, the following authors contributed to the work as follows:

The undersigned certify that:

1. They meet criteria for authorship in that they have participated in the conception, execution or interpretation of at least that part of the publication in their field of expertise;
2. They take public responsibility for their part of the publication, except for the responsible author who accepts overall responsibility for the publication;



- 3. There are no other authors of the publication according to these criteria;
- 4. Potential conflicts of interest have been disclosed to a) granting bodies, b) the editor or publisher of journals or other publications, and c) the head of the responsible academic unit; and
- 5. The original data will be held for at least five years from the date indicated below and is stored at the following **location(s)**:

Name(s) of Co-Author(s)	Contribution (%)	Nature of Contribution	Signature	Date
Shabbir Ahmed	5	Helped in measurements		26/02/20
Horace King	2	Review of draft		26/02/20
Ganesh Bharatula	2	Review of draft		20/2/20
John Campbell	3	Review of draft		14-2-20
Mike Faulkner	8	overall supervision and contribution to theory		14-2-20

Updated: September 2019

Chapter 7

Urban Microcell 39 GHz

Measurements

7.1 Overview

In Chapter 6, we characterized the mmWave channel in UMa scenarios. A key use case for mmWave 5G is expected to be the urban microcell (UMi) hotspot. Normally, UMi is characterised by low BS antenna heights, usually below rooftop and in the range of 5 m to 10 m. Considering this, Telstra were interested in street canyon and open square scenarios with emphasis on non line-of-sight (NLOS) coverage, particularly into cross streets and other hard to get at places. Also there was interest in the effect of BS antenna height and cross polar leakage. At the time there were few existing measurements covering these latter effects.

We concluded that:

- The signal does indeed penetrate into cross streets, but coverage might still be patchy due to a lack of angular diversity.
- The effect of antenna height gain was shown to be minimal.
- Signal depolarisation was similar for all NLOS positions when measured on an “omni” basis

7.2 Publication

The following paper has been published in IEEE Antennas and Wireless Propagation Letters.

Urban Microcell 39 GHz Measurements

Saurav Dahal¹, Student Member, IEEE, Shabbir Ahmed, Member, IEEE, Horace King¹, Senior Member, IEEE, Ganesh Bharatula, John Campbell, Member, IEEE, and Mike Faulkner¹, Member, IEEE

Abstract—Urban microcellular non-line-of-sight path gain measurements at 39.5 GHz are presented for open square (OS) and street canyon (SC) environments. The extracted parameters are in close agreement with the 3rd Generation Partnership Project specifications, particularly for the close-in free-space reference distance model with path-loss exponents within 3%. Base station antenna height diversity in the OS environment provided only a small 0.5 dB benefit. In the SC measurements, corner losses of 18 dB were reported and cross-polar discrimination reduced by 2.5 dB per 10 dB increase in path loss using directional antennas, but this correlation disappeared on an omnidirectional basis.

Index Terms—5G, channel models, millimeter waves, urban microcellular (UMi).

I. INTRODUCTION

PROPAGATION measurements are required for different environments and from different organizations in the derivation of channel models. This heterogeneity removes measurement bias and improves model confidence. Measurement campaigns and ray-tracing simulations at millimeter (mm)-wave bands have been conducted to develop channel models above 6 GHz [1]–[6]. More specifically, urban microcellular (UMi) propagation measurements have been reported for street canyon (SC) and open square (OS) scenarios [7]–[12], of which some included the 5G proposed frequency range 2 (FR2) near 40 GHz [13]–[18]. Few of these considered the effect of *in situ* base station (BS) antenna heights in OS [17] or polarization in SC [18], and fewer (none to our knowledge) have completed such measurements concurrently as presented here. Additional contributions include: 1) the isolation of height gain effect and the macro diversity effect of the dual height BS in OS, and 2) the identification of different relationships between cross-polar discrimination (XPD) and the path gain for omni and directional antennas in SC.

Of most interest are non-line-of-sight (NLOS) scenarios. We first, however, validate the large-scale parameters, shadow fading standard deviations (σ) of the two UMi 3rd Generation Partnership Project (3GPP) channel models (see Table I) [19], the AB-3GPP model [20] and the CI-NYU model (by New York

Manuscript received July 9, 2019; revised August 13, 2019; accepted August 22, 2019. Date of publication August 27, 2019; date of current version October 4, 2019. This work was supported by Telstra. (Corresponding author: Saurav Dahal.)

S. Dahal, S. Ahmed, H. King, and M. Faulkner are with the Institute of Sustainable Industries and Liveable Cities, Victoria University, Melbourne, VIC 3011, Australia (e-mail: saurav.dahal@live.vu.edu.au; shabbir.ahmed@vu.edu.au; horace.king@vu.edu.au; Mike.Faulkner@vu.edu.au).

G. Bharatula is with the Telstra Corporation Ltd., Melbourne, VIC 3000, Australia (e-mail: Ganesh.Bharatula@team.telstra.com).

J. Campbell, retired, was with the Telstra Corporation Ltd., Melbourne, VIC 3000, Australia (e-mail: jcccqq@gmail.com).

Digital Object Identifier 10.1109/LAWP.2019.2937539

TABLE I
UMi 3GPP NLOS PATH-LOSS MODELS

Model	Path Loss (dB)	σ (dB)	Applicability
AB-3GPP	$35.3 \log(d) + 22.4 + 21.3 \log(f_c)$ $-0.3(h_{UT} - 1.5)$	7.82	$h_{BS} = 10\text{m}$ $1.5\text{m} < h_{UT} < 22.5\text{m}$
CI-NYU	$32.4 + 20 \log(f_c) + 31.9 \log(d)$	8.2	-



Fig. 1. (a) UMi OS looking southwest from Tx lower balcony. (b) Tx balconies seen from #11.

University). Both models can be recast into the following AB form:

$$PL(f_c, d)[\text{dB}] = \beta(f_c, d_0, h_{UT})[\text{dB}] + 10\alpha \log_{10}(d/d_0) \quad (1)$$

where f_c is the carrier frequency in GHz, d is the distance in meters, d_0 is the reference distance (normally 1 m), h_{UT} is the terminal height, β is the intercept, and α represents the path-loss exponent (PLE). For close-in free-space reference distance (CI) model, β is equal to the free-space path gain (FSPG) [21] at $d_0 = 1$ m, and the PLE (α) is set by the scenario, 3.19 for UMi NLOS [13].

II. MEASUREMENT APPROACH

A. UMi OS

Two transmitters were placed on balconies overlooking a campus open area on level 2 ($h_T = 5.2$ m @ 39.499 GHz) and on level 3 ($h_T = 8.9$ m @ 39.501 GHz), enabling the study of height diversity (see Fig. 1). The small frequency offset allowed concurrent measurements using a spectrum analyzer. This minimized errors from pedestrian traffic and environmental dynamics. Equivalent isotropically radiated power (EIRP) continuous-wave (CW) signals of 18.7 dBm were transmitted from horn antennas with $\pm 27^\circ$ half-power beamwidth (HPBW).

For reception, a 25 dBi horn antenna (10° HPBW) was fixed on a rotating table ($h_R = 1.6$ m), enabling signal strength measurements over 360° of azimuth and from -20° to $+40^\circ$ of elevation [1]. Eleven receiver locations were chosen inside the campus as shown in Fig. 2. The three-dimensional (3-D) transmitter–receiver (Tx–Rx) separation distance ranged from 19 to 85 m.

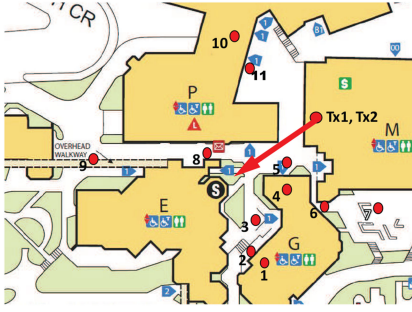


Fig. 2. UMi OS receiver locations: 1, 4, and 10 are indoor; 5 and 11 are LOS. The arrow indicates the Tx bore direction.



Fig. 3. UMi SC Tx antennas looking east on Little Lonsdale.

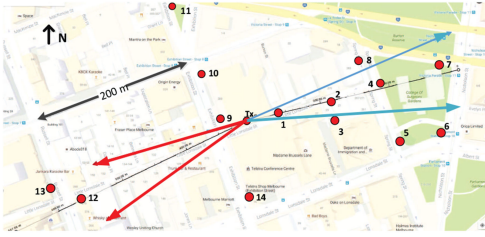


Fig. 4. UMi SC receiver locations: Red and blue arrows indicate 3 dB HPBW of Tx antenna of Fig. 3.

B. UMi SC

For the Melbourne CBD measurements, the Tx was mounted on a first-floor balcony (height = 6.1 m) at the Telstra Exchange building on Little Lonsdale St. (see Fig. 3). Two 33.85 dBm EIRP CW signals were transmitted up or down the street from two 20.5 dBi gain antennas ($\pm 10^\circ$ HPBW) arranged cross-polar with the bore site marked in Fig. 4. Building density was high with a number of very tall structures. The receive antenna was vertically polarized, enabling vertical-to-vertical (co-) and horizontal-to-vertical (cross-) polarization measurements. The receiver setup was as for the OS, and 3-D Tx-Rx distances ranged from 50 to 300 m (see Fig. 4).

III. MEASURED OUTDOOR NLOS PATH-LOSS RESULTS

Two power measurements are defined—the signal from the strongest direction [called “peak” (P_{Peak})] and the sum of all incoming signals [called “omni” (P_{Omni})]. The traditional way to calculate the received “omni” power is to sample the polar reception pattern in angular steps of HPBW (10°) in both azimuth

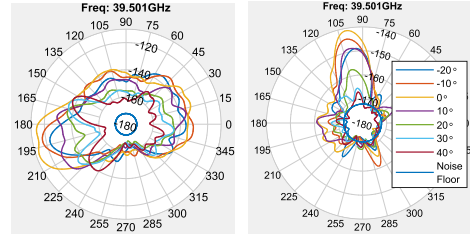


Fig. 5. Angle of arrival (AoA) versus directional path gain for antenna elevations between -20° (dark blue) to 40° (red) in intervals of 10° . (a) Alley entrance at #2. (b) Courtyard, 30 m down the alley at #3. AoA of 90° is due north in Fig. 4.



Fig. 6. Receiver position when (a) looking down the alley at #2 and (b) looking east at #3.

and elevation, weighting each measurement to account for the lower arc as elevation increases, and then, sum [22]

$$P_{\text{Peak}} = \max(P(\theta, \phi))$$

$$P_{\text{Omni}} = \sum \sum P(\theta_i, \phi_j) \cos(\theta_i) \quad (2)$$

where azimuth $\phi_j = 0^\circ$: HPBW: 360° , elevation $\theta_i = -20^\circ$: HPBW: 40° , and $P(\theta, \phi)$ is the received signal power seen by the measuring antenna aperture. After removing the transmitter EIRP and the measurement antenna gain, we obtain the path gains PG_{Peak} and PG_{Omni} .

A. Cross-Street Path Gain in UMi SC

Signal strengths were always strong for the near line-of-sight (LOS) conditions on Little Lonsdale St. (#2, #4, #7, and #12). Strong back and side scattering from walls, parked vehicles, lamp posts, and other street furniture generated broad lobes 15–20 dB below the LOS level. The signal at the head of the alley (position #2) was in direct LOS of the Tx and had a measured peak path gain (PG_{Peak}) of -112.4 dB at $\phi = 199^\circ$ [see Figs. 5(a), 6(a)] and strong back reflections between 350° and 50° . Of high interest is how much the path gain degrades when the receiver moves into the cross streets from the LOS junction. At the courtyard at the end of the 30 m long alley (#3), the signal strength had experienced an additional 28 dB loss in PG_{Peak} [see Figs. 5(b), 6(b)]. In all measured cross streets, the dominant lobes always faced toward the main LOS junction (positions #3, #5, #8, #10, #14) indicating the channeling effect of the street canyon. Back reflections were also apparent, but with greater variability. When signals were weakest, they often came in from higher elevations (e.g., #13 with $+10^\circ$ to $+20^\circ$; #6 with $+10^\circ$).

TABLE II
 SCATTER LOSS INTO CROSS STREETS FROM LOS JUNCTION BASED ON PG_{OMNI}

Location (junction)	Dist. to junction	PG_{omni} at junction (dB)	PG_{omni} cross-street (dB)	Scattering loss (dB)
#3 (#2)	30 m	-105	-135	30
#13 (#12)	20 m	-132	-150	18
#9 (#1)	14 m	-104	-122	18
#10 (#1)	90 m	-104	-137	33
#14 (#1)	112 m	-104	-134	30
#8 (#4)	45 m	-105	-134	29
#5 (#4)	96 m	-105	-150	45

Note: We use the signal strength at #1 to represent the Exhibition/Little Lonsdale junction due to its similar distance to the BS (there was too much traffic within the junction).

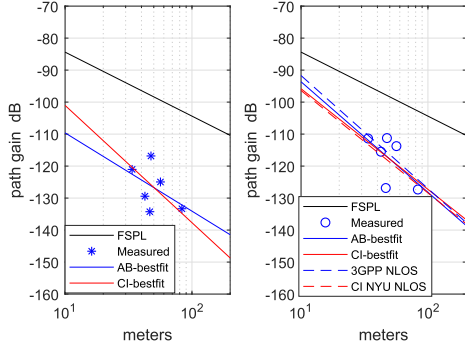

 Fig. 7. Scatter plot of PG_{peak} (left) and PG_{omni} (right) versus distance in UMi OS with BS $h_T = 5.2$ m.

Table II shows PG_{omni} at different positions from which the additional scattering loss, required to penetrate a given distance down a number of cross streets (from the street junction carrying the main LOS signal), is calculated. For example, the first row shows that the additional scatter loss between #3 and the LOS junction #2 is 30 dB. Positions #10, #14, and #8 are all one block (~ 100 m) away from the main LOS street and have similar scatter losses of ~ 31 dB. Some 18 dB of this loss occurs “just around the corner” (#9 and #13), slightly less than the 20 dB value suggested by ITU-R P.1411-9 [23]. The increasing corner loss with increasing distance to the Tx, predicted by [24] was not apparent. Narrower alleys have additional loss (30 dB for #3) as do streets bounded only on one side (45 dB for #5).

B. Path-Loss Model Comparison

For all NLOS measurement locations, PG_{omni} versus distance is compared against a number of channel models (see Figs. 7 and 8) and summarized in Table III. In both figures, the top line represents the well-known FSPG equation. The two solid lines are best-fit lines for AB and CI models, and the dotted lines are based on the CI-NYU and AB-3GPP NLOS parameters.

The AB-bestfit model has two degrees of freedom (β, α) to fit the measured data and has the lowest RMS error (e.g., $\sigma = 7.8$ dB for SC), but can give large anomalies in α and β when the number of points is few and the distance span is small, as is the case here for OS with $h_T = 8.9$ m ($\alpha = 0.9$) and SC ($\alpha = 2$). Therefore, extrapolating outside the measurement range is not recommended as indicated in [13]. The CI-bestfit model has only one degree of freedom (the slope α) and always crosses the

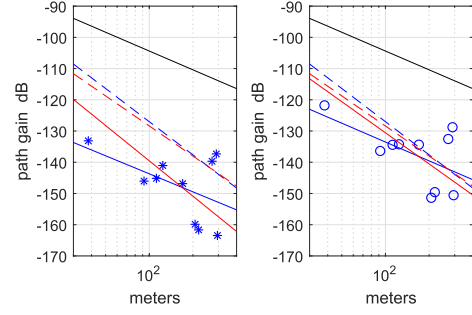

 Fig. 8. Scatter plot of PG_{peak} (left) and PG_{omni} (right) versus distance in UMi SC.

 TABLE III
 PATH-LOSS MODELS BASED ON PG_{OMNI}

Scenario	Models	σ (dB)	α	β (dB)
UMi Open Square	AB-Bestfit	6.0 / 5.4	0.9 / 3.5	-103.8 / -59.1
	CI-Bestfit	6.6 / 5.4	3.2 / 3.1	-64.4 / -64.4
	CI-NYU	6.7 / 5.5	3.2 / 3.2	-64.4 / -64.4
	AB-3GPP	7.5 / 5.6	3.5 / 3.5	-56.4 / -56.4
UMi Street Canyon	AB-Bestfit	7.8	2	-93.5
	CI-Bestfit	8.5	3.3	-64.4
	CI-NYU	8.9	3.2	-64.4
	AB-3GPP	9.5	3.5	-56.4

Note: The two values shown in the table represent measurements for two different BS heights (8.9 m/5.2 m) in UMi OS.

free-space line at $d_0 = 1$ m, giving a larger $\sigma = 8.5$ dB for SC. For the OS scenario, the difference in σ is less than 0.6 dB. Apart from the above-mentioned anomalies, the “bestfit” parameters almost perfectly agree with the specified 3GPP values for both OS and SC (e.g., α values within 3%). The low number of scatter points can reduce the confidence; however, the CI α is robust with one standard deviation error at $\approx \pm 0.16$ (5%) since the β anchor point is far (1.5 decades).

The CI-NYU has lower RMS error than AB-3GPP by less than 1 dB in all scenarios. The values of both are within the range suggested by the standards for OS (see Table I), whereas for SC, both are out of the range, CI-NYU by 0.7 dB and AB-3GPP by 1.7 dB, indicating a greater difficulty in predicting PL from distance in NLOS SCs.

All the 3GPP models are based on omni PG and, therefore, include signals from all directions. However, for beam-steered directional antennas, peak PG might be more appropriate. The cumulative distribution functions (CDFs) of peak and omni PGs, expressed relative to the FSPG, are shown in Fig. 9(a) and (b) for OS and SC, respectively. Both measurement locations show an almost constant offset between peak and omni, averaging approximately 10 dB, making the 3GPP models appear optimistic unless handled correctly [19].

C. Height Gain, Diversity, and XPD

1) *Height Gain and Diversity in UMi OS*: The two Tx antennas will, in general, provide different path gains due to their different heights, and their separation could be used to provide macro-diversity against shadowing. The height gain between Tx antenna heights h_1 and h_2 at NLOS position i is

$$\Delta G(h_1, h_2, i) = (PG_{h_1}(i) - PG_{h_2}(i)), \quad h_1 > h_2. \quad (3)$$

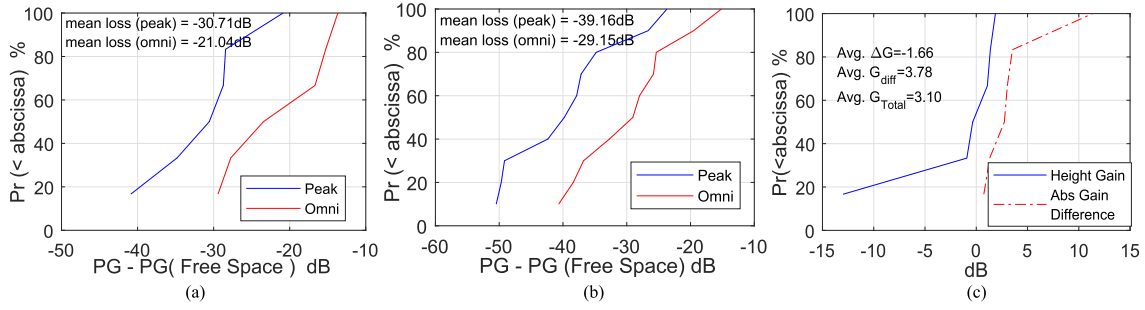


Fig. 9. CDF of additional PG w.r.t. FSPG (a) OS and (b) SC, and (c) CDF of OS height gain, ΔG , and absolute gain difference G_{diff} .

The average height gain is then $\overline{\Delta G} = \sum_i \Delta G(i)/N$, where h_1, h_2 are dropped for conciseness. The absolute gain difference due to diversity is isolated by removing the $\overline{\Delta G}$ bias from the upper antenna

$$G_{\text{diff}}(i) = \text{abs}[(PG_{h_1}(i) - \overline{\Delta G}) - PG_{h_2}(i)]. \quad (4)$$

The mean absolute gain difference is $\overline{G_{\text{diff}}} = \sum_i G_{\text{diff}}(i)/N$. Thus, the diversity gain (DG) would be half of this value, since the equiprobability of the diversity antenna being stronger than the main antenna $DG = \overline{G_{\text{diff}}}/2$.

The CDFs of height gain and absolute gain difference are shown in Fig. 9(c). Interestingly, the average height gain of $\overline{\Delta G} = -1.66$ dB indicates that the antenna from the lower balcony has, on average, the stronger signal. Further analysis shows that the averaging was dominated by one position (#6 at $\Delta G(i) = -13$ dB), indicating strong scatters (reflections) from the lower balcony, not seen from the upper balcony. The red plot shows the CDF of the absolute gain difference—the difference between the strongest and weakest antenna due to diversity. It varies between 1 and 11 dB, with mean $\overline{G_{\text{diff}}} = 3.78$ dB. The DG would be 1.89 dB in this case. The average absolute total gain difference $G_{\text{Total}} = \text{abs}[(PG_{h_1}(i) - \overline{\Delta G}) - PG_{h_2}(i)] = 3.1$ dB includes both diversity and height gain effects. Half of this value gives the combined height and diversity gain (DHG) of 1.55 dB.

Interestingly, had the dominating position (#6) been discounted, the average height gain ($\overline{\Delta G}$) would move to 0.61 dB. Similarly the DG would be 0.5 dB and the DHG would be 0.56 dB. The low values indicate little improvement using height diversity for the OS scenario. This is contrary to the results of [17], which showed a height gain of almost 3 dB over the same height range.

2) *XPD in UMi SC*: The XPD is defined as the ratio between the cross-polar component (H to V) to the copolar component (V to V). The CDF of XPD [see Fig. 10(a)] implies that the isolation between the H and V components holds up well in these NLOS conditions despite multiple reflections. The median values indicate 10.1 dB XPD for “peak” and 11.6 dB for “omni.” The respective average values are 11.7 and 12.3 dB, and the worst-case value is 5.8 dB, which can enhance diversity and multiple-input–multiple-output (MIMO) performance. (The channel dominates the depolarization since the antenna XPD was measured at 27 dB.) On a “peak” basis, XPD deteriorates 2.5 dB for every decade dB increase in path loss [over the measurement range, Fig. 10(b)]. However, on an “omni” basis, as used by channel models, there appears to be zero correlation

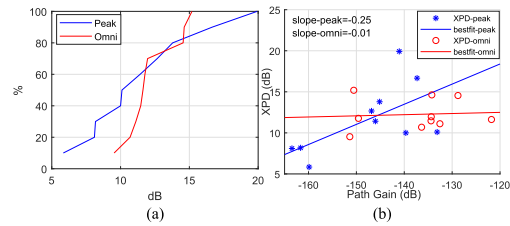


Fig. 10. (a) CDF of XPD in UMi SC. (b) XPD versus PG.

with path loss. This supports the use of a fixed offset term in channel models rather than varying the PLE (α) to accommodate for XPD effects [25].

IV. CONCLUSION

UMi NLOS measurements are performed in OS and SC. The parameters extracted by the reconstructed omnidirectional measurements closely match with the path-loss parameters specified in the 3GPP standard. The AB model has the lowest bestfit RMS error, but requires a large number of points to get consistent α and β values. Of the predefined models, the CI-NYU outperforms AB-3GPP having up to 1 dB reduced σ values. However, for SC, the measured σ values are generally ~ 1 dB higher than the 3GPP specification. We use measurements from two antenna heights to isolate height gain and diversity gain contributions. The negative average height gain in UMi OS indicated the stronger signal from the lower height transmitter. However, omitting one dominant position (#6), the height gain was marginal as was the diversity gain (0.5 dB). Height diversity appears to be ineffective on these measurements, which is contrary to [17].

The scattering loss into CBD side streets was measured at 18 dB for “just around the corner” rising to 31 dB ~ 100 m down the side street. Narrower streets have higher losses. Although it should be possible to place microcells at every major junction (every 200 m) and get a reasonable signal penetration into side alleys, the signal in the side alley often has reduced directional diversity (comes from one direction only) making reception sensitive to body shadowing effects. No such problem exists in the LOS streets where back and side scattered signals remain strong. The median XPD measured in the CBD was 11.6 dB, dropping to 5.8 dB at the weakest signal location. XPD drops with path loss on a “peak” basis, but appeared uncorrelated on an “omni” basis.

REFERENCES

- [1] S. Dahal, S. Ahmed, H. King, and M. Faulkner, "Antenna gain in a millimetre-wave multipath environment," in *Proc. IEEE 3rd Aust. Microw. Symp.*, 2018, pp. 93–94.
- [2] S. Dahal, M. Faulkner, H. King, and S. Ahmed, "27.1 GHz millimetre wave propagation measurements for 5G urban macro areas," in *Proc. IEEE 85th Int. Conf. Veh. Technol.*, 2017, pp. 1–5.
- [3] M. Cudak, T. Kovarik, T. A. Thomas, A. Ghosh, Y. Kishiyama, and T. Nakamura, "Experimental mm wave 5G cellular system," in *Proc. IEEE Globecom Workshops*, 2014, pp. 377–381.
- [4] A. Ghosh *et al.*, "Millimeter-wave enhanced local area systems: A high-data-rate approach for future wireless networks," *IEEE J. Sel. Areas Commun.*, vol. 32, no. 6, pp. 1152–1163, Jun. 2014.
- [5] S. Hur, Y.-J. Cho, J. Lee, N.-G. Kang, J. Park, and H. Benn, "Synchronous channel sounder using horn antenna and indoor measurements on 28 GHz," in *Proc. IEEE Int. Black Sea Conf. Commun. Netw.*, 2014, pp. 83–87.
- [6] W. Roh *et al.*, "Millimeter-wave beamforming as an enabling technology for 5G cellular communications: Theoretical feasibility and prototype results," *IEEE Commun. Mag.*, vol. 52, no. 2, pp. 106–113, Feb. 2014.
- [7] Y. Azar *et al.*, "28 GHz propagation measurements for outdoor cellular communications using steerable beam antennas in New York City," in *Proc. IEEE Int. Conf. Commun.*, 2013, pp. 5143–5147.
- [8] M. R. Akdeniz *et al.*, "Millimeter wave channel modeling and cellular capacity evaluation," *IEEE J. Sel. Areas Commun.*, vol. 32, no. 6, pp. 1164–1179, Jun. 2014.
- [9] H. Zhao *et al.*, "28 GHz millimeter wave cellular communication measurements for reflection and penetration loss in and around buildings in New York City," in *Proc. IEEE Int. Conf. Commun.*, 2013, pp. 5163–5167.
- [10] M. Samimi *et al.*, "28 GHz angle of arrival and angle of departure analysis for outdoor cellular communications using steerable beam antennas in New York City," in *Proc. IEEE 77th Veh. Technol. Conf.*, 2013, pp. 1–6.
- [11] H. C. Nguyen, G. R. MacCartney, T. Thomas, T. S. Rappaport, B. Vejlggaard, and P. Mogensen, "Evaluation of empirical ray-tracing model for an urban outdoor scenario at 73 GHz E-band," in *Proc. IEEE 80th Veh. Technol. Conf.*, 2014, pp. 1–6.
- [12] M. Kyro, V.-M. Kolmonen, and P. Vainikainen, "Experimental propagation channel characterization of mm-wave radio links in urban scenarios," *IEEE Antennas Wireless Propag. Lett.*, vol. 11, pp. 865–868, 2012.
- [13] S. Sun *et al.*, "Investigation of prediction accuracy, sensitivity, and parameter stability of large-scale propagation path loss models for 5G wireless communications," *IEEE Trans. Veh. Technol.*, vol. 65, no. 5, pp. 2843–2860, May 2016.
- [14] S. S. Oh *et al.*, "Path loss characteristics for urban street canyon environments from 0.75 to 24 GHz," in *Proc. IEEE 88th Veh. Technol. Conf.*, 2019, pp. 1–3.
- [15] S. S. Oh *et al.*, "An empirical propagation prediction model for urban street canyon environments at 6, 10, and 18 GHz," *Microw. Opt. Technol. Lett.*, vol. 61, no. 6, pp. 1574–1578, 2019.
- [16] F. Qamar *et al.*, "Investigation of future 5G-IoT millimeter-wave network performance at 38 GHz for urban microcell outdoor environment," *Electronics*, vol. 8, no. 5, 2019, Art. no. 495.
- [17] Z. Zhong, C. Li, J. Zhao, and X. Zhang, "Height-dependent path loss model and large-scale characteristics analysis of 28 GHz and 38.6 GHz in urban micro scenarios," in *Proc. 11th Eur. Conf. Antennas Propag.*, 2017, pp. 1818–1822.
- [18] M. N. Hindia, A. M. Al-Samman, T. A. Rahman, and T. Yazdani, "Outdoor large-scale path loss characterization in an urban environment at 26, 28, 36, and 38 GHz," *Phys. Commun.*, vol. 27, pp. 150–160, 2018.
- [19] ETSI 3rd Generation Partnership Project, "Study on channel model for frequency spectrum above 6 GHz," Eur. Telecommun. Standards Inst., Sophia Antipolis, France, ETSI Tech. Rep. 138 900 V14.2.0, Jun. 2017.
- [20] P. Kyosti, "Winner II channel models," Inf. Soc. Technol., Tech. Rep. IST-4-027756 WINNER II D1.1.2 V1.2, Oulu, Finland, 2007.
- [21] T. S. Rappaport, *Wireless Communications: Principles and Practice*, vol. 2. Englewood Cliffs, NJ, USA: Prentice-Hall, 1996.
- [22] G. R. MacCartney, M. K. Samimi, and T. S. Rappaport, "Omnidirectional path loss models in New York City at 28 GHz and 73 GHz," in *Proc. IEEE 25th Annu. Int. Symp. Personal, Indoor, Mobile Radio Commun.*, 2014, pp. 227–231.
- [23] *Propagation Data and Prediction Methods for the Planning of Short-Range Outdoor Radiocommunication Systems and Radio Local Area Networks in the Frequency Range 300 MHz to 100 GHz*, Rec. P.1411-9, Int. Telecommun. Union, Geneva, Switzerland, Jun. 2017.
- [24] K.-W. Kim and S.-J. Oh, "Geometric optics-based propagation prediction model in urban street canyon environments," *IEEE Antennas Wireless Propag. Lett.*, vol. 15, pp. 1128–1131, 2016.
- [25] A. Al-Samman, T. Rahman, M. Azmi, M. Hindia, I. Khan, and E. Hanafi, "Statistical modelling and characterization of experimental mm-wave indoor channels for future 5G wireless communication networks," *PLoS One*, vol. 11, no. 9, 2016, Art. no. e0163034.

OFFICE FOR RESEARCH TRAINING, QUALITY AND INTEGRITY

DECLARATION OF CO-AUTHORSHIP AND CO-CONTRIBUTION: PAPERS INCORPORATED IN THESIS

This declaration is to be completed for each conjointly authored publication and placed at the beginning of the thesis chapter in which the publication appears.

1. PUBLICATION DETAILS (to be completed by the candidate)

Title of Paper/Journal/Book:	Millimetre Wave Propagation Reverse Measurements for 5G Urban Micro Scenario		
Surname:	Dahal	First name:	Saurav
Institute:	Institute for Sustainable Industries and Liveable	Candidate's Contribution (%):	80
Status:		Date:	
Accepted and in press:	<input type="checkbox"/>	Date:	
Published:	<input checked="" type="checkbox"/>	Date:	28-04-2019

2. CANDIDATE DECLARATION

I declare that the publication above meets the requirements to be included in the thesis as outlined in the HDR Policy and related Procedures – policy.vu.edu.au.

<input type="text"/>	<input type="text"/>	18-12-2019
	Signature	Date

3. CO-AUTHOR(S) DECLARATION

In the case of the above publication, the following authors contributed to the work as follows:

The undersigned certify that:

1. They meet criteria for authorship in that they have participated in the conception, execution or interpretation of at least that part of the publication in their field of expertise;
2. They take public responsibility for their part of the publication, except for the responsible author who accepts overall responsibility for the publication;



- 3. There are no other authors of the publication according to these criteria;
- 4. Potential conflicts of interest have been disclosed to a) granting bodies, b) the editor or publisher of journals or other publications, and c) the head of the responsible academic unit; and
- 5. The original data will be held for at least five years from the date indicated below and is stored at the following **location(s)**:

Name(s) of Co-Author(s)	Contribution (%)	Nature of Contribution	Signature	Date
Euripides A. Stephanou	5	Helped in measurements		24/02/2020
Nathaniel Talukdar	5	Helped in measurements		21/02/2020
Shabbir Ahmed	2.5	Review of drafts		26/02/20
Horace King	2.5	Review of drafts		26/02/20
Mike Faulkner	5	Overall supervision and contribution to theory		28/02/2020

Updated: September 2019

Chapter 8

Millimetre Wave Propagation Reverse Measurements for 5G Urban Micro Scenario

8.1 Overview

In Chapter 7, we presented mmWave channel characterization for UMi scenarios. High gain directive antennas are likely to be used in the next generation of mobile systems. These antennas have the potential to increase the spectral efficiency through MIMO processing, provided the channel is sufficiently compliant. Similarly, beamforming schemes work better if the base station can resolve users with sufficient angular separation. A double-directional channel gives both the path loss as well as angle of arrival and departure information. In this Chapter, we present double directional experimental

measurements for a UMi OS scenario. This study provides an insight into the MIMO and beamforming performance of mmWaves in this scenario.

We show that multiple AoD's from the UE can have a single AoA at the BS indicating a potential limitation on the number of usable MIMO streams (rank reduction) (see eq. 1.12) [38].

8.2 Publication

This paper has been published in IEEE Vehicular Technology (VTC) Conference 2019.

S. Dahal, E. A. Stephanou, N. Talukdar, S. Ahmed, H. King and M. Faulkner, "Millimetre Wave Propagation Reverse Measurements for 5G Urban Micro Scenario," 2019 IEEE 89th Vehicular Technology Conference (VTC2019-Spring), Kuala Lumpur, Malaysia, 2019, pp. 1-5, doi: 10.1109/VTCSpring.2019.8746428.

The full-text of this article is subject to copyright restrictions, and cannot be included in the online version of the thesis.

The full-text is available from: <https://ieeexplore.ieee.org/document/8746428>

OFFICE FOR RESEARCH TRAINING, QUALITY AND INTEGRITY

DECLARATION OF CO-AUTHORSHIP AND CO-CONTRIBUTION: PAPERS INCORPORATED IN THESIS

This declaration is to be completed for each conjointly authored publication and placed at the beginning of the thesis chapter in which the publication appears.

1. PUBLICATION DETAILS (to be completed by the candidate)

Title of Paper/Journal/Book:	Slant-Path Building Entry Loss at 24 GHz		
Surname:	Dahal	First name:	Saurav
Institute:	Institute for Sustainable Industries and Liveable	Candidate's Contribution (%):	80
Status:		Date:	
Accepted and in press:	<input type="checkbox"/>	Date:	
Published:	<input checked="" type="checkbox"/>	Date:	22-10-2019

2. CANDIDATE DECLARATION

I declare that the publication above meets the requirements to be included in the thesis as outlined in the HDR Policy and related Procedures – policy.vu.edu.au.

	18-12-2019
Signature	Date

3. CO-AUTHOR(S) DECLARATION

In the case of the above publication, the following authors contributed to the work as follows:

The undersigned certify that:

1. They meet criteria for authorship in that they have participated in the conception, execution or interpretation of at least that part of the publication in their field of expertise;
2. They take public responsibility for their part of the publication, except for the responsible author who accepts overall responsibility for the publication;



- 3. There are no other authors of the publication according to these criteria;
- 4. Potential conflicts of interest have been disclosed to a) granting bodies, b) the editor or publisher of journals or other publications, and c) the head of the responsible academic unit; and
- 5. The original data will be held for at least five years from the date indicated below and is stored at the following location(s):

Name(s) of Co-Author(s)	Contribution (%)	Nature of Contribution	Signature	Date
Shabbir Ahmed	2.5	Helped in measurements		26/02/20
Horace King	2.5	Helped in measurements		26/02/20
Ganesh Bharatula	2.5	Review of draft		20-02-20
John Campbell	2.5	Review of draft		14-2-20
Mike Faulkner	10	Overall supervision and contribution to theory		14-2-20

Updated: September 2019

Chapter 9

Slant-Path Building Entry Loss at 24

Ghz

9.1 Overview

In Chapters 7 and 8, we presented the single and double-directional propagation characteristics of mmWaves in UMi scenarios. Millimetre waves are subject to higher attenuation due to scattering, diffraction and building penetration. In this chapter, we provide mmWave propagation channel measurements in an outdoor to indoor (O2I) environment where the outdoor station is a high altitude platform (such as from satellite, balloons, drones). Sometimes it is desirable to minimise transmission loss to inside the building, and sometimes it is required to maximise transmission loss, depending on whether the signals are desired or interference. The latter occurs when signals emanating from inside the building interfere with a satellite's uplink. An example being Australia's NBN

satellite uplink (28.5 GHz to 29.1 GHz) which co-exists with some of the proposed mmWave 5G spectra.

The initial path loss measurements were taken using the high gain narrow beam ($\pm 5^\circ$) antenna. It was found that the limited vertical scan (-20° to $+40^\circ$) did not capture all the incoming signals from high slant angle transmissions. The measurements were then repeated with a lower gain antenna ($\pm 23^\circ$) with enhanced vertical capture capability ($\pm 83^\circ$). The collected data was used to synthesise the response of an isotropic antenna and the results were submitted to the ITU [7] for their May 2017 channel model. The model did not include the effect of directional antennas, which was left as future work [152].

Thus, in this chapter, we present building entry loss results featuring mmWaves, elevation slant paths, building depths, directional antennas and isotropic antennas with full spherical scanning. This study provides an insight into

- the effect of beamforming on desired signals from HAPs
- the effect of beamforming on satellite co-existing uplink channels
- the effect of terminal depth on BEL (from the exposed outside wall)

We show that, compared to isotropic antennas, beamforming increases the desired HAP signal, while it also decreases interference into the satellite uplink.

9.2 Publication

The following article has been published in IEEE Access.

Received September 16, 2019, accepted October 12, 2019, date of publication October 22, 2019,
date of current version November 12, 2019.

Digital Object Identifier 10.1109/ACCESS.2019.2948938

Slant-Path Building Entry Loss at 24 Ghz

SAURAV DAHAL¹, (Student Member, IEEE), **SHABBIR AHMED**¹, (Member, IEEE),
HORACE KING¹, (Senior Member, IEEE), **GANESH BHARATULA**²,
JOHN CAMPBELL², (Member, IEEE), AND **MICHAEL FAULKNER**¹, (Member, IEEE)

¹Institute for Sustainable Industries and Liveable Cities, Victoria University, Melbourne, VIC 3011, Australia

²Telstra Corp Ltd., Melbourne, VIC 3000, Australia

Corresponding author: Saurav Dahal (saurav.dahal@live.vu.edu.au)

This research was supported by Telstra Corp Ltd.

ABSTRACT Results from an outdoor to indoor (O2I) measurement campaign emulating the satellite to indoor propagation channel at millimetre wave frequencies are presented in this paper. A link between a transmitter at a high altitude and a receiver placed at several locations on different floors of a building provided different slant path angles from the transmitter. The indoor receiver uses directional antennas with full spherical scanning capability which allows the measurement of signal strength as a function of antenna pointing direction, thus providing localized angle of arrival (AoA) information. Two directional horn antennas with different beamwidths are used for the indoor receiver. This allows the modelling of equipment incorporating adaptive beamforming. We synthesise the isotropic (0 dBi) antenna performance to enable comparison with the recent ITU (International Telecommunications Union) model. We observed that the mean building entry loss (BEL) increases by 0.43 dB per degree of slant elevation angle, almost twice the ITU recommendation. The signal decay with distance into the building had path loss slopes varying between 1.9 dB/m for a slant angle of 34° and 3.4 dB/m for a slant angle of 51°. We show that high gain narrow beam antennas outperform lower gain wider beamwidth antennas for reception (signal maximisation), but the performance improvement is significantly less than the gain difference between the two antennas. In terms of coexistence (interference minimisation), random alignment of the beam direction modestly enhances building entry loss (≈6 dB to 9 dB) which, after a certain limit, changes little with antenna gain.

INDEX TERMS Beamforming, building entry loss, indoor coverage, millimeter wave, penetration loss, satellite co-existence, slant angle.

I. INTRODUCTION

Millimetre waves (mmWave) enable an order of magnitude increase in bandwidth to greater than 1 GHz, but are subject to higher attenuation due to number of factors such as scattering, diffraction and building penetration. High Altitude Platforms (HAPs) want good indoor coverage whereas satellites want to restrict indoor coverage due to potential interference from mobile terminals into the satellite uplink channels. Building Entry Loss (BEL) is a parameter which determines the additional loss beyond that expected from just outside the building structure [1]. BEL measurements have been reported for frequencies below 6 GHz [2]–[6] but less have been reported for frequencies above 6 GHz [2], [7], [8]. A compilation of empirical data on BEL from different authors in different countries is available in [2], but only

three out of the thirteen compiled mmWave measurements included slant angle of arrivals (one of which is a sub-set of the measurements presented here). Standardized models from organisations such as Third Generation Partnership Project (3GPP) provide only 0 dBi isotropic path loss characteristics as functions of distance and frequency [9]. However, directional beamforming is normally required for reliable mmWave links, therefore the isotropic characteristics may be less informative for the design and evaluation of systems employing directional antennas (or beamforming). Authors in [10]–[12] investigated the effect of antenna beamwidth on the BEL at 28, 32 and 38 GHz and found BEL increases as the beamwidth narrows. However, these were based on transmitter (Tx) and receiver (Rx) antennas at the same height. A ray tracing study has been done to study the BEL for a single slant path in [13]. To the best of our knowledge, there are very few reported BEL measurements that include mmWaves, directional antennas, slant path and full spherical

The associate editor coordinating the review of this manuscript and approving it for publication was Chow-Yen-Desmond Sim¹.

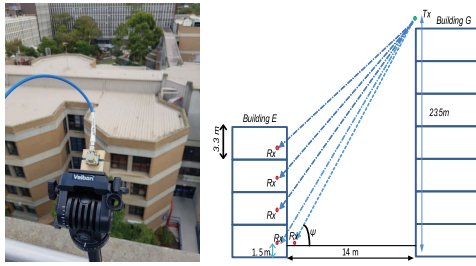


FIGURE 1. Building E from the Tx site on building G.

scanning over all azimuth and elevation angles ($0^\circ > \phi > 360^\circ$, $-90^\circ > \theta > +90^\circ$).

For frequencies below 6 GHz, the ITU-R Report M.2135 [14] reported a linear increase in path loss with internal distance, d , from the illuminated external wall, with a path loss slope of $m = 0.5$ dB/m. Authors in [7] studied the variation of BEL with in-building depth for 24 to 31 GHz and indicated that the increase in the path loss with internal distance at these frequencies could be higher than the $m * d$ suggested by the ITU-R Report M.2135. Other researchers measured m values between 0.2 dB/m and 1.0 dB/m for upward looking (i.e. transmitter on the ground) elevation angles between 0° to 30° [15], indicating a large variability when operating at mmWave frequencies. Here we report measurements for downward looking (elevated transmitter see Fig. 1) slant angles (ψ) of over 30° and show even greater m values.

Recently a model for BEL has been developed by ITU for frequencies up to 100 GHz given by a combination of two log-normal distributions, based upon the frequency and the slant angle as:

$$L_{BE}(P) = 10 \log(10^{0.1A(P)} + 10^{0.1B(P)} + 10^{0.1C}) \text{ dB} \quad (1)$$

where $L_{BE}(P)$ is the BEL not exceeded for probability P , and other variables defined as in the Appendix [16], [17]. The model specifies isotropic antennas, has a single median loss term and is not a function of d ; the depth into the building being incorporated into the distribution itself. We compare our mmWave BEL measurements with this model.

We present results from a measurement campaign on slant-path building entry loss in the K/Ka bands around 24 GHz. We calibrated out the errors wherever possible, but some were out of our control such as human movement and small changes in environment between the two receive horn antenna measurement campaigns. Previous experience has shown that these differences average out in terms of macro parameters which are based on many measurements.

The signal received from a high rooftop transmitter into different floors of an adjacent building was used to determine path loss variation with slant angle, ψ . This enables the assessment of a) the unwanted signal leakage from transmitters within a building into a satellite's uplink channel for co-existence purposes and b) the desired signal in-building coverage from a high altitude platform (HAP) such as a drone

or a balloon. The two use cases are identical when isotropic antennas are used for the indoor unit, but this changes when directional antennas are used. Indoor units employing adaptive antennas will adjust differently depending on whether the incoming signal is desired or not. Phase array antennas will be incorporated into future 5G user equipment to overcome increase path loss at mmWave frequencies. Thus, it is necessary to study how adaptive beamforming affects the building entry loss. We derive from our measurements the behaviour of a phase array antenna having the same beamwidths (gains) of our horn. Measurements were performed using two horn antennas of gain 9.6 dBi and 23.5 dBi from the same locations to identify how gain affects the results. The two antennas broadly model what can be expected from a user equipment (UE) with a 4 patch array (6 dB array factor + 5 dBi patch = 11 dBi) (approximately similar to 9.6 dBi gain horn) or a customer premises equipment (CPE) with a 64 patch array (18 dB array factor + 5 dBi patch = 23 dBi) (approximately similar to 23.5 dBi horn). In addition, we synthesise the isotropic antenna performance on which most channel models are based [16].

II. MEASUREMENT APPROACH

The measurement campaign was undertaken on the campus of Victoria University in Melbourne, Australia. The target building comprised of steel-reinforced concrete for structure and floors, with double-brick infill for external walls and a mix of double-brick and stud-and-plaster internal walls, topped by a near-flat zinc-coated ribbed-steel roof. The windows are single-glazed and set into aluminium frames. The lower 25% of the windows are reinforced with internal wire mesh. The general structural situation of building E under test is shown in Fig. 1, including the two transmitting antennas (Tx2 shown only) on top of building G. The building can generally be considered as 'traditional masonry construction' with minimal thermal efficiency measures.

The transmit horn antennas illuminated two of the target building's tower sections and were down-tilted and adjusted for bore-sight illumination of the particular target floor (Fig. 2). Each floor provides a certain slant-angle of incidence. Both antennas transmitted a 24 GHz continuous-wave (CW) signal. A small frequency offset of 2 MHz between the two transmitted signals was used to identify each transmission.

The 'mobile' receiver (Rx) consisted of a calibrated standard horn antenna, placed on a rotating table, fed into a swept-frequency spectrum analyser; thus allowing concurrent measurements of the two slightly offset transmitted frequencies. The first set of slant path measurements was taken with the narrow half power beamwidth (HPBW) antenna ($\pm 5^\circ$, 23.5 dBi gain, here termed as 'narrow beam' (NB)). The azimuth (ϕ) coverage was in 7° steps over 360° , but the antenna size mechanically restricted the vertical coverage (θ) to seven steps of 10° , covering elevations between -25° to $+45^\circ$ [19], which in normal circumstances is more than enough to capture all received multipaths [13], [20]. However,

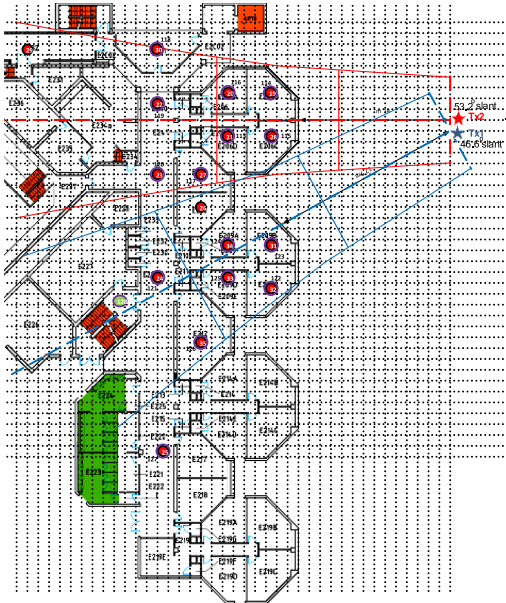


FIGURE 2. Receiver locations at level 2 of target building E. We replicate the positions on each floor as far as practically possible. Red and blue lines show the location within the HPBW of the transmit antenna. Receiver locations at level 1 in [18].



FIGURE 3. Modified receiver with 9.6 dBi antenna.

since we are dealing with signals from high altitude platforms, some multipaths could be missed. The measurements were repeated from the same locations with a smaller, but less directive antenna of $\pm 23^\circ$ HPBW (9.6 dBi, here termed as ‘wide beam’ (WB)), enabling expanded θ coverage between $+83^\circ$ and -83° from four pointing elevations of $+60^\circ$, $+20^\circ$, -20° , -60° (Fig. 3), giving close to full spherical coverage. In both cases the measurements are oversampled in the azimuth angle, ϕ , enabling interpolation down to 1° , but are close to critically sampled in the elevation angle θ making interpolation difficult.

For each orientation of the receiver horn (θ, ϕ), the spectrum analyser made 10 sweeps and recorded the average received power over these sweeps, and this process repeated

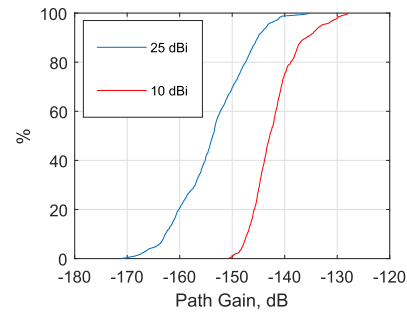


FIGURE 4. CDF of $PG(\theta, \phi)$ over all θ and ϕ measurement angles at position 2.

3 times. The received power $P(\theta, \phi)$ was used to obtain the mean path gain $PG(\theta, \phi)$ by removing the Tx Effective Isotropic Radiated Power (EIRP) and the Rx antenna gain, $G_{Rx}(boresight)$.

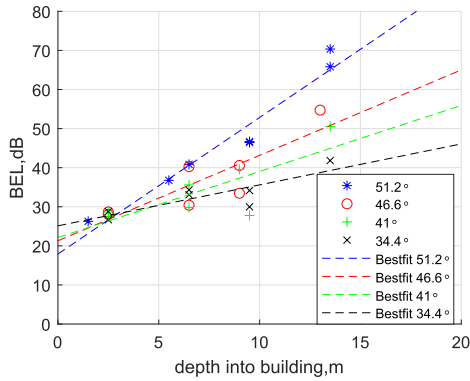
As an example, Fig. 4 shows the CDF (cumulative distribution function) of the directional dependent path gain ($PG(\theta, \phi)$) at position 2 (level 1) directly below position 20 on level 2 (Fig. 2) over all antenna pointing directions from the NB (23.5 dBi) and the WB (9.6 dBi) antenna. As $PG(\theta, \phi)$ is based on the *normalised* antenna radiation patterns ($G_{Rx}(boresight)} = 0$ dBi) and does not include the Rx antenna gain, the NB antenna has lower $PG(\theta, \phi)$ compared to the WB antenna, since it is capturing less signal. The angular averaging effect of the WB antenna is evident in the reduced null depth and reduced dynamic range of the RHS (red) trace.

The signal level just outside the building is necessary as a reference for the BEL calculations, and is calculated from the free space path loss based on the 3D link distance from the transmitter (Fig. 2). Ground level measurements were used as a check and agreed within 0.5 dB of the calculated free space path loss (FSPL).

III. RESULTS

For each measurement location and each antenna we extracted the peak path gain (PG_{peak}) and reconstructed the isotropic (or omni) path gain (PG_{iso}) from the measured signals as follows [18], [21], [22].

For PG_{peak} , the path gain from the strongest direction is taken i.e. $PG_{peak} = \max(PG(\theta, \phi))$, where $PG(\theta, \phi)$ is the path gain measured by the Rx antenna aperture. For PG_{iso} , we first sampled the polar path gain pattern in angular steps of HPBW in both azimuth and elevation, weighting each measurement to account for the lower arc as elevation increases and then sum i.e. $PG_{iso} = \sum \sum PG(\theta_i, \phi_j) \cos(\theta_i)$, where azimuth $\phi_j = 0^\circ : HPBW : 360^\circ$ and elevation $\theta_i = -90^\circ : HPBW : 90^\circ$. In theory, both antennas should give the same ‘isotropic’ result for the same location, but in practice there is some variance since the measurements were not taken concurrently, and there was a bias due to the mechanically constrained elevation search angles, θ_i particularly for the NB antenna. Synthesis based on the WB antenna would


FIGURE 5. Isotropic BEL vs depth based on NB antenna for Tx1.

therefore give the closest isotropic approximation. Next we discuss BEL based upon these extracted PGs.

BEL WITH ISOTROPIC ANTENNAS

Building Entry Loss (BEL) (L_{BE}) is the difference between the measured PGs and the reference free space path gain (FSPG) obtained outside the illuminated face of the building structure [1];

$$L_{BE_{xxx}} = FSPG - PG_{yyy} \quad (2)$$

Thus BEL ($L_{BE_{xxx}}$) can be “minimum” ($L_{BE_{min}}$) or “isotropic” ($L_{BE_{iso}}$) or “directional” ($L_{BE}(\theta, \phi)$), corresponding to which path gain PG_{yyy} is used, PG_{peak} , PG_{iso} or $PG(\theta, \phi)$ respectively. BEL increases with depth into the building and is usually modelled by a linear dB variation with building depth (eq. 3)

$$L_{BE_{iso}}(d) [dB] = c + m d \quad (3)$$

where, d and m have been defined previously and c represents the loss through the building’s outer wall measured at the facing wall’s internal edge ($d = 0$). However the odd shape of the construction, with different angled faces and multiple entry points (windows) at different depths into the building made c more of an aggregate quantity. Therefore c was obtained along with m in a minimum mean square error (MMSE) estimate of the ‘line-of-best-fit’. We also explored a power law variation based on the AB model [23]. In all cases, the linear model gave at least a 1 dB closer fit than the AB model for our measurements.

Fig. 5 and Fig. 6 show the scatter plot of the isotropic BEL ($L_{BE_{iso}}$) with building depth into the south tower from Tx1 for different slant angles (ψ) corresponding to each floor level. Generally, BEL increases with increased slant angle and this applies to both measurement antennas. As expected, the BEL increases as the measurement locations recede deeper inside the building and the variance increases, suggesting the existence of a complex multipath environment within the building. The ‘line of best fit’ for each floor shows the expected steeper slope (increase in m) with increase in

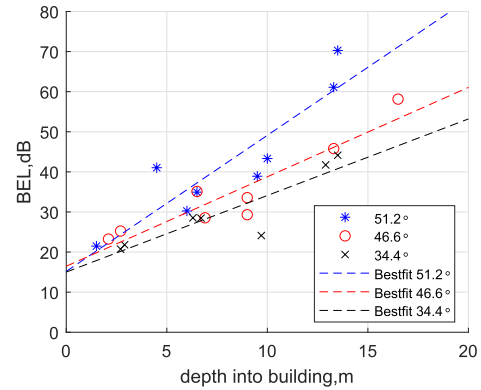

FIGURE 6. Isotropic BEL vs depth based on WB antenna for Tx1.

TABLE 1. BEL parameters with WB and NB antenna for Tx1.

Lvl	slant ψ	Bestfit (Isotropic)					
		σ (dB)		m		c (dB)	
		WB	NB	WB	NB	WB	NB
1	51.2	6.5	3.4	3.4	3.4	15.2	17.9
2	46.6	4.0	4.4	2.2	2.2	16.5	21.3
3	41.0	-	4.9	-	1.7	-	22.1
4	34.4	3.9	2.5	1.9	1.1	15.0	25.1

TABLE 2. Mean BEL with WB and NB antenna.

Lvl	Slant ψ	Tx1				Slant ψ	Tx2			
		$L_{BE_{min}}$		$L_{BE_{iso}}$			$L_{BE_{min}}$		$L_{BE_{iso}}$	
		WB	NB	WB	NB		WB	NB	WB	NB
1	51.2°	46.6	58.7	42.7	47.6	57.5°	43.7	55.2	40.6	44.8
2	46.6°	36.9	44.8	34.9	36.6	53.2°	41.2	53.6	38.1	43.7
3	41.0°	-	42.1	-	34.2	47.8°	37.9	46.1	34.4	37.9
4	34.4°	33.2	39.9	29.9	32.7	40.8°	37.2	43.5	33.8	34.9

slant angle, ψ , which is consistent with the more vertically orientated floor-ceiling reflections inside the building. Details of the ‘line-of-best-fit’ with, m , c are shown in Table 1 for Tx1 where σ is the standard deviation of the fit. Both NB and WB antennas have a similar path loss slope, $m = 3.4$ dB/m on level 1 ($\psi = 51.2^\circ$), but this decreases to $m = 1.1$ and 1.9 for the NB and WB antennas respectively on level 4 ($\psi = 34.4^\circ$). These figures are much higher than $m = 0.5$ dB/m for the M.2135 ITU model for <6 GHz [14] and the $0.7 \sin \psi$ variation in m for frequencies up to 38 GHz proposed by [15]. This is due to the higher slant angles under test and the internal walls and heavy clutter within the building. The effective loss through the buildings exterior wall (skin) $c \approx 15.3$ dB as measured by the WB antenna where as it is ≈ 21.5 dB as measured by the NB antenna. The latter measurement partially reflects the reduced signal collection from the mechanically constrained elevation angle, θ , of the NB measurement equipment.

The current ITU recommendation for BEL does not model the depth inside the building, relying instead on a single BEL distribution for each slant angle (ψ) [16]. The mean of the BEL measurements for each floor and from each transmitter are tabulated in Table 2 for both ‘min’ and ‘isotropic’ measurements. The mean is taken across all contributing

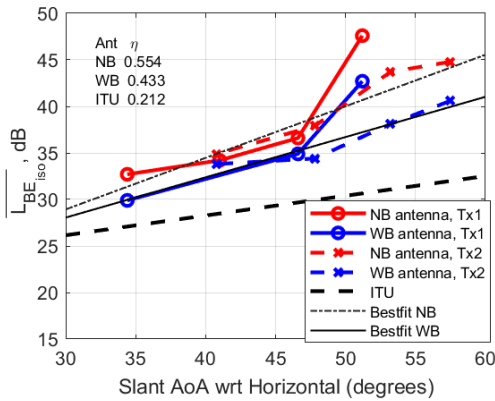


FIGURE 7. Mean Isotropic BEL ($\overline{L_{BE_{iso}}}$) vs slant angle for NB and WB antennas for Tx1 and Tx2.

locations in the Tx antennas HPBW for each slant angle ψ , as illustrated by Fig. 2 for floor level 2. The different geometries mean that Tx1 and Tx2 have different slant angle ψ values for the same floor level. Fig. 7 shows how the mean isotropic BEL ($\overline{L_{BE_{iso}}}$) values vary with ψ for each Tx. $\overline{L_{BE_{iso}}}$ increases with increasing slant angle, ψ . The restricted elevation coverage of the NB antenna shows up as a 1 dB to 5 dB additional path loss (compared to the WB antenna), particularly evident when ψ is over 50° . The abrupt increase in BEL from Tx1 at $\psi = 51.2^\circ$ is due to tree clutter and a low iron roof partially shading the building's south tower ground floor (level 1) entrance. Leaving out this point a best fit line of all the remaining WB antenna based measurements (solid black) has a slope of $\eta = 0.433$ dB/degree of slant with a $\sigma = 0.77$ dB, which is a good fit. The slope is approximately twice the steepness of the ITU's recent model prediction of 0.212 dB/degree (shown as a black dashed line) for this type of building [16]. The mean BEL is closest to the ITU prediction at low slant angles, being within 3 dB for $\psi < 37^\circ$.

Fig. 8 compares the ITU cdf of eq. 1 with the cdf of our isotropic BEL ($L_{BE_{iso}}$) measurements for three slant angles taking results from both Tx1 and Tx2 towers. It is not possible to compare the tails of the distributions as in [10] due to the limited number of measurements, however the average slope is not too dissimilar to the ITU recommendation. The WB antenna (dot-dashed line) closely aligns to the mid region of the ITU curves for $\psi = 34.4^\circ$, but shifts to higher BEL at increased ψ . The higher loss of the NB antenna is clearly evident in the positive offset of the solid curves at low BEL (cdf < 60%) when depth into the building is small. However this is not apparent for higher BEL's (cdf > 60%) which would occur deeper into the building. Here, the NB and WB lines undergo a series of crossings indicating little signal is present outside the NB capture range ($|\theta| \approx > 45^\circ$). Such signals have been reduced by reflection losses and scattering off internal objects converting the elevated signals into more horizontally propagating waves.

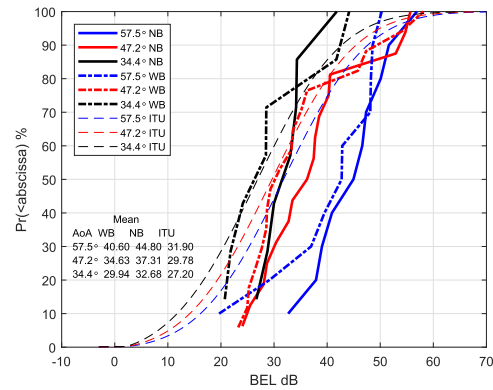


FIGURE 8. CDF of Isotropic BEL ($L_{BE_{iso}}$) with NB, WB and the ITU model at different slant angles.

BEL WITH ADAPTIVE BEAMFORMING

In this section we include the effect of the receive antenna directivity and gain, G_{Rx} , to give the realistic antenna experience (rather than reconstruct the “isotropic” performance as per the previous section). This effectively removes the normalisation on Fig. 4. Including the directivity of the receive antenna is regarded as future work for the ITU standard [17].

The combined building entry loss (CBEL) measured at the receiver antenna port, $L_{BE,Grx}$, can be represented as a combination of loss due to building entry L_{BE} and gain due to receiver antenna G_{Rx} i.e.

$$L_{BE,Grx} = L_{BE} - G_{Rx} \quad (4)$$

For an isotropic Rx antenna, $G_{Rx} = 0$ dBi and $L_{BE_{iso}}$ of Fig. 7 equals $L_{BE,Grx_{iso}}$. With isotropic antennas BEL is the same whether it is being used to estimate the coverage from a high altitude platform or the co-existence with a high altitude platform. In the former the platform signal is desired, while in the latter case the platform signal is unwanted interference. This situation changes when adaptive beamforming is used, as in the case for mmWaves. Although, in all cases, the BEL is essentially the same, the effects of multiple entry points and the internal multipath environment combined with the antenna array pattern, gain and orientation makes for quite different receiver experiences. CBEL uses the same outside (0 dBi antenna) reference for comparing these different scenarios. When the high altitude platform forms the desired signal, the Rx array will beamsteer to the strongest direction, while in the co-existence case the array is focussed on signals from another basestation and so we assume the orientation is random with respect to the platform signal. Then, only occasionally will the beamsteered array coincide with the direction of max interference from the platform. We discuss these two situations next.

The lower 4 traces of Fig. 9 show the desired signal case when the Rx antenna is always beamformed to the direction of the strongest signal (minimum CBEL). Then $\overline{L_{BE,Grx_{min}}}$, the mean of the minimum combined entry loss from just

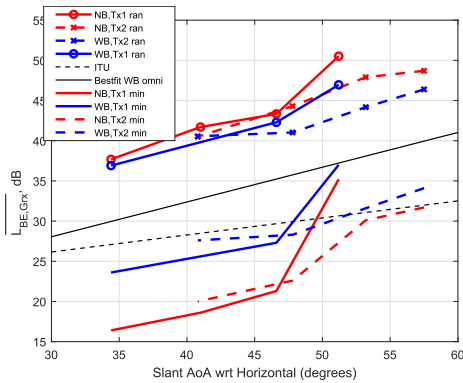


FIGURE 9. Mean directional CBEL ($\overline{L_{BE,Grx}(\theta, \phi)}$) and Mean minimum CBEL ($\overline{L_{BE,Grx_{min}}}$) vs slant angle for NB and WB antennas for Tx1 and Tx2.

outside the building to the receiver’s input port (which now includes the Rx antenna gain), is plotted against the slant angle, ψ . The WB antenna (blue) gives an average of ≈ 7 dB reduced CBEL than the isotropic best fit line (solid black) which is 2.6 dB short of the antennas 9.6 dBi gain. Similarly, comparing the NB antenna with the NB derived isotropic gives an average of ≈ 17.5 dB less CBEL which is 6 dB short of the 23.5 dBi gain of the antenna. The specified gain of the antennas is not fully realised because of the complex multiple direction of arrivals within the building [18], [24]–[26]. In this environment the gain reduction is 26% for both antennas. Also note that as the slant angles move from low ($\psi = 35^\circ$) to high ($\psi > 50^\circ$) the difference between the NB and WB antennas reduces from ≈ 7 dB to < 3 dB caused by a fall in NB antenna gain as a growing proportion of signals from higher elevations are not being seen by the NB antenna. The cdf for three slant angles is shown in Fig. 10. Slopes are similar or slightly steeper than the ITU specified 0 dBi curves and the NB antenna outperforms the WB antenna in all except two locations, (characterised by low CBEL and a high slant angle).

The co-existence situation with random alignment is shown by the upper four traces in Fig. 9 (marked ‘ran’) where the mean is taken over all the measured angles from all locations contributing to the specified slant angle. Compared to the bestfit isotropic line we see a ≈ 7 dB increase in BEL for the WB antenna and ≈ 9 dB for the higher gain NB antenna (or ≈ 6 dB compared to the NB isotropic bestfit of Fig. 7). The increased CBEL is because the directive antenna’s bore-sight is often pointing away from the incoming signals. Occasionally however the antenna will beamform into the minimum CBEL direction and the occurrence of this can be checked by the cdf of $\overline{L_{BE,Grx_{min}}}$, Fig. 11. Again we use the ITU cdf of eq. 1 as a reference. The higher number of measurement points gives a smoother curve with better rendition of the tails. The median value of CBEL is between 35 dB and 50 dB, but the tails go as low as 10 dB as they incorporate the wanted signal situation of Fig. 10 when the antenna is aligned for maximum response (minimum BEL). The cdf

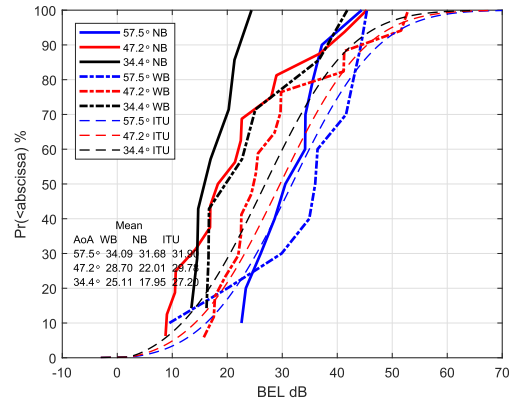


FIGURE 10. CDF of minimum CBEL ($\overline{L_{BE,Grx_{min}}}$) with NB, WB and the ITU model at different slant angles.

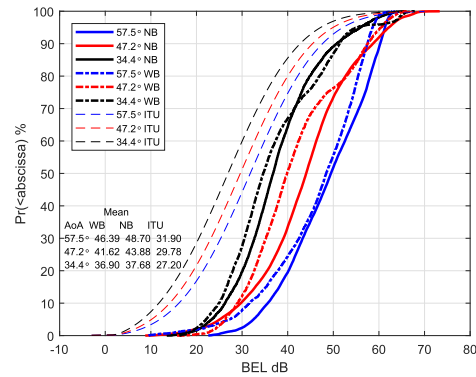


FIGURE 11. CDF of Directional CBEL ($\overline{L_{BE,Grx}(\theta, \phi)}$) with NB, WB and the ITU model at different slant angles.

shows CBELs below 20 dB only occur with a probability of 2% for the most sensitive slant angle of $\psi = 34^\circ$.

IV. CONCLUSION

Slant path BEL using directional antennas at mmWaves is important for both coverage and coexistence studies. BEL measurements at 24 GHz into an older style building are presented for different slant angles and different depths into the building, using 9.6 dBi and 23.5 dBi horn antennas for the indoor unit. The isotropic (0 dBi) performance is synthesised to allow comparisons to the recent ITU model. The signal loss into the building was best modelled as a linear increase in path loss (dB) with distance into the building. The slope increases with slant angle up to 3.4 dB/m; higher than previous published predictions [15]. The effective loss through the outside wall and windows was 15 dB. The variation of mean BEL with ψ is twice that suggested by the ITU indicating a much higher increased loss with slant angle for this building. The higher gain, NB antenna had a limited vertical scan angle that meant it could not see signals from above 45° or below -25° elevations. We use this fact to identify conditions where high elevation signals dominate, and this shows up at high

slant paths $\psi > 50^\circ$ where the NB synthesised Isotropic BEL increased 5 dB compared to the WB synthesised Isotropic which had unrestricted scanning. Clearly the NB antenna misses the majority of the signal because the internal floor to ceiling reflections have elevation angles set by the incoming slant. The difference between NB and WB synthesised BEL measurements drops to ≈ 1 dB at $\psi = 30^\circ$. Now, both NB and WB antennas give similar results.

Slant path BEL using beamformed antennas are not as yet covered by the ITU. We introduce the term CBEL, which combines BEL with the indoor antenna gain, to give a consistent outside reference and then present measurements for two conditions, the desired signal condition and the co-existence condition. When the HAP is the desired signal source the CBEL is significantly reduced by beamforming, but not by the full antenna directivity gain as might be expected. Scattering within the building causes multiple AoAs which reduce the effective (dB) antenna gain by about 26% for both NB and WB antennas. In the co-existence case beamforming actually increases the CBEL compared to the Isotropic case, which is clearly a benefit and somewhat counter to the supposition in [17] indicating there would be no difference. However, the improvement is modest (in this case 6 dB to 9 dB dependent on slant angle) and limited by diminishing returns as the beamwidth is narrowed (1 dB to 3 dB further improvement going from WB to NB). We conclude that beamforming at mmWave frequencies is beneficial for slant path building entry in both coverage enhancement and co-existence with HAPs and satellites.

APPENDIX

The ITU parameters for building entry loss of equation (1) are given as [16]:

$$A(P) = F^{-1}(P)\sigma_1 + \mu_1 \quad (5)$$

$$B(P) = F^{-1}(P)\sigma_2 + \mu_2 \quad (6)$$

$$C = -3.0 \quad (7)$$

$$\mu_1 = L_h + L_e \quad (8)$$

$$\mu_2 = w + x \log(f) \quad (9)$$

$$\sigma_1 = u + v \log(f) \quad (10)$$

$$\sigma_2 = y + z \log(f) \quad (11)$$

$$\quad \quad \quad (12)$$

where:

$$L_h = r + s \log(f) + t (\log(f))^2 \quad (13)$$

L_e is the correction for slant elevation angle, ψ :

$$L_e = 0.212 |\psi| \quad (14)$$

- f = frequency (GHz)
 ψ = slant elevation angle (degrees)
 P = probability that loss is not exceeded ($0 < P < 1$)
 $F^{-1}(P)$ = inverse cumulative normal distribution as a function of probability.

For the traditional building, the coefficients are given as: $r = 12.64$, $s = 3.72$, $t = 0.96$, $u = 9.6$, $v = 2.0$, $w = 9.1$, $x = -3.0$, $y = 4.5$, $z = -2.0$

REFERENCES

- [1] *Effects of Building Materials and Structures on Radiowave Propagation Above About 100 MHz*, document ITU-R, ITU-R P.2040-1, International Telecommunication Union, Report, 2015. [Online]. Available: <https://www.itu.int/rec/R-REC-P.2040-1-201507-1/en>
- [2] *Compilation of Measurement Data Relating to Building Entry Loss*, document ITU-R 2346-2, International Telecommunication Union, 2017. [Online]. Available: <https://www.itu.int/pub/R-REP-P.2346>
- [3] F. Perez-Fontan, V. Hovinen, M. Schönhuber, R. Prieto-Cerdeira, J. A. Delgado-Penín, F. Teschl, J. Kyröläinen, and P. Valtr, "Building entry loss and delay spread measurements on a simulated HAP-to-indoor link at S-band," *EURASIP J. Wireless Commun. Netw.*, vol. 2008, no. 11, pp. 11:1–11:6, Jan. 2008.
- [4] T. Jost, G. Carrié, F. Pérez-Fontán, W. Wang, and U.-C. Fiebig, "A deterministic satellite-to-indoor entry loss model," *IEEE Trans. Antennas Propag.*, vol. 61, no. 4, pp. 2223–2230, Apr. 2013.
- [5] D. I. Axiotis and M. E. Theologou, "An empirical model for predicting building penetration loss at 2 GHz for high elevation angles," *IEEE Antennas Wireless Propag. Lett.*, vol. 2, pp. 234–237, 2003.
- [6] D. Axiotis and M. E. Theologou, "Building penetration loss at 2 GHz for mobile communications at high elevation angles by HAPS," in *Proc. 5th Int. Symp. Wireless Pers. Multimedia Commun.*, vol. 1, Oct. 2002, pp. 282–285.
- [7] B. Guo, Y. Wu, J. Jiao, B. Lv, F. Zhou, Z. Ma, and J.-L. Sun, "Building entry loss model for 24 to 31GHz band," in *Proc. Int. Symp. Antennas Propag. (ISAP)*, Oct. 2016, pp. 60–61.
- [8] C. R. Anderson, T. S. Rappaport, K. Bae, A. Verstak, N. Ramakrishnan, W. H. Tranter, C. A. Shaffer, and L. T. Watson, "In-building wideband multipath characteristics at 2.5 and 60 GHz," in *Proc. IEEE 56th Veh. Technol. Conf.*, vol. 1, Sep. 2002, pp. 97–101.
- [9] *Study on Channel Model for Frequency Spectrum Above 6 GHz Version 14.1.0*, document 3GPP.38.900, Technical Specification, 3rd Generation Partnership Project, Jun. 2017.
- [10] J. Lee, K.-W. Kim, M.-D. Kim, J.-J. Park, and H. K. Chung, "Empirical investigation of antenna beamwidth effects on the ITU-R building entry loss (BEL) model based on 32 GHz measurements," in *Proc. 11th Global Symp. Millim. Waves (GSMM)*, May 2018, pp. 1–3.
- [11] J. Lee, M.-D. Kim, J.-J. Park, and Y. J. Chong, "Field-measurement-based received power analysis for directional beamforming millimeter-wave systems: Effects of beamwidth and beam misalignment," *ETRI J.*, vol. 40, no. 1, pp. 26–38, Feb. 2018.
- [12] J. Lee, J. Liang, J.-J. Park, and M.-D. Kim, "Beamwidth-dependent directional propagation loss analysis based on 28 and 38 GHz urban micro-cellular (UMi) measurements," in *Proc. IEEE 86th Veh. Technol. Conf. (VTC-Fall)*, Sep. 2017, pp. 1–5.
- [13] M. U. Sheikh, K. Hiltunen, and J. Lempiäinen, "Enhanced outdoor to indoor propagation models and impact of different ray tracing approaches at higher frequencies," *Adv. Sci. Technol. Eng. Syst. J.*, vol. 3, no. 2, pp. 58–68, 2018.
- [14] *Guidelines for Evaluation of Radio Interface Technologies for IMT-Advanced*, document ITU-R M.2135, ITU, 2008.
- [15] M. Inomata, W. Yamada, M. Sasaki, and T. Onizawa, "Outdoor-to-indoor path loss model for 8 to 37 GHz band," in *Proc. Int. Symp. Antennas Propag. (ISAP)*, Nov. 2015, pp. 1–4.
- [16] *Prediction of Building Entry Loss*, document ITU-R, ITU-R P.2109-0, International Telecommunication Union, Recommendation, 2017.
- [17] R. Rudd, J. Medbo, F. Lewicki, F. S. Chaves, and I. Rodriguez, "The development of the new ITU-R model for building entry loss," in *Proc. 12th Eur. Conf. Antennas Propag. (EuCAP)*, Apr. 2018, pp. 1–5.
- [18] S. Dahal, S. Ahmed, H. King, and M. Faulkner, "Antenna gain in a millimetre-wave multipath environment," in *Proc. Austral. Microw. Symp. (AMS)*, Feb. 2018, pp. 93–94.
- [19] S. Dahal, M. Faulkner, H. King, and S. Ahmed, "27.1 GHz millimetre wave propagation measurements for 5G urban macro areas," in *Proc. IEEE 85th Veh. Technol. Conf. (VTC Spring)*, Jun. 2017, pp. 1–5.
- [20] M. U. Sheikh, K. Hiltunen, and J. Lempiäinen, "Angular wall loss model and extended building penetration model for outdoor to indoor propagation," in *Proc. 13th Int. Wireless Commun. Mobile Comput. Conf. (IWCMC)*, Jun. 2017, pp. 1291–1296.

- [21] S. Dahal, S. Ahmed, H. King, G. Bharatula, J. Campbell, and M. Faulkner, "Urban microcell 39 GHz measurements," *IEEE Antennas Wireless Propag. Lett.*, vol. 18, no. 10, pp. 2071–2075, Oct. 2019.
- [22] S. Sun, G. R. MacCartney, M. Samimi, and T. S. Rappaport, "Synthesizing omnidirectional antenna patterns, received power and path loss from directional antennas for 5G millimeter-wave communications," in *Proc. IEEE Global Commun. Conf. (GLOBECOM)*, Dec. 2015, pp. 1–7.
- [23] P. Kyosti, "Winner ii channel models," IST, Las Vegas, NV, USA, Tech. Rep. IST-4-027756 WINNER II D1.1.2V1.2, 2007.
- [24] T. Taga, "Analysis for mean effective gain of mobile antennas in land mobile radio environments," *IEEE Trans. Veh. Technol.*, vol. 39, no. 2, pp. 117–131, May 1990.
- [25] A. A. Glazunov, A. F. Molisch, and F. Tufvesson, "Mean effective gain of antennas in a wireless channel," *IET Microwaves, Antennas Propag.*, vol. 3, no. 2, pp. 214–227, Mar. 2009.
- [26] A. A. Glazunov, "Theoretical analysis of mean effective gain of mobile terminal antennas in Ricean channels," in *Proc. IEEE 56th Veh. Technol. Conf.*, vol. 3, Sep. 2002, pp. 1796–1800.



SAURAV DAHAL received the bachelor's degree in electronics and communication engineering from Tribhuvan University, Kathmandu, Nepal, in 2011, and the master's degree in computer engineering with a major in wireless communication and networking from Chosun University, Gwangju, South Korea, in 2015. He is currently pursuing the Ph.D. degree in telecommunication with Victoria University, Melbourne, VIC, Australia. He received the Brain Korea 21 (BK 21) Plus

Scholarship for studying master's degree in South Korea and is receiving the Victoria University Postgraduate Scholarship (VUPRS) for studying Ph.D. degree with Victoria University. His current research interests include networks and RF and millimeter wave systems.



SHABBIR AHMED received the Ph.D. degree from Victoria University, Melbourne, in 2013. His Ph.D. research involved the investigation of the major causes of interference that arise in co-locating base station transceivers. After his Ph.D. degree, he continued as a Research Fellow of wireless systems with the College of Engineering and Science, Victoria University, until 2017. He is currently a Senior EMC and RF Engineer with EMC Technologies, Melbourne. He is also

a Lecturer with Victoria University. His current research interests include software radios, and RF and millimeter-wave systems.



HORACE KING received the degree from RMIT University, where he was with the research Centre for Advanced Technology in Telecommunication (CATT) doing research in Telecommunication and Teaching of Engineering Design Units for the third and fourth year Engineering streams after which he was with Swinburne and Monash. He is currently a Senior Lecturer in electrical engineering with the College of Engineering and Science, involved in teaching and coordinating telecommu-

nication units at both undergraduate and postgraduate levels. He is also an active research member of Telecommunications, Electronics, Photonics and Sensors (TEPS) Research Centre. His current research interest includes telecommunication technologies, specifically in wireless communication of CDMA, LTE, and microwave and satellite communication systems.



GANESH BHARATULA received the master's degree in microwave communications and electronics and another master's degree in solid state physics from Delhi University, India.

He was with the Tata Institute of Fundamental Research (India's premier research organization), developing microwave and satellite communication products for India's space research. He has been with Telstra Corporation Ltd., since 1984, starting first with IT Research Laboratories and then joining its CTO Department and Wireless Engineering. He is currently a Networks Principal with the Wireless Access Group and looks after assessment and development of emerging wireless technologies. Over the last 35 years, he has been providing technology leadership in regards to Telstra's current and future national and international mobile and fixed radio networks deployments in terms of standards influence, technology strategy, roadmap development, and performance assessment and tools. He has played key roles in Telstra's decisions to deploy 3G, 4G, and 5G.

He has authored several articles for reputed national and international journals and conferences.



JOHN CAMPBELL received the B.E. and M.Eng.Sc. degrees from The University of Melbourne. He started to work with Telstra (then Telecom Australia), in 1978. He was with Telstra's Research Laboratories, until 2006, then in their as a CTO, and Wireless Network Engineering Departments. He has recently retired from Telstra Corporation Ltd., where he was a Senior Wireless Technology Specialist. In his early years, he involved in pair cable, optical fiber, and high

capacity digital radio systems after which his work focused on mobile wireless systems, involving the assessment of emerging wireless technologies and their impact on network capacity and performance, propagation measurements and modeling, network design tools, spectrum matters, and technology strategy. He presented the postgraduate subject wireless communication system at The University of Melbourne, from 1999 to 2016. His current research interests include physical layer technologies for 5G with focus on performance targets, coexistence, mm-wave systems, new waveforms, massive MIMO, 3GPP influence and the application of 5G to both mobile and fixed wireless access. He is currently involved with the Antennas and Propagation Society, Melbourne, Australia.



MICHAEL FAULKNER received the B.Sc. (Eng.) degree from the Queen Mary University of London, U.K., and the Ph.D. degree from the University of Technology, Sydney, Australia, in 1993. He is currently a Professor in telecommunications with Victoria University, Australia. His main research interest was in the application of (digital) signal processing techniques to the correction of the non-ideal characteristics of practical RF components; for example, quadrature modulators and

power amplifiers. He has given tutorials, seminars, and invited articles on the above topic. Since then, his interests have broadened to encompass all physical layer aspects of wireless systems, with an emphasis on implementation. He has supervised research projects in radio propagation measurements (wideband channel sounding and direction of arrival), MIMO, transceiver algorithms, architectures and circuits, physical layer signal processing, and modulation. He has authored or coauthored over 100 publications and is regularly involved with industry sponsored research. His current research interests include wireless system design and fifth generation wireless technologies.

...

OFFICE FOR RESEARCH TRAINING, QUALITY AND INTEGRITY

DECLARATION OF CO-AUTHORSHIP AND CO-CONTRIBUTION: PAPERS INCORPORATED IN THESIS

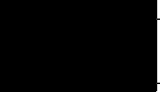
This declaration is to be completed for each conjointly authored publication and placed at the beginning of the thesis chapter in which the publication appears.

1. PUBLICATION DETAILS (to be completed by the candidate)

Title of Paper/Journal/Book:	Antenna gain in a Millimetre-Wave Multipath Environment		
Surname:	Dahal	First name:	Saurav
Institute:	Institute for Sustainable Industries and Liveable	Candidate's Contribution (%):	80
Status:		Date:	
Accepted and in press:	<input type="checkbox"/>	Date:	
Published:	<input checked="" type="checkbox"/>	Date:	06-02-2018

2. CANDIDATE DECLARATION

I declare that the publication above meets the requirements to be included in the thesis as outlined in the HDR Policy and related Procedures – policy.vu.edu.au.

	18-12-2019
Signature	Date

3. CO-AUTHOR(S) DECLARATION

In the case of the above publication, the following authors contributed to the work as follows:

The undersigned certify that:

1. They meet criteria for authorship in that they have participated in the conception, execution or interpretation of at least that part of the publication in their field of expertise;
2. They take public responsibility for their part of the publication, except for the responsible author who accepts overall responsibility for the publication;



- 3. There are no other authors of the publication according to these criteria;
- 4. Potential conflicts of interest have been disclosed to a) granting bodies, b) the editor or publisher of journals or other publications, and c) the head of the responsible academic unit; and
- 5. The original data will be held for at least five years from the date indicated below and is stored at the following **location(s)**:

Name(s) of Co-Author(s)	Contribution (%)	Nature of Contribution	Signature	Date
Shabbir Ahmed	5	Helped in measurements		26/02/20
Horace King	5	Helped in measurements		26/02/20
Mike Faulkner	10	Overall supervision and contribution to theory		28/02/2020

Updated: September 2019

Chapter 10

Antenna gain in a Millimetre-Wave

Multipath Environment

10.1 Overview

Chapter 9 showed the O2I performance of terminal beamforming inside a building. Mobile terminals inside buildings are likely to receive many multipaths. In such a scenario, the antenna gain is not fully utilised. In this chapter, we show the effective antenna gain is reduced (from its specified gain) because multipaths outside the main lobe are rejected. This study will help in planning link budgets in multipath environments.

10.2 Publication

The following article has been published in IEEE Australian Microwave Symposium (AMS) 2018.

S. Dahal, S. Ahmed, H. King and M. Faulkner, "Antenna gain in a millimetre-wave multipath environment," 2018 Australian Microwave Symposium (AMS), Brisbane, QLD, 2018, pp. 93-94, doi : 10.1109/AUSMS.2018.8346998.

The full-text of this article is subject to copyright restrictions, and cannot be included in the online version of the thesis.

The full-text is available from: <https://ieeexplore.ieee.org/document/8346998>

Chapter 11

Conclusion

This chapter summarizes the channel measurements performed in different scenario, RMa, UMa, UMi and O2I, and then discusses some of the topics for future work. Measurements involved either continuous wave (CW) narrowband transmissions at 24 GHz and 39.5 GHz or wide band multi-carrier transmissions at 27.1 GHz.

11.1 Research Contributions

11.1.1 RMa

CW Measurements at 24 GHz in an open park area with many sports fields were used to emulate a rural (RMa) environment. Some of the key findings are:

- The parameters such as path loss exponent, angle of arrival (AoA) spread closely aligned with parameters of the pre 2016 RMa path loss model in R1-163909 [53].

As a result of this work, the 3GPP RMa path loss model in R1-163909 [53] was extended from 7 GHz to to 30 GHz as described in TS 38.9 version 14.1.0 [100] .

- Tree foliage measured through the crown of a eucalyptus tree can cause up to 20 dB attenuation.

11.1.2 UMa

UMa measurements were performed at 27.1 GHz in NLOS Light and NLOS Dense scenarios. Some of the key findings were:

- The 'Alpha-Beta (AB)' model having two degrees of freedom (PLE α and intercept β) had a lower bestfit RMS error (σ) compared to the 'close-in reference distance (CI)' model (with only one degree of freedom (α)). However the CI model was more stable when there was a limited number of measurement points.
- With "omni" measurements, AB-3GPP outperformed CI-NYU in the more sub-urban (or light) setting while the CI-NYU preferred the more dense environments. The CI model performed particularly well when the coverage area included zones with vastly different parameter sets (street widths, building heights)

11.1.3 UMi

UMi measurements were categorized into two different scenarios, UMi Open Square (OS) and UMi Street Canyon (SC). We performed forward measurements (BS to MS) with two different antenna heights in OS and two different polarisations in SC scenario.

Additionally, reverse measurements (MS to BS) were performed in OS scenario. Some of the key findings were:

- For OS and SC, the CI α parameter extracted from the synthesised omnidirectional measurements matched those from the CI-NYU model within 3%. The shadow fading σ parameter was within limits for OS, but 0.7 dB higher in SC.
- The height gain was marginal and slightly negative. Increasing BS height appears to be ineffective in these conditions, contrary to [128] which obtained a 3 dB power boost over a similar 4 m height increase. Generally the lower antenna would encounter more ground clutter but, as shown here, it can experience less tree clutter by avoiding (getting below) the leaf canopy. These effects nullify each other.
- The scattering loss into SC side streets was measured at 18 dB for “just around the corner” rising to 31 dB ~ 100 m down the side street.
- The signal in the side alley often has reduced directional diversity (comes from one direction only) making hand-held reception sensitive to body shadowing effects.
- The mean XPD measured in the UMi SC was 12.3 dB, dropping to 5.8 dB at the weakest signal location.
- XPD drops with path loss on a “peak” basis, but appeared uncorrelated on an “omni” basis. The latter implies existing co-polar channel models can be used for predicting cross-polar signal strengths, just by adding an additional 12.3 dB path loss.

Reverse measurements were conducted in an OS UMi environment to see the correspondence between the UE AoDs and BS AoAs.

- Multiple Angles of Departure (AoD) from a given UE position often result in few (often just one) Angles of Arrival (AoA) at the BS.
- Multiple UE positions have signals arriving at few (often just one) Angles of Arrival (AoA) at the BS. The channelling effect of streets and scattering from the same object appear to be dominant mechanisms in NLOS situations.
- The reduced number of resolvable paths imply limited performance in MIMO and beamforming applications.

11.1.4 O2I

BEL measurements at 24 GHz into a 'traditional' building were presented for different slant angles and different depths into the building, using 9.6 dBi (WB) and 23.5 dBi (NB) horn antennas for the indoor unit. Some of the key findings were:

- The signal loss into the building was best modelled as a linear increase in path loss (dB) with distance into the building from the exposed face. The path loss slope increased with slant angle up to 3.4 dB/m (@slant of 51.2°) ; higher than the $(0.7 \sin(\psi))$ dB/m proposed by [153].
- The effective loss through the outside wall and windows was 15 dB \pm 2 dB.
- The variation of mean BEL with slant angle ψ was twice that suggested by the ITU, indicating a much higher increased loss with slant angle for this building.

- Beamforming at mmWave frequencies is beneficial for slant path building entry in both coverage enhancement and co-existence with high altitude platforms (HAPs) and satellites.
- Measurements using a 9.6 dBi horn antenna showed an effective gain of 5.7 dBi, a loss of 3.87 dB due to the multipath nature of the indoor environment.

11.2 Future Work

Some ideas for future work are:

- A number of researchers have reported on path loss through trees, however few researchers have considered back-scattering from trees. A study into scattering from trees and vegetation would therefore be useful.
- MmWaves have been considered for wireless fixed access as low cost alternative to optical fibre for internet to the home. Fixed access measurements would identify feasibility in terms of coverage and link quality.
- Reverse measurements were only performed for UMi. Other scenarios should be considered.
- Path Loss and AoA data have been obtained for many scenarios. How this relates to terminal performance is not clear. A study, using the existing measurement data to predict performance of hand held antennas in different environments is required.

References

- [1] 3GPP, “New measurements at 24 GHz in a rural macro environment,” 3rd Generation Partnership Project, Technical Report TDOC R1-164975, Telstra, Ericsson, May 2016. [Online]. Available: http://www.3gpp.org/ftp/TSG_RAN/WG1_RL1/TSGR1_85/Docs/R1-164975.zip
- [2] S. Dahal, S. Ahmed, H. King, G. Bharatula, J. Campbell and M. Faulkner, “Slant-Path Building Entry Loss at 24 GHz,” *IEEE Access*, vol. 7, pp. 158 525–158 532, 2019.
- [3] ———, “Urban microcell 39 GHz measurements,” *IEEE Antennas and Wireless Propagation Letters*, vol. 18, no. 10, pp. 2071–2075, 2019.
- [4] S. Dahal, E. A. Stephanou, N. Talukdar, S. Ahmed, H. King, and M. Faulkner, “Millimetre Wave Propagation Reverse Measurements for 5G Urban Micro Scenario,” in *IEEE 89th Vehicular Technology Conference*, 2019, pp. 1–5.
- [5] S. Dahal, S. Ahmed, H. King, and M. Faulkner, “Antenna gain in a millimetre-wave multipath environment,” in *IEEE Australian Microwave Symposium (AMS)*, 2018, pp. 93–94.

References

- [6] S. Dahal, M. Faulkner, H. King, and S. Ahmed, “27.1 GHz Millimetre Wave Propagation Measurements for 5G Urban Macro Areas,” in *IEEE 85th International Conference on Vehicular Technology*, 2017, pp. 1–5.
- [7] ITU-R, “Compilation of measurement data relating to building entry loss,” International Telecommunication Union, Report ITU-R 2346-2, 2017. [Online]. Available: <https://www.itu.int/pub/R-REP-P.2346>
- [8] —, “Measurements on urban building clutter loss,” International Telecommunication Union, Report ITU-R WP3K Contribution 102, 2017. [Online]. Available: <https://www.itu.int/md/R15-WP3K-C-0102/en>
- [9] P. Cerwall, “Ericsson mobility report,” *White Paper*, 2016. [Online]. Available: <https://www.ericsson.com/assets/local/mobility-report/documents/2016/Ericsson-mobility-report-june-2016.pdf>
- [10] ShareTechnote. Svd model. [Online]. Available: https://www.sharetechnote.com/html/Communication_ChannelModel_SVD.html
- [11] Design World. (2015) A new way to accelerate 5G research. [Online]. Available: <https://www.designworldonline.com/a-new-way-to-accelerate-5g-research/>
- [12] I. Ahmed, H. Khammari, A. Shahid, A. Musa, K. S. Kim, E. De Poorter, and I. Moerman, “A survey on hybrid beamforming techniques in 5G: Architecture and system model perspectives,” *IEEE Communications Surveys & Tutorials*, vol. 20, no. 4, pp. 3060–3097, 2018.

References

- [13] Qualcomm. (2017) Understanding 3GPP – starting with the basics. [Online]. Available: <https://www.qualcomm.com/news/onq/2017/08/02/understanding-3gpp-starting-basics>
- [14] Telewave Inc. Ant150d3 -folded dipole antenna 138-174 mhz. [Online]. Available: <https://www.telewave.com/product/ant150d3-folded-dipole-antenna-138-174-mhz/>
- [15] S. Basu, A. Srivastava, and A. Goswami, “Dual frequency hexagonal microstrip patch antenna,” *International Journal of Scientific and Research Publications*, vol. 3, no. 11, pp. 1–9, 2013.
- [16] Remcom. Beamforming for an 8x8 Planar Phased Patch Antenna Array for 5G at 28 GHz. [Online]. Available: <https://www.remcom.com/examples/2018/7/26/beamforming-for-an-8x8-planar-phased-patch-antenna-array-for-5g-at-28-ghz>
- [17] tutorialspoint. Antenna theory - radiation pattern. [Online]. Available: https://www.tutorialspoint.com/antenna_theory/antenna_theory_radiation_pattern.htm
- [18] ——. Antenna theory - beam width. [Online]. Available: https://www.tutorialspoint.com/antenna_theory/antenna_theory_beam_width.htm
- [19] C. Gustafson, “60 GHz Wireless Propagation Channels: Characterization, Modeling and Evaluation,” Ph.D. dissertation, Lund University, 2014.
- [20] T. S. Rappaport, J. N. Murdock, and F. Gutierrez, “State of the art in 60-GHz integrated circuits and systems for wireless communications,” *Proceedings of the IEEE*, vol. 99, no. 8, pp. 1390–1436, 2011.

- [21] T. S. Rappaport, S. Sun, R. Mayzus, H. Zhao, Y. Azar, K. Wang, G. N. Wong, J. K. Schulz, M. Samimi, and F. Gutierrez, “Millimeter wave mobile communications for 5G cellular: It will work!” *IEEE access*, vol. 1, pp. 335–349, 2013.
- [22] ITU-R, “Attenuation by atmospheric gases,” International Telecommunication Union, Recommendation ITU-R P.676-11, 2016. [Online]. Available: <https://www.itu.int/rec/R-REC-P.676/en>
- [23] Z. Qingling and J. Li, “Rain attenuation in millimeter wave ranges,” in *IEEE 7th International Symposium on Antennas, Propagation & EM Theory*, 2006, pp. 1–4.
- [24] J. Poutanen, “Geometry-based radio channel modeling: Propagation analysis and concept development,” Ph.D. dissertation, Aalto University, 2011.
- [25] G. R. MacCartney Jr, S. Sun, T. S. Rappaport, Y. Xing, H. Yan, J. Koka, R. Wang, and D. Yu, “Millimeter wave wireless communications: New results for rural connectivity,” in *Proceedings of the 5th Workshop on All Things Cellular: Operations, Applications and Challenges*, 2016, pp. 31–36.
- [26] S. Ahmed, R. A. Antiohos, and M. Faulkner, “Millimeter-wave measurements for 5G,” in *IEEE 2nd Australian Microwave Symposium*, Feb 2016, pp. 39–40.
- [27] A. M. Al-Samman, M. H. Azmi, Y. Al-Gumaei, T. Al-Hadhrami, Y. Fazea, A. Al-Mqdashi *et al.*, “Millimeter Wave Propagation Measurements and Characteristics for 5G System,” *Applied Sciences*, vol. 10, no. 1, p. 335, 2020.
- [28] S. Dahal, J. Proud, N. Hodson, H. King, M. Faulkner, and S. Ahmed, “Millimeter Wave Propagation Measurements and Channel Models for Fifth Generation

References

- Mobile Communication in Urban Macro Areas.” Poster presented at Australian Communications Theory Workshop (AusCTW), Canberra, Australia, 2017.
- [29] 3GPP, “Study on channel model for frequencies from 0.5 to 100 GHz,” 3rd Generation Partnership Project, Technical Report TR 38.901 V14.3.0, Dec 2017.
- [30] ARPANSA RPS3. Maximum exposure levels to radiofrequency fields - 3 khz to 300 ghz. [Online]. Available: https://www.arpana.gov.au/sites/default/files/legacy/pubs/rps/rps3.pdf?acsf_files_redirect
- [31] V. N. I. Cisco, “Forecast and methodology, 2012–2017,” *White Paper*, 2013.
- [32] N. R. Ani Pappachen, “Efficient mobile broadband systems based on millimeter wave and tact framework,” *International Journal of Advanced Research in Electrical, Electronics and Instrumentation Engineering*, vol. 4, no. 8, pp. 6964–6969, 2015.
- [33] F. Khan, *LTE for 4G mobile broadband: air interface technologies and performance*. Cambridge University Press, 2009.
- [34] Z. Pi and F. Khan, “An introduction to millimeter-wave mobile broadband systems,” *IEEE Communications Magazine*, vol. 49, no. 6, pp. 101–107, 2011.
- [35] Nokia, “5g use cases and requirements,” *White Paper*, 2013.
- [36] T. S. Rappaport, *Wireless communications: principles and practice*. prentice hall PTR New Jersey, 1996, vol. 2.
- [37] D. Tse and P. Viswanath, *Fundamentals of wireless communication*. Cambridge university press, 2005.

References

- [38] P. Almers, F. Tufvesson, and A. F. Molisch, “Keyhole effects in mimo wireless channels-measurements and theory,” *GLOBECOM-NEW YORK-*, vol. 4, pp. 1781–1785, 2003.
- [39] D. Tse and P. Viswanath, *Fundamentals of wireless communication*. Cambridge university press, 2005.
- [40] C. A. Balanis, “Antenna theory: Analysis & design, john willey & sons,” *Inc. Publication*, 1997.
- [41] A. F. Molisch, V. V. Ratnam, S. Han, Z. Li, S. L. H. Nguyen, L. Li, and K. Haneda, “Hybrid beamforming for massive MIMO: A survey,” *IEEE Communications Magazine*, vol. 55, no. 9, pp. 134–141, 2017.
- [42] T. L. Marzetta, “Noncooperative cellular wireless with unlimited numbers of base station antennas,” *IEEE Transactions on Wireless Communications*, vol. 9, no. 11, pp. 3590–3600, 2010.
- [43] F. Rusek, D. Persson, B. K. Lau, E. G. Larsson, T. L. Marzetta, O. Edfors, and F. Tufvesson, “Scaling up MIMO: Opportunities and challenges with very large arrays,” *IEEE Signal Processing Magazine*, vol. 30, no. 1, pp. 40–60, 2013.
- [44] H. Q. Ngo, E. G. Larsson, and T. L. Marzetta, “Energy and spectral efficiency of very large multiuser mimo systems,” *IEEE Transactions on Communications*, vol. 61, no. 4, pp. 1436–1449, 2013.
- [45] L. Lu, G. Y. Li, A. L. Swindlehurst, A. Ashikhmin, and R. Zhang, “An overview of massive mimo: Benefits and challenges,” *IEEE journal of selected topics in signal processing*, vol. 8, no. 5, pp. 742–758, 2014.

- [46] E. G. Larsson, O. Edfors, F. Tufvesson, and T. L. Marzetta, “Massive MIMO for next generation wireless systems,” *IEEE Communications Magazine*, vol. 52, no. 2, pp. 186–195, 2014.
- [47] I. Ahmed, H. Khammari, and A. Shahid, “Resource allocation for transmit hybrid beamforming in decoupled millimeter wave multiuser-MIMO downlink,” *IEEE Access*, vol. 5, pp. 170–182, 2016.
- [48] F. Boccardi, R. W. Heath, A. Lozano, T. L. Marzetta, and P. Popovski, “Five disruptive technology directions for 5G,” *IEEE Communications Magazine*, vol. 52, no. 2, pp. 74–80, 2014.
- [49] International Telecommunication Union. (2017) About ITU. [Online]. Available: <https://www.itu.int/en/about/Pages/default.aspx>.
- [50] ITU-R, “ITU-R P. 1411-3: Propagation data and prediction methods for the planning of short-range outdoor radiocommunication systems and radio local area networks in the frequency range 300 MHz to 100 GHz,” International Telecommunication Union, Technical Report, 2005.
- [51] —, “Propagation data and prediction methods for the planning of short-range outdoor radiocommunication systems and radio local area networks in the frequency range 300 MHz to 100 GHz,” International Telecommunication Union, Recommendation P.1411-9, Jun 2017.
- [52] —, “Effects of building materials and structures on radiowave propagation above about 100 MHz,” International Telecommunication Union, Report

References

- ITU-R P.2040-1, 2015. [Online]. Available: <https://www.itu.int/rec/R-REC-P.2040-1-201507-I/en>
- [53] 3GPP, “Wf on the rural macro scenario,” 3rd Generation Partnership Project, Technical Report TDOC R1-163909, Ericsson, Vodafone, Samsung, Nokia, 2016. [Online]. Available: https://www.3gpp.org/ftp/TSG_RAN/WG1_RL1/TSGR1_84b/Docs
- [54] ITU-R, “Prediction of building entry loss,” International Telecommunication Union, Recommendation ITU-R P.2109-0, 2017. [Online]. Available: <https://www.itu.int/rec/R-REC-P.2109/en>
- [55] S. Dahal, S. Ahmed, H. King, and M. Faulkner, “Antenna gain in a millimetre-wave multipath environment,” in *IEEE Australian Microwave Symposium*, 2018, pp. 93–94.
- [56] S. Dahal, M. Faulkner, H. King, and S. Ahmed, “27.1 GHz millimetre wave propagation measurements for 5g urban macro areas,” in *IEEE 85th Vehicular Technology Conference*, 2017, pp. 1–5.
- [57] C. A. Balanis, “Antenna theory: A review,” *Proceedings of the IEEE*, vol. 80, no. 1, pp. 7–23, 1992.
- [58] Antenna types. [Online]. Available: <http://www.antenna-theory.com/antennas/main.php>
- [59] P. D. Vita. (2012) An4190 application note: Antenna selection guidelines. [Online]. Available: <http://www.stmicroelectronics.com.cn/>

internet/com/TECHNICAL_RESOURCES/TECHNICAL_LITERATURE/
APPLICATION_NOTE/DM00068254.pdf

- [60] R. K. Chand, M. V. Raghavendra and K.Sathyavathi, “Radiation analysis and design of pyramidal horn antenna,” *INTERNATIONAL JOURNAL OF ENGINEERING RESEARCH and TECHNOLOGY*, vol. 2, no. 10, 2013.
- [61] Ericsson, “Advanced antenna systems for 5G networks,” *White Paper*, 2018. [Online]. Available: <https://www.ericsson.com/en/reports-and-papers/white-papers/advanced-antenna-systems-for-5g-networks>
- [62] D. B. Miron, “Chapter 2 - antenna fundamentals i,” in *Small Antenna Design*, D. B. Miron, Ed. Burlington: Newnes, 2006, pp. 9 – 41. [Online]. Available: <http://www.sciencedirect.com/science/article/pii/B9780750678612500040>
- [63] S. Farahani, “Chapter 5 - rf propagation, antennas, and regulatory requirements,” in *ZigBee Wireless Networks and Transceivers*, S. Farahani, Ed. Burlington: Newnes, 2008, pp. 171 – 206. [Online]. Available: <http://www.sciencedirect.com/science/article/pii/B9780750683937000054>
- [64] G. R. MacCartney, M. K. Samimi, and T. S. Rappaport, “Omnidirectional path loss models in New York City at 28 GHz and 73 GHz,” in *IEEE 25th Annual International Symposium on Personal, Indoor, and Mobile Radio Communication*, 2014, pp. 227–231.
- [65] M. K. Samimi and T. S. Rappaport, “Local multipath model parameters for generating 5G millimeter-wave 3GPP-like channel impulse response,” in *10th European Conference on Antennas and Propagation*, 2016, pp. 1–5.

- [66] I. WINNER, “WINNER II channel models,” *Deliverable D1*, vol. 1, p. 9, 2007.
- [67] B. H. Fleury, “First-and second-order characterization of direction dispersion and space selectivity in the radio channel,” *IEEE Transactions on Information Theory*, vol. 46, no. 6, pp. 2027–2044, 2000.
- [68] B. Clerckx and C. Oestges, “Chapter 3 - analytical mimo channel representations for system design,” in *Mimo Wireless Networks*, second edition ed., B. Clerckx and C. Oestges, Eds. Oxford: Academic Press, 2013, pp. 59 – 100. [Online]. Available: <http://www.sciencedirect.com/science/article/pii/B9780123850553000031>
- [69] J.-P. Kermoal, L. Schumacher, K. I. Pedersen, P. E. Mogensen, and F. Frederiksen, “A stochastic MIMO radio channel model with experimental validation,” *IEEE Journal on selected areas in Communications*, vol. 20, no. 6, pp. 1211–1226, 2002.
- [70] W. Weichselberger, M. Herdin, H. Ozelik, and E. Bonek, “A stochastic MIMO channel model with joint correlation of both link ends,” *IEEE Transactions on Wireless Communications*, vol. 5, no. 1, pp. 90–100, 2006.
- [71] J. Karedal, F. Tufvesson, N. Czink, A. Paier, C. Dumard, T. Zemen, C. F. Mecklenbrauker, and A. F. Molisch, “A geometry-based stochastic mimo model for vehicle-to-vehicle communications,” *IEEE Transactions on Wireless Communications*, vol. 8, no. 7, pp. 3646–3657, 2009.

- [72] H. Hofstetter, A. F. Molisch, and N. Czink, “A twin-cluster MIMO channel model,” in *Antennas and Propagation, 2006. EuCAP 2006. First European Conference on*. IEEE, 2006, pp. 1–8.
- [73] L. Liu, C. Oestges, J. Poutanen, K. Haneda, P. Vainikainen, F. Quitin, F. Tufvesson, and P. De Doncker, “The COST 2100 MIMO channel model,” *IEEE Wireless Communications*, vol. 19, no. 6, pp. 92–99, 2012.
- [74] A. F. Molisch, H. Asplund, R. Heddergott, M. Steinbauer, and T. Zwick, “The COST259 directional channel model-part I: Overview and methodology,” *IEEE Transactions on Wireless Communications*, vol. 5, no. 12, 2006.
- [75] H. Asplund, A. A. Glazunov, A. F. Molisch, K. I. Pedersen, and M. Steinbauer, “The COST 259 directional channel model-part II: macrocells,” *IEEE Transactions on Wireless Communications*, vol. 5, no. 12, 2006.
- [76] X. Gao, F. Tufvesson, O. Edfors, and F. Rusek, “Channel behavior for very-large MIMO systems-initial characterization,” in *COST IC1004, 2012*, 2012.
- [77] J. Meinilä, P. Kyösti, T. Jämsä, and L. Hentilä, “WINNER II channel models,” *Radio Technologies and Concepts for IMT-Advanced*, pp. 39–92, 2009.
- [78] 3GPP, “Study on 3D channel model for LTE (Release 12),” 3rd Generation Partnership Project, Technical Report TR 36.873 V12.2.0, Jun 2015.
- [79] ITU-R, “ITU-R M. 2412: Guidelines for evaluation of radio interface technologies for IMT-2020,” International Telecommunication Union, Technical Report, 2017.

References

- [80] ———, “ITU-R M. 1225: Guidelines for evaluation of radio interface technologies for IMT-2000,” International Telecommunication Union, Technical Report, 1997.
- [81] METIS, “Project management plan,” METIS, Technical Report D1.2, Mar 2013.
- [82] 5GCM, “5G channel model for bands up to 100 GHz,” 5GCM, Technical Report, Oct 2016. [Online]. Available: <http://www.5gworkshops.com/5GCM.html>.
- [83] A. Maltsev, A. Pudeyev, A. Lomayev, and I. Bolotin, “Channel modeling in the next generation mmWave Wi-Fi: IEEE 802.11 ay standard,” in *22th European Wireless Conference*. VDE, 2016, pp. 1–8.
- [84] K. Hiraga, “TG3e Channel Modelling Document (CMD),” IEEE P802.15 Working Group for Wireless Personal Area Networks (WPANs), Technical Report TR 15-15-0279-02-003e, Mar 2015. [Online]. Available: <https://mentor.ieee.org/802.15/dcn/14/15-14-0310-18-003d-channel-modeling-document.docx>
- [85] A. Frickel, “TG3d Channel Modelling Document (CMD),” IEEE P802.15 Working Group for Wireless Personal Area Networks (WPANs), Technical Report TR 15-14-0310-19-003d, Mar 2016. [Online]. Available: <https://mentor.ieee.org/802.15/dcn/14/15-14-0310-18-003d-channel-modeling-document.docx>
- [86] R. J. Weiler, M. Peter, W. Keusgen, A. Maltsev, I. Karls, A. Pudeyev, I. Bolotin, I. Siaud, and A.-M. Ulmer-Moll, “Quasi-deterministic millimeter-wave channel models in MiWEBA,” *EURASIP Journal on Wireless Communications and Networking*, vol. 2016, no. 1, p. 84, 2016.

- [87] mmMAGIC, “Measurement campaigns and initial channel models for preferred suitable frequency ranges,” MAGIC, Technical Report H2020-ICT-671650-mmMAGIC/D2.1, Mar 2016.
- [88] S. Jaeckel, L. Raschkowski, K. Börner, and L. Thiele, “QuaDRiGa: A 3-D multi-cell channel model with time evolution for enabling virtual field trials,” *IEEE Transactions on Antennas and Propagation*, vol. 62, no. 6, pp. 3242–3256, 2014.
- [89] S. Sun, G. R. MacCartney, and T. S. Rappaport, “A novel millimeter-wave channel simulator and applications for 5G wireless communications,” in *IEEE International Conference on Communications*, 2017, pp. 1–7.
- [90] K. Haneda, L. Tian, Y. Zheng, H. Asplund, J. Li, Y. Wang, D. Steer, C. Li, T. Balercia, and S. Lee, “5G 3GPP-like channel models for outdoor urban microcellular and macrocellular environments,” *arXiv preprint arXiv:1602.07533*, 2016.
- [91] Q. Li, H. Shirani-Mehr, T. Balercia, A. Papathanassiou, G. Wu, S. Sun, M. K. Samimi, and T. S. Rappaport, “Validation of a geometry-based statistical mmwave channel model using ray-tracing simulation,” in *IEEE 81st Vehicular Technology Conference*, 2015, pp. 1–5.
- [92] K. Guan, G. Li, T. Kürner, A. F. Molisch, B. Peng, R. He, B. Hui, J. Kim, and Z. Zhong, “On millimeter wave and THz mobile radio channel for smart rail mobility,” *IEEE Transactions on Vehicular Technology*, vol. 66, no. 7, pp. 5658–5674, 2016.

- [93] R. He, B. Ai, G. L. Stüber, G. Wang, and Z. Zhong, “Geometrical-based modeling for millimeter-wave MIMO mobile-to-mobile channels,” *IEEE Transactions on Vehicular Technology*, vol. 67, no. 4, pp. 2848–2863, 2017.
- [94] T. S. Rappaport, G. R. MacCartney, M. K. Samimi, and S. Sun, “Wideband millimeter-wave propagation measurements and channel models for future wireless communication system design,” *IEEE Transactions on Communications*, vol. 63, no. 9, pp. 3029–3056, 2015.
- [95] J. Meinilä, P. Kyösti, T. Jämsä, and L. Hentilä, “WINNER II channel models,” *Radio Technologies and Concepts for IMT-Advanced*, pp. 39–92, 2009.
- [96] M. Hata, “Empirical formula for propagation loss in land mobile radio services,” *IEEE transactions on Vehicular Technology*, vol. 29, no. 3, pp. 317–325, 1980.
- [97] S. Sun, G. R. MacCartney, and T. S. Rappaport, “Millimeter-wave distance-dependent large-scale propagation measurements and path loss models for outdoor and indoor 5G systems,” in *IEEE 10th European Conference on Antennas and Propagation*, 2016, pp. 1–5.
- [98] ITU-R, “Guidelines for evaluation of radio interface technologies for IMT-Advanced,” International Telecommunication Union, Report ITU-R M. 2135, 2008. [Online]. Available: <https://www.itu.int/pub/R-REP-M.2135>
- [99] S. Sun, T. S. Rappaport, T. A. Thomas, A. Ghosh, H. C. Nguyen, I. Z. Kovacs, I. Rodriguez, O. Koymen, and A. Partyka, “Investigation of Prediction Accuracy,

References

- Sensitivity, and Parameter Stability of Large-Scale Propagation Path Loss Models for 5G Wireless Communications,” *IEEE Transactions on Vehicular Technology*, vol. 65, no. 5, pp. 2843–2860, 2016.
- [100] 3GPP, “Study on channel model for frequency spectrum above 6 GHz,” 3rd Generation Partnership Project (3GPP), Technical Specification (TS) 38.900, Jun 2017, version 14.1.0. [Online]. Available: <https://portal.3gpp.org/desktopmodules/Specifications/SpecificationDetails.aspx?specificationId=2991>
- [101] G. R. MacCartney and T. S. Rappaport, “Rural macrocell path loss models for millimeter wave wireless communications,” *IEEE Journal on Selected Areas in Communications*, vol. 35, no. 7, pp. 1663–1677, 2017.
- [102] T. S. Rappaport, Y. Qiao, J. I. Tamir, J. N. Murdock, and E. Ben-Dor, “Cellular broadband millimeter wave propagation and angle of arrival for adaptive beam steering systems,” in *IEEE Radio and Wireless Symposium*, 2012, pp. 151–154.
- [103] H. C. Nguyen, I. Rodriguez, T. B. Sorensen, L. L. Sanchez, I. Kovacs, and P. Mogenssen, “An empirical study of urban macro propagation at 10, 18 and 28 GHz,” in *IEEE 83rd Vehicular Technology Conference*, 2016, pp. 1–5.
- [104] J. N. Murdock, E. Ben-Dor, Y. Qiao, J. I. Tamir, and T. S. Rappaport, “A 38 GHz cellular outage study for an urban outdoor campus environment,” in *IEEE Wireless Communications and Networking Conference (WCNC)*, 2012, pp. 3085–3090.
- [105] M. Samimi, K. Wang, Y. Azar, G. N. Wong, R. Mayzus, H. Zhao, J. K. Schulz, S. Sun, F. Gutierrez, and T. S. Rappaport, “28 GHz angle of arrival and angle

- of departure analysis for outdoor cellular communications using steerable beam antennas in New York City,” in *IEEE 77th Vehicular Technology Conference*, 2013, pp. 1–6.
- [106] T. S. Rappaport, F. Gutierrez, E. Ben-Dor, J. N. Murdock, Y. Qiao, and J. I. Tamir, “Broadband millimeter-wave propagation measurements and models using adaptive-beam antennas for outdoor urban cellular communications,” *IEEE transactions on antennas and propagation*, vol. 61, no. 4, pp. 1850–1859, 2013.
- [107] H. C. Nguyen, G. R. MacCartney, T. Thomas, T. S. Rappaport, B. Vejlgaard, and P. Mogensen, “Evaluation of empirical ray-tracing model for an urban outdoor scenario at 73 GHz E-band,” in *IEEE 80th Vehicular Technology Conference*, 2014, pp. 1–6.
- [108] C. Larsson, B.-E. Olsson, and J. Medbo, “Angular Resolved Pathloss Measurements in Urban Macrocell Scenarios at 28 GHz,” in *IEEE 84th Vehicular Technology Conference*, 2016, pp. 1–5.
- [109] M. Sasaki, M. Nakamura, M. Inomata, Y. Takatori, K. Kitao, and T. Imai, “Path loss frequency dependence at 2–26 GHz in an urban macro cell environment,” in *IEEE International Symposium on Antennas and Propagation & USNC/URSI National Radio Science Meeting*, 2017, pp. 601–602.
- [110] M. R. Akdeniz, Y. Liu, M. K. Samimi, S. Sun, S. Rangan, T. S. Rappaport, and E. Erkip, “Millimeter wave channel modeling and cellular capacity evaluation,” *IEEE journal on selected areas in communications*, vol. 32, no. 6, pp. 1164–1179, 2014.

- [111] A. I. Sulyman, A. T. Nassar, M. K. Samimi, G. R. MacCartney, T. S. Rappaport, and A. Alsanie, “Radio propagation path loss models for 5G cellular networks in the 28 GHz and 38 GHz millimeter-wave bands,” *IEEE Communications Magazine*, vol. 52, no. 9, pp. 78–86, 2014.
- [112] J.-J. Park, J. Liang, J. Lee, H.-K. Kwon, M.-D. Kim, and B. Park, “Millimeter-wave channel model parameters for urban microcellular environment based on 28 and 38 GHz measurements,” in *IEEE 27th Annual International Symposium on Personal, Indoor, and Mobile Radio Communications*, 2016, pp. 1–5.
- [113] T. S. Rappaport, E. Ben-Dor, J. Murdock, and Y. Qiao, “38 GHz and 60 GHz angle-dependent propagation for cellular & peer-to-peer wireless communications,” in *IEEE International Conference on Communications*, 2012, pp. 4568–4573.
- [114] M. K. Samimi, T. S. Rappaport, and G. R. MacCartney, “Probabilistic omnidirectional path loss models for millimeter-wave outdoor communications,” *IEEE Wireless Communications Letters*, vol. 4, no. 4, pp. 357–360, 2015.
- [115] G. R. MacCartney and T. S. Rappaport, “73 GHz millimeter wave propagation measurements for outdoor urban mobile and backhaul communications in New York City,” in *IEEE International Conference on Communications*, 2014, pp. 4862–4867.
- [116] M. K. Samimi and T. S. Rappaport, “3-D millimeter-wave statistical channel model for 5G wireless system design,” *IEEE Transactions on Microwave Theory and Techniques*, vol. 64, no. 7, pp. 2207–2225, 2016.

References

- [117] G. R. Maccartney, T. S. Rappaport, M. K. Samimi, and S. Sun, “Millimeter-wave omnidirectional path loss data for small cell 5G channel modeling,” *IEEE Access*, vol. 3, pp. 1573–1580, 2015.
- [118] A. Al-Samman, T. Rahman, M. Azmi, M. Hindia, I. Khan, and E. Hanafi, “Statistical modelling and characterization of experimental mm-wave indoor channels for future 5G wireless communication networks,” *PloS one*, vol. 11, no. 9: e0163034, 2016.
- [119] Y. Azar, G. N. Wong, K. Wang, R. Mayzus, J. K. Schulz, H. Zhao, F. Gutierrez, D. Hwang, and T. S. Rappaport, “28 GHz propagation measurements for outdoor cellular communications using steerable beam antennas in New York city,” in *IEEE International Conference on Communications*, 2013, pp. 5143–5147.
- [120] A. I. Sulyman, A. Alwarafy, G. R. MacCartney, T. S. Rappaport, and A. Alsanie, “Directional radio propagation path loss models for millimeter-wave wireless networks in the 28-, 60-, and 73-GHz bands,” *IEEE Transactions on Wireless Communications*, vol. 15, no. 10, pp. 6939–6947, 2016.
- [121] W. Roh, J.-Y. Seol, J. Park, B. Lee, J. Lee, Y. Kim, J. Cho, K. Cheun, and F. Aryanfar, “Millimeter-wave beamforming as an enabling technology for 5G cellular communications: Theoretical feasibility and prototype results,” *IEEE communications magazine*, vol. 52, no. 2, pp. 106–113, 2014.
- [122] M. Kyro, V. Kolmonen, and P. Vainikainen, “Experimental propagation channel characterization of mm-wave radio links in urban scenarios,” *IEEE Antennas and Wireless Propagation Letters*, vol. 11, pp. 865–868, 2012.

References

- [123] A. I. Sulyman, H. Seleem, A. Alwarafy, K. M. Humadi, and A. Alsanie, "Effects of Solar Radio Emissions on Outdoor Propagation Path Loss Models at 60 GHz bands for Access/backhaul links and D2D communications," *IEEE Transactions on Antennas and Propagation*, vol. 65, no. 12, pp. 6624–6635, 2017.
- [124] S. Hur, Y.-J. Cho, T. Kim, J. Park, A. F. Molisch, K. Haneda, and M. Peter, "Wideband spatial channel model in an urban cellular environments at 28 GHz," in *IEEE 9th European Conference on Antennas and Propagation*, 2015, pp. 1–5.
- [125] G. Lovnes, J. Reis, and R. Raekken, "Channel sounding measurements at 59 GHz in city streets," in *5th IEEE International Symposium on Personal, Indoor and Mobile Radio Communications, Wireless Networks-Catching the Mobile Future.*, vol. 2, 1994, pp. 496–500.
- [126] P. F. Smulders and L. Correia, "Characterisation of propagation in 60 GHz radio channels," *Electronics & communication engineering journal*, vol. 9, no. 2, pp. 73–80, 1997.
- [127] Keysight. (2018) 5G Flexible Numerology – What is it? Why should you care? [Online]. Available: <https://community.keysight.com/community/keysight-blogs/next-generation-wireless-communications/blog/2018/04/11/5g-flexible-numerology-what-is-it-why-should-you-care?>
- [128] Z. Zhong, C. Li, J. Zhao, and X. Zhang, "Height-dependent path loss model and large-scale characteristics analysis of 28 GHz and 38.6 GHz in urban micro scenarios," in *11th European Conference on Antennas and Propagation*, 2017, pp. 1818–1822.

- [129] A. Al-Samman, M. Hindia, and T. Rahman, "Path loss model in outdoor environment at 32 GHz for 5G system," in *IEEE 3rd International Symposium on Telecommunication Technologies*, 2016, pp. 9–13.
- [130] F. Qamar, M. Hindia, K. Dimyati, K. A. Noordin, M. B. Majed, T. Abd Rahman, and I. S. Amiri, "Investigation of Future 5G-IoT Millimeter-Wave Network Performance at 38 GHz for Urban Microcell Outdoor Environment," *Electronics*, vol. 8, no. 5, p. 495, 2019.
- [131] S. S. N., D. Dash, H. E. Madi, and G. Gopalakrishnan, "WiGig and IEEE 802.11ad - For multi-gigabyte-per-second WPAN and WLAN," 2012.
- [132] E. J. Violette, R. H. Espeland, R. O. DeBOLT, and F. Schwering, "Millimeter-wave propagation at street level in an urban environment," *IEEE Transactions on Geoscience and Remote Sensing*, vol. 26, no. 3, pp. 368–380, 1988.
- [133] M. Celidonio, E. Fionda, M. Vaser, and E. Restuccia, "NLOS mm Wave Propagation Measurements through Vegetation in Urban Area: a Case Study," in *2018 AEIT International Annual Conference*. IEEE, 2018, pp. 1–6.
- [134] H. Zhao, R. Mayzus, S. Sun, M. Samimi, J. K. Schulz, Y. Azar, K. Wang, G. N. Wong, F. Gutierrez, and T. S. Rappaport, "28 GHz millimeter wave cellular communication measurements for reflection and penetration loss in and around buildings in New York City," in *IEEE International Conference on Communications*, 2013, pp. 5163–5167.

- [135] C. Larsson, F. Harrysson, B.-E. Olsson, and J.-E. Berg, “An outdoor-to-indoor propagation scenario at 28 GHz,” in *IEEE 8th European Conference on Antennas and Propagation*, 2014, pp. 3301–3304.
- [136] E. Semaan, F. Harrysson, A. Furuskär, and H. Asplund, “Outdoor-to-indoor coverage in high frequency bands,” in *IEEE Globecom Workshops*, 2014, pp. 393–398.
- [137] G. R. Maccartney, T. S. Rappaport, S. Sun, and S. Deng, “Indoor office wideband millimeter-wave propagation measurements and channel models at 28 and 73 GHz for ultra-dense 5G wireless networks,” *IEEE Access*, vol. 3, pp. 2388–2424, 2015.
- [138] A. Sayeed, J. Brady, P. Cheng, and U. Tayyab, “Indoor channel measurements using a 28GHz multi-beam MIMO prototype,” in *IEEE 84th Vehicular Technology Conference*, 2016, pp. 1–5.
- [139] S. Hur, Y.-J. Cho, J. Lee, N.-G. Kang, J. Park, and H. Benn, “Synchronous channel sounder using horn antenna and indoor measurements on 28 GHz,” in *IEEE International Black Sea Conference on Communications and Networking*, 2014, pp. 83–87.
- [140] I. A. Hemadeh, K. Satyanarayana, M. El-Hajjar, and L. Hanzo, “Millimeter-wave communications: Physical channel models, design considerations, antenna constructions, and link-budget,” *IEEE Communications Surveys & Tutorials*, vol. 20, no. 2, pp. 870–913, 2017.

- [141] D. Axiotis and M. Theologou, "Building penetration loss at 2 GHz for mobile communications at high elevation angles by HAPS," in *IEEE 5th International Symposium on Wireless Personal Multimedia Communications*, vol. 1, 2002, pp. 282–285.
- [142] A. Al-Hourani, S. Chandrasekharan, and S. Kandeepan, "Path loss study for millimeter wave device-to-device communications in urban environment," in *IEEE international conference on communications workshops (ICC)*, 2014, pp. 102–107.
- [143] A. Al-Hourani, R. J. Evans, P. M. Farrell, B. Moran, M. Martorella, S. Kandeepan, S. Skafidas, and U. Parampalli, "Millimeter-wave integrated radar systems and techniques," in *Academic Press Library in Signal Processing, Volume 7*. Elsevier, 2018, pp. 317–363.
- [144] C. C. Chan, F. G. Kurnia, A. Al-Hourani, K. M. Gomez, S. Kandeepan, and W. Rowe, "Open-Source and Low-Cost Test Bed for Automated 5G Channel Measurement in mmWave Band," *Journal of Infrared, Millimeter, and Terahertz Waves*, vol. 40, no. 5, pp. 535–556, 2019.
- [145] A. Al-Hourani and K. Gomez, "Modeling cellular-to-UAV path-loss for suburban environments," *IEEE Wireless Communications Letters*, vol. 7, no. 1, pp. 82–85, 2017.
- [146] A. Al-Hourani, S. Kandeepan, and A. Jamalipour, "Modeling air-to-ground path loss for low altitude platforms in urban environments," in *IEEE global communications conference*, 2014, pp. 2898–2904.

- [147] C. C. Chan, A. Al-Hourani, J. Choi, K. M. Gomez, and S. Kandeepan, "Performance Modeling Framework for IoT-over-Satellite Using Shared Radio Spectrum," *Remote Sensing*, vol. 12, no. 10, p. 1666, 2020.
- [148] A. Al-Hourani, "On the Probability of Line-of-Sight in Urban Environments," *IEEE Wireless Communications Letters*, 2020.
- [149] B. Al Homssi, A. Al-Hourani, R. J. Evans, K. G. Chavez, S. Kandeepan, W. S. Rowe, and M. Loney, "Free spectrum for iot: How much can it take?" in *2018 IEEE International Conference on Communications Workshops (ICC Workshops)*. IEEE, 2018, pp. 1–6.
- [150] T. Wu, T. S. Rappaport, and C. M. Collins, "The human body and millimeter-wave wireless communication systems: Interactions and implications," in *IEEE International Conference on Communications (ICC)*, 2015, pp. 2423–2429.
- [151] ICNIRP. GUIDELINES FOR LIMITING EXPOSURE TO ELECTROMAGNETIC FIELDS (100 kHz to 300 GHz). [Online]. Available: <https://www.icnirp.org/cms/upload/publications/ICNIRPrfgdl2020.pdf>
- [152] R. Rudd, J. Medbo, F. Lewicki, F. S. Chaves, and I. Rodriguez, "The development of the new ITU-R model for building entry loss," in *12th European Conference on Antennas and Propagation*, 2018, pp. 1–5.
- [153] M. Inomata, W. Yamada, M. Sasaki, and T. Onizawa, "Outdoor-to-indoor path loss model for 8 to 37 GHz band," in *IEEE International Symposium on Antennas and Propagation*, 2015, pp. 1–4.